Rijkswaterstaat
Ministry of Infrastructure and Water Management

RWS INFORMATION

Datareport Kustgenese 2.0.

Date November 2019
Status Final

Colofon

Uitgegeven door	Rijkswaterstaat WVL
Auteur	Gezamenlijke auteurs Kustgenese 2.0 en SEAWAD
Informatie	Kustgenese 2.0. / Coastal genesis 2.0 Website
NL website	https://www.helpdeskwater.nl/onderwerpen/waterveiligheid/programma-projecten/kustgenese-2-0/
EN website	https://www.helpdeskwater.nl/secundaire-navigatie/english/water-and-safety/@179039/factsheet-coastal/
Datum	November 2019
Status	Final

Voorwoord / Preface (Dutch)

Voor u ligt het datarapport van Kustgenese 2.0, uitgevoerd door Rijkswaterstaat in opdracht van het Ministerie van Infrastructuur en Waterstaat. Het programma Kustgenese 2.0 onderzoekt tussen 2015 en 2028 hoeveel zand op lange termijn nodig is, waar en wanneer het zand nodig is en hoe we het zand kunnen toevoegen aan de kust. In dit rapport is de gehele opzet en uitvoering van de meetcampagne, de dataprocessing, dataopslag en indicatieve resultaten van de gemeten data beschreven.

Dit rapport is tot stand gekomen door een unieke samenwerking tussen de Universiteiten van Twente, Delft en Utrecht verenigd in het STW programma SEAWAD, Deltares en Rijkswaterstaat CIV en WVL. Rijkswaterstaat is alle partijen en individuele auteurs zeer erkentelijk voor hun inhoudelijke bijdrages aan dit rapport en houding tot samenwerken binnen het Kustgenese 2.0 programma.

Team Kustgenese 2.0,

November 2019

Universiteit Utrecht

TU Delft

Delft University of Technology

UNIVERSITY OF TWENTE.

Deltares

Enabling Delta Life

Rijkswaterstaat

Ministry of Infrastructure and Water Management

Deltares

Data report Kustgenese 2.0 measurements

Jebbe van der Werf
José Antonio Álvarez Antolínez
Laura Brakenhoff
Matthijs Gawehn
Kees den Heijer
Harry de Looff
Marcel van Maarsseveen
Harriëtte Meijer - Holzhauer
Jan-Willem Mol
Stuart Pearson
Bram van Prooijen
Giorgio Santinelli
Cor Schipper
Marion Tissier
Pieter Koen Tonnon
Lodewijk de Vet
Tommer Vermaas
Rinse Wilmink
Floris de Wit

Deltares

Title
Data report Kustgenese 2.0 measurements

Client	Project	Attribute	Pages
Rijkswaterstaat Water, Verkeer en Leefomgeving, UTRECHT	1220339-015	1220339-015-ZKS-0004	85

Nederlandse samenvatting
Rijkswaterstaat, Deltares en de partners van het STW SEAWAD onderzoeksproject, Technische Universiteit Delft, Universiteit Utrecht en Universiteit Twente, ontwikkelen in het programma Kustgenese 2.0 (KG2) kennis van het Nederlandse kustsysteem. Een belangrijk onderdeel is de grootschalige meetcampagne rondom het Amelander Zeegat en op de diepe onderwateroever van Ameland, Terschelling en Noordwijk in 2017-2018.

Dit datarapport bevat een beschrijving van de metingen, dataverwerking, kalibratie, en datakwaliteitscontroles en toont voorbeeldresultaten. De data-analyse komt niet aan bod.

De KG2 data is uniek, vanwege 1) het grote aantal meetlocaties, waaronder 14 verschillende framelocaties, 2) het groot aantal geavanceerde meetinstrumenten (20, waaronder 3D SONAR) en 3) de veelzijdigheid van de metingen zoals waterbeweging, zwevend stof, sedimentsamenstelling, bodemvormen, morfologie en macrobenthos.

Deze dataset zal helpen de waterbeweging en sedimenttransportprocessen in complexe kustsystemen, zoals zeegaten en buitendelta's, beter te begrijpen en te modelleren.

De data is publiekelijk beschikbaar via Waterinfo Extra, http://waterinfo-extra.rws.nl/, en het *4TU Centre for Research Data* via twee gedeeltelijk overlappende repositories: https://data.4tu.nl/repository/collection:kustgenese2 en https://data.4tu.nl/repository/collection:seawad.

Deltares

Title
Data report Kustgenese 2.0 measurements

Client	Project	Attribute	Pages
Rijkswaterstaat Water, Verkeer en Leefomgeving, UTRECHT	1220339-015	1220339-015-ZKS-0004	85

Keywords
Kustgenese 2.0, measurement campaign, Ameland Inlet, Dutch lower shoreface

Summary
Rijkswaterstaat, Deltares and the SEAWAD STW research project partners Delft University of Technology, Utrecht University and University of Twente work together in the framework of the Kustgenese 2.0 (KG2) programme to develop knowledge on the Dutch coastal system. The main source is formed by a large measurement campaign on the ebb-tidal delta of the Ameland Inlet and the lower shoreface offshore Ameland Inlet, Terschelling and Noordwijk, The Netherlands in 2017-2018.

This data report includes a description of this measurement campaign, data-processing, calibration, data-quality checks and illustrative example results. It does not include data-analysis results.

The KG2 data set is unique, because of 1) the large number of measuring locations, including 14 different frame positions, 2) the large number of advanced instrumentation (20 different devices, including 3D SONAR), and 3) the versatility of the measurements including hydrodynamics, suspended matter, sediment composition, bedforms, bed levels and macrobenthos.

This dataset will help to increase the understanding and modelling of fundamental processes over complex bathymetries under the combined influence of waves and tidal currents.

The data is publicly available at *Waterinfo Extra*, http://waterinfo-extra.rws.nl/, and at 4TU Centre for Research Data at two partly overlapping repositories: https://data.4tu.nl/repository/collection:kustgenese2 and https://data.4tu.nl/repository/collection:seawad.

Version	Date	Author	Initials	Review	Initials	Approval	Initials
1.	18 Jul 2019	Jebbe van der Werf		Bart Grasmeijer			
2.	1 Nov 2019	Jebbe van der Werf		Bart Grasmeijer			
3.	8 Nov 2019	Jebbe van der Werf		Bart Grasmeijer		Frank Hoozemans	

Status
final

Contents

1 Introduction

1.1 Background

The Dutch coastal policy aims for a safe, economically strong and attractive coast (Deltaprogramma, 2015). This is achieved by maintaining the part of the coast that supports these functions; the coastal foundation. The offshore boundary of the coastal foundation is taken at the NAP -20 m depth contour, the onshore limit is formed by the landward edge of the dune area (closed coast) and by the tidal inlets (open coast). The borders with Belgium and Germany are the lateral boundaries. The coastal foundation is maintained by means of sand nourishments; the total nourishment volume is about 12 million m^3/year since 2000.

In 2020 the Dutch Ministry of Infrastructure and Environment will make a new decision about the nourishment volume. The Kustgenese-2 (KG2) programme is aimed to deliver knowledge to enable this decision making. The scope of the KG2 project, commissioned by Rijkswaterstaat to Deltares, is determined by three main questions:

1 What are possibilities for an alternative offshore boundary of the coastal foundation?
2 How much sediment is required for the coastal foundation to grow with sea level rise?
3 What are the possibilities for large scale nourishments along the interrupted coastline (inlets), and what could be the added value compared to regular nourishments?

The KG2 project cooperates with the SEAWAD STW research project by Delft University of Technology, Utrecht University and University of Twente. SEAWAD develops the system knowledge and tools to predict the effects of mega-nourishments on the Ameland ebb-tidal delta on morphology and ecology (benthos distribution).

The main source of these studies is formed by a large measurement campaign at the Ameland Inlet and Ameland, Terschelling and Noordwijk lower shorefaces in 2017-2018.

1.2 Objective and scope

This report aims to describe the measurements and the datasets of the complete KG2 measurement campaign.

It serves as a data user manual which is publicly available at Water Info Extra, http://waterinfo-extra.rws.nl/, and at the 4TU Centre for Research Data at two partly overlapping repositories: https://data.4tu.nl/repository/collection:kustgenese2 and https://data.4tu.nl/repository/collection:seawad. The data is also published in the journal paper of Van Prooijen et al. (in prep).

The report includes a description of the measurements campaign, data-processing, calibration, data-quality checks and illustrative example results. It does not include data-analysis results.

1.3 Outline report

Chapter 0 describes the measurement campaign, including practical considerations. The steps from raw to processed data are discussed in Chapter 0. Chapter 4 presents example measurement results. Finally, Chapter 5 summarizes the report.

1.4 Author contributions

This report is the product of collaboration between Rijkswaterstaat, SEAWAD and Deltares. A number of people from these organisations have contributed to the report, which is reflected in the list of authors. The report was edited by Jebbe van der Werf (Deltares).

2 KG2 measurement campaign

2.1 Introduction

The objective of the KG2 measurement campaign is to deliver hydrodynamic, sediment, morphological and ecological data of the Dutch lower shoreface and Ameland Inlet to develop system knowledge and modelling tools to support the Rijkswaterstaat advise on i) the seaward boundary of the Coastal Foundation, ii) the total nourishment volume, iii) the feasibility of nourishing the Wadden Sea ebb-tidal delta.

The Ameland Inlet, between barrier islands Terschelling and Ameland, was chosen as one of the main study areas (Figure 2.1). The reason for this choice is that this inlet shows a more natural morphodynamic behaviour than other inlets, and that field measurements were performed here during previous projects (within the SBW project, see Aqua Vision, 2008, 2012).

The lower shoreface measurements were carried out offshore Ameland Inlet, Terschelling and Noordwijk (Figure 2.1). The lower shoreface, with water depths between ~8 and ~20 m, is the zone with mixed action of waves and currents. These locations cover the diversity of the Dutch lower shoreface and link to existing and ongoing field work. More details on the choice for these three lower shoreface locations can be found in Van der Werf et al. (2017).

Table 2.1 presents the general time line of the KG2 measurement campaign. Details will follow in the sections below.

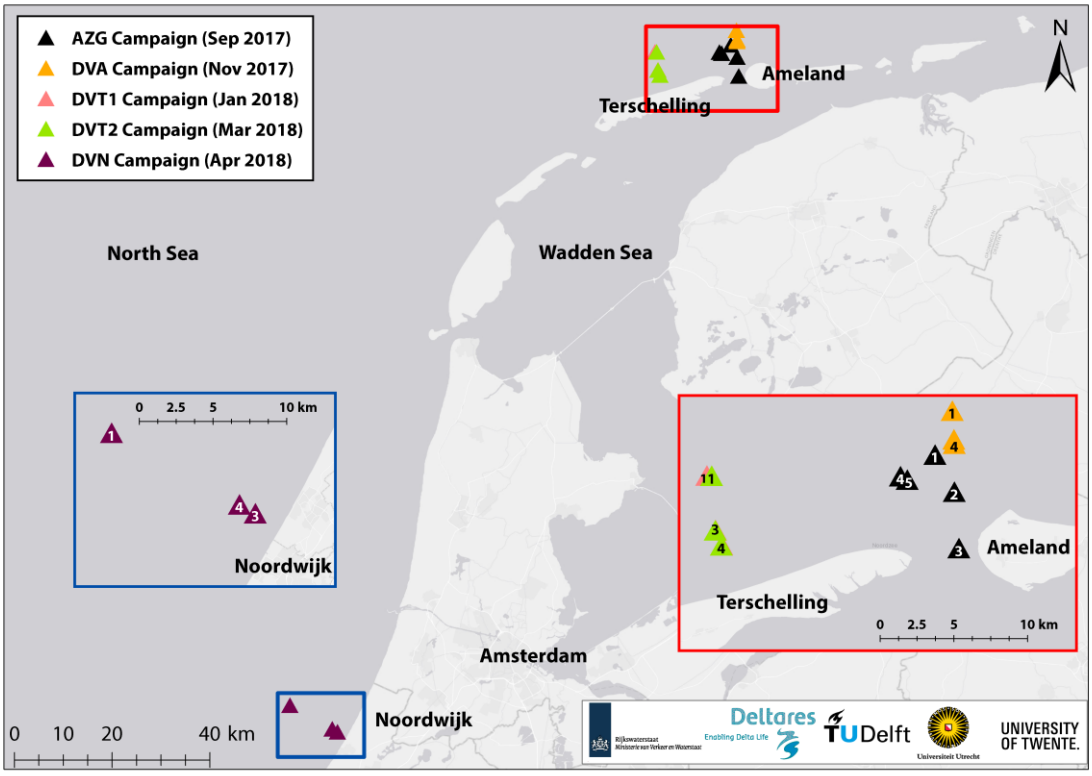

Figure 2.1 Overview of the five frame measurement campaigns carried out in the Kustgenese 2.0 project at the four study sites: Ameland Inlet (AZG), and the lower shorefaces of Ameland (DVA), Terschelling (DVT) and

Noordwijk (DVN). Note that DVA frame 3 is located very close to DVA frame 4 and is hidden behind it. Frames for DVT campaigns 1 and 2 were placed in approximately the same positions, so their marker symbols overlap.

Table 2.1 General time line of the KG2 measurement campaign. AZG = Amelander Zeegat (Ameland Inlet), DV = Diepe Vooroever (Lower Shoreface), DVA/DVT/DVN refer to the lower shoreface measurements offshore Ameland, Terschelling and Noordwijk. "2019" refers to measurements carried out in and beyond 2019.

Campaign	**Measurement**	**2016**	**2017**				**2018**				**2019**
			Q1	Q2	Q3	Q4	Q1	Q2	Q3	Q4	
General	Wave buoys										
AZG	Frames										
	ADC transects										
	Pressures sensors										
	Watersheds										
	Drifters										
	Tracers										
	XBand radar										
	Single-beam										
	Multi-beam										
	Survey pilot nourishment										
	Box cores										
	Fish										
DV	Frames					DVA	DVT	DVN			
	Vibrocores										
	Boxcores										
	Multibeam										

2.2 Measurement frames

Frame measurements were carried out during five campaigns at Ameland Inlet (AZG), Ameland lower shoreface (DVA), Terschelling lower shoreface (DVT1, DVT2) and Noordwijk lower shoreface (DVN). Locations and deployment times can be found in Figure 2.1 and Table 2.2.

Four frames (Frames 1, 2, 3 and 4) were constructed specifically for this campaign in order to house the required scientific instruments (Figure 2.2). The 2.4 m high stainless-steel frames were initially built for the AZG campaign and then the physical structures were reused for subsequent campaigns. However, not all instruments were used in each campaign due to lack of availability for instruments shared by partner institutions. A fifth frame (Frame 5) was also used for the AZG campaign. This frame, belonging to Utrecht University, was the prototype of the other frames, but made from steel (not stainless). Frame 2 was only used during the AZG campaign, since it became irretrievably buried by sand during a large storm.

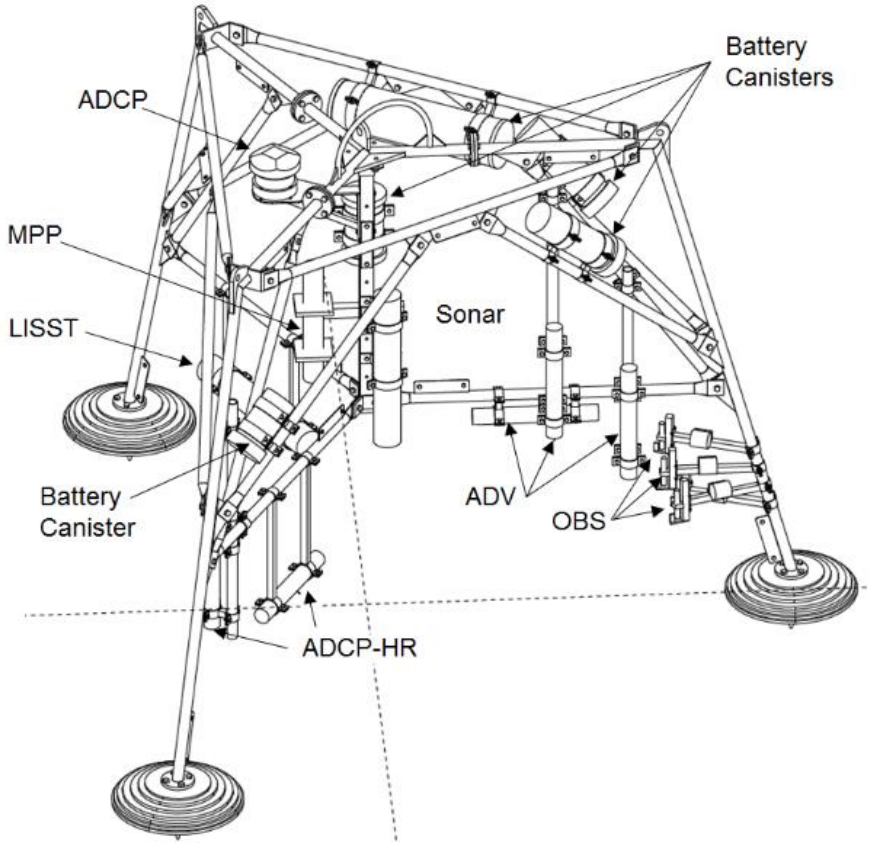

Figure 2.2 Design of the measurement frames used during the KG2 field campaigns. Each 2.4 m high stainless-steel frame was mounted with up to 14 instruments and their accompanying battery packs. This drawing indicates Frame 4 from the AZG campaign; not all instruments shown here were present on all other frames.

Table 2.2 Overview of frame locations and deployment times for all frames on all campaigns.

Campaign	Frame	Begin time	End time	Lat [°]	Lon [°]	Approx. depth (to m NAP)
AZG	1	30/08/2017 10:11	09/10/2017 15:20	53.50	5.57	8
	2	30/08/2017 16:38	N/A[1]	53.48	5.59	9
	3	30/08/2017 15:37	10/10/2017 07:10	53.44	5.59	20
	4	29/08/2017 15:55	09/10/2017 15:50	53.49	5.54	5
	5	29/08/2017 15:28	09/10/2017 16:45	53.49	5.54	4
DVA	1	08/11/2017 13:00	11/12/2017 13:15	53.53	5.59	20
	3	08/11/2017 11:00	11/12/2017 14:15	53.51	5.59	16
	4	08/11/2017 10:30	11/12/2017 15:00	53.51	5.59	10
DVT1	1	11/01/2018 12:20	06/02/2018 09:30	53.49	5.34	20
	3	11/01/2018 14:00	06/02/2018 10:30	53.45	5.35	14
	4	11/01/2018 15:15	06/02/2018 11:30	53.45	5.35	10
DVT2	1	12/03/2018 16:00	26/03/2018 10:10	53.49	5.34	20
	3	12/03/2018 19:50	26/03/2018 13:40	53.45	5.35	14
	4	12/03/2018 17:50	26/03/2018 12:40	53.45	5.35	10
DVN	1	04/04/2018 12:15	15/05/2018 13:30	52.28	4.24	20
	3	04/04/2018 14:10	15/05/2018 17:00	52.23	4.39	12
	4	04/04/2018 13:40	15/05/2018 14:50	52.24	4.37	16

[1] *irretrievably buried during a large storm*

Table 2.3 presents an instrument overview per measurement campaign.

Hydrodynamics measurements were carried out using upward- and downward-looking Acoustic Doppler Current Profilers (ADCPs). The near-bed flow was measured using a downward looking high-resolution (HR) ADCP (also known as AquaDopp) and three Acoustic Doppler Velocimeters (ADVs) at ~0.35, 0.65 m and 0.9 m above the bed (low, middle, high). For Frame 4 on the DVT and DVN campaigns, a downward-looking (non-HR) ADCP was used to measure near-bed velocity profiles. To measure suspended sediment concentrations, a Laser In-Situ Scattering and Transmissometer (LISST), a Multi-parameter probe (MPP) and 4 Optical Backscatter Sensors (OBS) at ~0.2, 0.3, 0.5, 0.8 m above the bed, were used. The MPP was also capable of measuring salinity, temperature, and other key water quality parameters. Frame 5 contained an additional array of 4 OBSs between ~0.1 and 0.25 m above the bed and a separate pressure sensor. Changes in the seabed below the frame were monitored using a 3D Sonar.

More specifications of the instruments per frame can be found in Appendix A.

Table 2.3 Instrument overview per campaign. ● = instrument is present on site; instrument is fully-working and processed data is usable. ● = instrument is present on site; instrument is partially working and/or processed data is partially useable. ○ = instrument is present on site; instrument is not working and/or processed data is not useable.

Instrument	**AZG frames**				**DVA frames**			**DVT1 frames**			**DVT2 frames**			**DVN frames**		
	1	**3**	**4**	**5**	**1**	**3**	**4**	**1**	**3**	**4**	**1**	**3**	**4**	**1**	**3**	**4**
ADCP upward	●	●	●	●	●	●	●	●	●	●	●	●	●	●	●	●
ADCP downward							●			●			●			●
ADCP HR	●	●	●	●	●	●	○	○	●	○	●	●	○	●	●	○
ADV low	●	●	●	○	●	●		●	○		○	○		●	○	
ADV middle	●	●	●	○	●	●		●	●		●	●		●	●	
ADV high			○	○												
LISST		●	●	○	○	●		○	●		○	●		○	●	
MPP	●	●	●	●	●	●	●	●	●	●	●	●	●	●	●	●
OBS low	●	●	●	○	●	●		●	●		●	●		●	●	
OBS middle 1	●	●	●		●	●		●	●		●	●		●	●	
OBS middle 2	●	●	●	○	●	●		●	●		●	●		●	●	
OBS high	●	●	●	○	●	●		●	●		●	●		●	●	
OBS array (4x)				○												
SONAR	●	●	●	●	●	●	●	●	○	●	●		●	●	○	

Table 2.3 distinguishes between fully-, partially- and not-working instruments. Data from not-working instruments are unusable; data from partially-working instruments have quality issues or parts of the data are missing.

Below we briefly discuss the rationale behind the data-quality flags; more details on data-quality can be found in Chapters 0 and 4, and Appendix D:

- The AZG upward ADCP data were flagged as “partially-working”, except for Frame 4, because before servicing these ADCPs were not equipped with pressure sensors to determine the water surface elevation.
- The data from the upward ADCP on DVT1 Frame 3 and DVN Frame 1 were flagged as “partially-working”, because of issues with directions (see Appendix D).

- The DVN-F3 upward ADCP data stopped at 21st of April 2018, which is more than 3 weeks before the end of the frame deployment.
- The DVN-F4 upward ADCP data is flagged as “partially-working”, as pressure measurements were not successful.
- The information of the heading, pitch and roll were missing for the ADCP-HR on DVA Frame 4, DVT1 Frames 1 and 4, DVT2 Frame 4 and DVN Frame 4 such that the East-North-Up (ENU) velocities could not be computed.
- The data from the ADCP-HR on AZG Frame 5 was flagged as “partially-working”, because of issues with directions (see Appendix D).
- The ADV’s on AZG Frames 1 and 3 unexplainably did not measure for 1-2 weeks.
- The head of the lowest ADV on AZG Frame 4 was broken during the retrieval of the frame.
- The lowest and middle ADV on AZG Frame 4 were flagged as “partially-working”, because of issues with directions (see Appendix D).
- The highest ADV on AZG Frame 4 has not been processed yet (see Appendix D). This will be done at a later stage.
- The ADV and OBS data on AZG Frame 5 have not been processed yet, because the file structure is different from the ADV- and OBS-files on the other frames. This will be done at a later stage.
- The information of the heading, pitch and roll were missing for the ADV low on DVT1 Frame 3, DVT2 Frame 3 and DVN Frame 3 such that the ENU-velocities could not be computed.
- There was no raw data file available for ADV low on DVT2 Frame 1.
- The LISST mounted on Frame 5 during the AZG campaign and Frame 1 during subsequent campaigns (LIS03) experienced a serious, unexplained malfunction, and did not produce usable data for any of the measurement periods (see Section 3.8).
- The MPP quality flags were based on whether there was a time series containing data within the normal operating range for each of the main variables measured. Instruments without measured time series for all variables were flagged as incomplete (see also Section 3.9).
- The relation between measured OBS voltages and suspended sediment concentrations is not clear, and therefore only the voltages are stored (see Section 3.10).
- The data from SONAR AZG-F1 and DVA-F4 is of poor quality for large part of the measurement period. The SONAR on DVA-F3, DVT1-F4 and DVT2-F4 has a lot of missing data. The SONAR on DVT2-F3 and DVN-F3 did not record data (see also Section 3.13).

2.3 Ameland Inlet campaign

The Ameland Inlet (Amelander Zeegat or AZG) campaign was the first to be carried out as part of the Kustgenese 2.0 project. Spanning a large area in and around the islands of Ameland and Terschelling (Figure 2.3), the campaign took place from August to October 2017. This location was of particular interest as it was the site of a planned pilot nourishment project set to take place in 2018. Hence, the AZG campaign served as a baseline or “T0” measurement of the natural system’s characteristics prior to intervention.

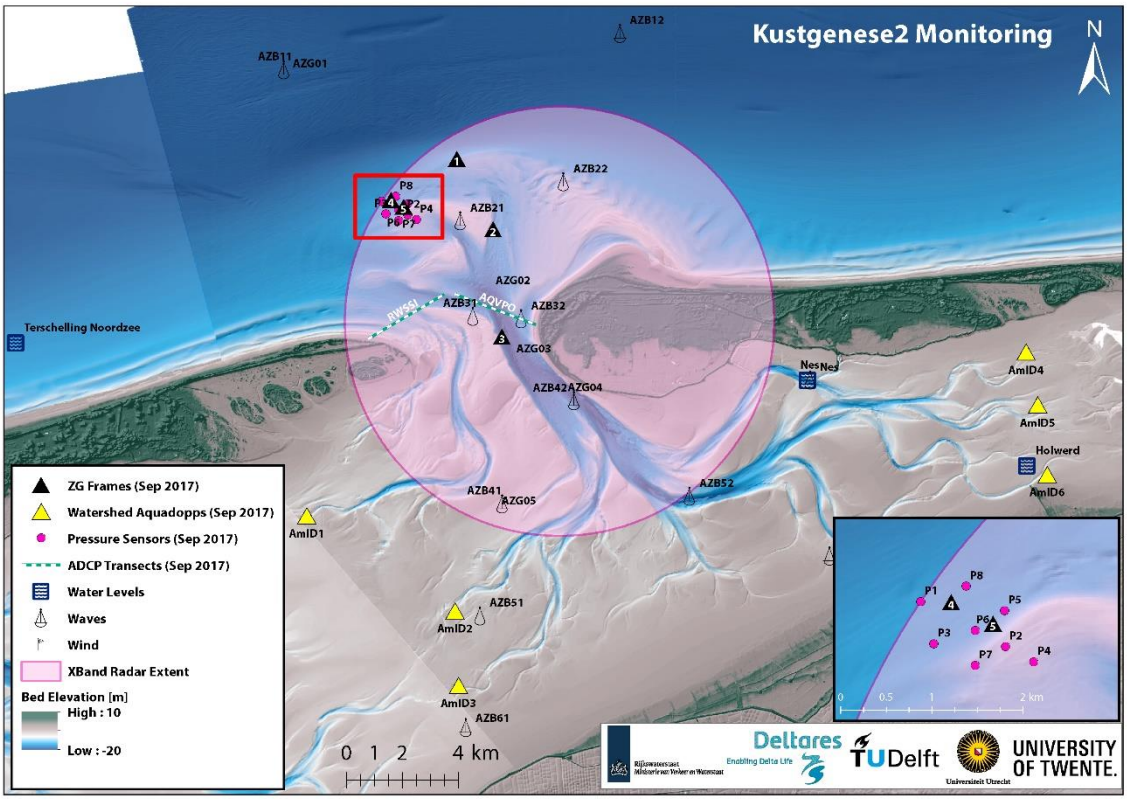

Figure 2.3 Overview of the Ameland Inlet (AZG) campaign, which took place in September 2017. Markers indicate the type and location of the different measurements carried out as part of the fieldwork. The inset map encompasses the location of the planned sand nourishment, which was also the area most intensely investigated. This figure also includes locations of previous wave height measurements carried out in the SBW project, and location of standard water level and wind stations.

This section is intended to shed light on the considerations behind the locations and placement of the frames and instruments used in the AZG Campaign. A range of measurements has been conducted.

Measurement frames

- Frame 1 was placed at the North end of the main ebb channel on the distal lobe of ebb-tidal delta.
- Frame 2 was placed in the middle of main ebb channel on its west bank. It was intended to form a direct line out of the inlet with Frames 1 and 3, and in doing so provide understanding of the flow and transport in the ebb-channel. Recent bathymetric surveys show this area to be highly dynamic, as the channel rotates clockwise with the eastward migration of the north-western ebb shoal (Elias et al., 2018).
- Frame 3 was placed along the west bank of Borndiep (primary inlet channel) in deep water (15-20 m). The results from this frame should provide insights in the dynamics (hydrodynamics and sediment dynamics) in the channel.
- Frame 4 was placed on the site of the planned pilot nourishment in water 8 m deep. This location was chosen to measure waves approaching the ebb-tidal delta from the NW and interacting with currents from the ebb channel. The nearby north-western ebb shoal is rapidly prograding and migrating; recent bathymetric surveys show this area to be highly dynamic (Elias et al., 2018).

- Frame 5 was also located on the site of the planned pilot nourishment at a depth of 5 m. It was intended to complement the measurements of Frame 4, aligned with it in an approximately NW/SE axis. This transect is in line with a major ebb channel. The frame is also shallow enough to be exposed to breaking waves in energetic conditions. Recent bathymetric surveys show this area to be highly dynamic.

Frames 1-3 were meant to be aligned with the main tidal channel. The final locations deviated somewhat from the design, to deal with local water depts and wave height to make deployment feasible for the vessels *Terschelling* and *Schuitengat.*

Unfortunately, Frame 2 was irretrievably buried in a large storm. Placed in the main ebb channel, it was rapidly buried under several metres of sand as the channel rotated and the north-western shoal migrated eastwards. Several attempts were made to excavate it in calmer weather, but these were until now unsuccessful, so the data from its instruments are likely lost.

ADCP transects
To monitor the incoming and outgoing water fluxes, 13-hours continuous ADCP transects were measured across the Ameland Inlet on 1, 5, 18 and 19 September 2017. On September 18 Section D was sailed, and on the other dates Section A-C (see Figure 2.5).

Water samples
The acoustic backscatter from ADCP signals can be used to estimate suspended matter concentrations. To convert the acoustic backscatter into a mass concentration of suspended sediment, it is necessary to calibrate using water samples. 198 water samples were obtained during the 13-hour ADCP transect measurements across the inlet on September 1st and 5th, 2017. Simultaneous in-situ readings of conductivity, depth, temperature, and turbidity were taken with a YSI 600 to provide context for the physical samples. Sample depths ranged from near-surface (0.72 m) to the deeper parts of the Borndiep channel (21.95 m).

Additional water samples were taken at the measurement frames. These were not processed in the laboratory as a result of being unsuitable for calibrating the OBS sensors. Instead, sediment from the bed was used for this purpose (Section 3.10).

Pressure sensors and wave buoys
The standalone pressure sensors were aligned in an approximately NW/SE axis with Frame 4/5 (Figure 2.3 inset, Table 2.4) to be in line with the ebb channel and main wave direction, in order to measure wave transformation along a transect. This configuration allows for the determination of gradients in wave characteristics over the topography. Note that the pressure was also measured by instruments on the frames. These measurements were supplemented by a series of wave buoys located throughout the inlet area.

Table 2.4 Pressure sensor locations, depths, and time series durations.

Sensor	Begin date and time	End date and time	Latitude [º]	Longitude [º]	Depth [m]
1	29/08/2017 08:30	08/10/2017 00:00	53.489000	5.530468	10.0
2	29/08/2017 13:30	08/10/2017 00:00	53.484550	5.544500	4.2
3	29/08/2017 09:00	08/10/2017 00:00	53.484843	5.532633	7.8
4	29/08/2017 13:30	08/10/2017 00:00	53.483052	5.549125	4.3
5	29/08/2017 11:00	08/10/2017 00:00	53.488092	5.544327	7.5
7	29/08/2017 12:30	08/10/2017 00:00	53.482702	5.539460	4.9
8	29/08/2017 10:30	08/10/2017 00:00	53.490500	5.537975	9.1

Watersheds

Three ADCPs-HR were placed on each watershed with the intent to observe inter-basin flows and test previous modelled theories about the role of wind-driven flow in the Wadden Sea (e.g. Duran-Matute and Gerkema, 2015). The instruments were intended to be placed at locations where small channels crossed the watersheds such that they were submerged most of the time (the target was a 90% submergence threshold), and also because these areas are where primary flows are conveyed. For practical reasons, i.e. the accessibility by boat or foot, the instrument locations were sometimes moved. AmID4 (Figure 2.3) was placed on foot at low tide on September 1st 2017, but the rest were placed via boat at high tide between August 30th-31st, recording until approximately October 2 (Table 2.5).

Table 2.5 Watershed ADCP-HR locations, sensor elevations with respect to NAP, and time series durations.

Sensor	Begin date and time	End date and time	Latitude [º]	Longitude [º]	Elev [m NAP]
AmID1	31/08/2017 00:00	03/10/2017 17:38	53.386881	5.489669	-0.74
AmID2	31/08/2017 00:00	03/10/2017 18:06	53.356310	5.569010	-0.60
AmID3	31/08/2017 00:00	03/10/2017 19:28	53.332295	5.570845	-0.35
AmID4	30/08/2017 00:00	03/10/2017 18:50	53.438537	5.876507	-0.71
AmID5	30/08/2017 00:00	03/10/2017 18:34	53.421485	5.882596	N/A[2]
AmID6	30/08/2017 00:00	03/10/2017 16:14	53.399147	5.887491	-0.40

Drifter Experiments

Lagrangian drifter experiments were carried out with the intention of observing spatial variations in flow patterns at the site of the planned nourishment. The main experiments were conducted in the area surrounding Frame 4/5 and pressure sensors (Figure 2.3). In addition, a single large-scale experiment was conducted around the entire inlet over course of a single tidal cycle to better understand large-scale circulation patterns and flow pathways. Details are given in Table 2.6.

[2] *No GPS was recorded for this point, and the position is based only on the proposed location.*

Table 2.6 Details for all drifter deployments during the AZG campaign.

Date and time	Deployments	Tide	# Drifters	# Deployments
01/09/2017 13:00-17:00	Small scale	Flood	20	5
02/09/2017 14:00-19:00	Small scale	Flood	30	8
03/09/2017 09:00-13:00	Small scale	Ebb	30	7
04/09/2017 09:30-15:30	Small scale	Ebb	30	9
05/09/2017 11:00-15:00	Small scale	Ebb	30	6
09/09/2017 08:00-17:00	Small scale	Ebb and flood	20	15
09/09/2017 08:30-18:00	Large scale	Ebb and flood	10	1

Tracer Study

A sediment tracer study was conducted in the area between Frames 4 and 5 (Figure 2.9), which corresponds to the planned nourishment location that was heavily monitored. The tracer study was intended to provide a prediction of potential pathways for nourished sediment. The tracer was initially deployed on August 29th, 2017, then sampled intensively for the following week. Several additional samples were taken during servicing and retrieval of the measurement frames, up until October 9th, 2017.

XBand radar

An XBand radar unit mounted in the lighthouse at Ameland's tip was used for remotely and continuously sensing both hydrodynamic and bathymetric changes in the inlet (Gawehn, 2018; in prep). The extent of the measured area is visualized in Figure 2.3.

Single beam bed surveys

Within the Kustgenese 2.0 project, half-yearly single beam bed surveys of the ebb tidal delta of Ameland inlet were (will be) carried out by Rijkswaterstaat between fall 2016 and spring 2020 (Figure 2.4, Table 2.7). These measurements are similar to those carried out within the regular MWTL 'Vaklodingen' survey program by Rijkswaterstaat. In the 'Vaklodingen' program, the ebb-tidal delta and adjacent island coasts of the Wadden Sea are surveyed every 3 years, while the basins are surveyed every 6 years. Note that in the MWLT program, the nearshore area is measured separately every year in spring within the JARKUS program. The end result of the regular 'Vaklodingen' program is the combined data of the ebb-tidal delta and the nearshore area, interpolated to a 20x20 m grid.

Note that the spring 2017 and spring 2020 bed surveys were carried out within the regular 'Vaklodingen' survey program and thus cover a larger domain compared to the Kustgenese 2.0 surveys and are also not part of the Kustgenese 2.0 data set. Between 2007 and 2010, additional bed surveys were carried of the ebb-tidal delta and main channels of Ameland basin within the SBW project (Zijderveld & Peters, 2008).

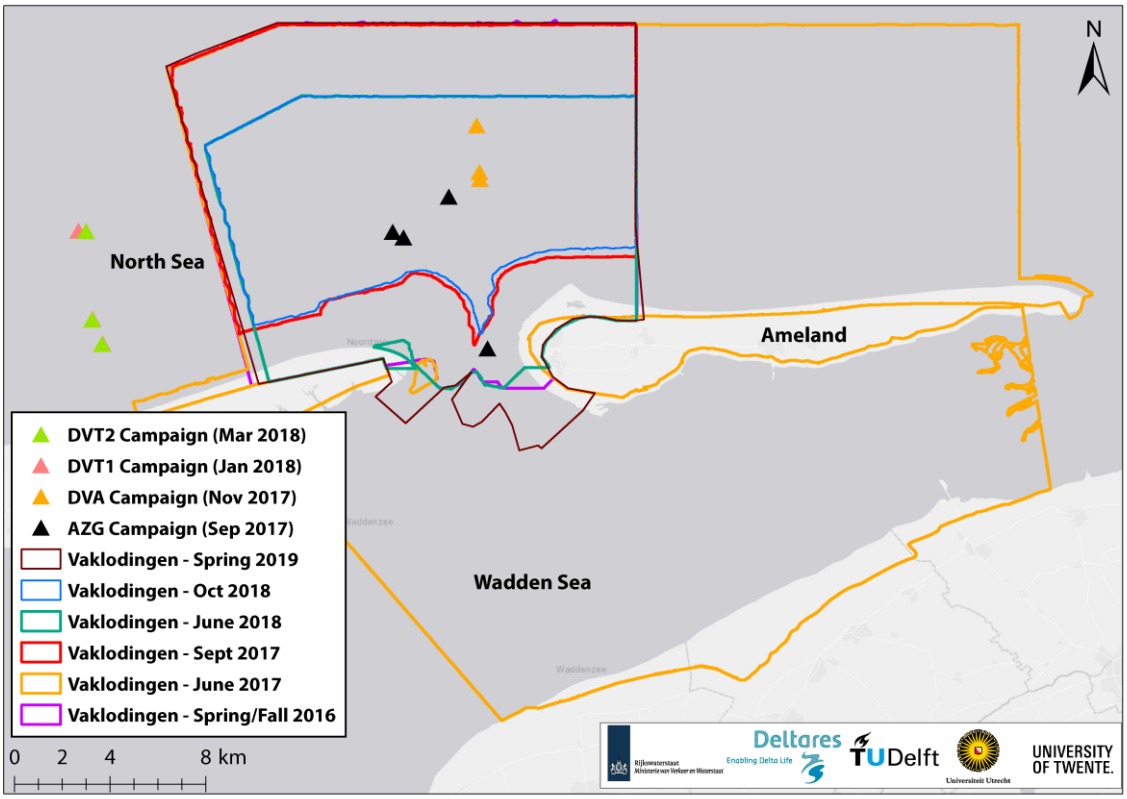

Figure 2.4 Overview of KG2 AZG Vaklodingen bathymetric measurements.

Table 2.7 Overview of data sources for resulting, half-yearly gridded bathymetric files. Note that the fall data is composed of measurements from fall for the ebb tidal delta and from spring of that year for the nearshore zone. At the time of writing of this report bathymetries for 2016, 2017 and 2018 were available.

Period	Data ebb tidal delta	Data island coasts	Project
2016, spring	-	Jarkus transects for coast of Terschelling and Ameland	
2016, fall	Singlebeam survey of the ebb tidal delta of Ameland inlet		Kustgenese 2.0
2017, spring	Singlebeam survey of the ebb tidal delta of Ameland inlet	Jarkus transects for coast of Terschelling and Ameland	regular MWTL 'Vakloding'
2017, fall	Singlebeam survey of the ebb tidal delta of Ameland inlet		Kustgenese 2.0
2018, spring	Singlebeam survey of the ebb tidal delta of Ameland inlet	Jarkus transects for coast of Terschelling and Ameland	Kustgenese 2.0
2018, fall	Singlebeam survey of the ebb tidal delta of Ameland inlet		Kustgenese 2.0
2019, spring	Singlebeam survey of the ebb tidal delta of Ameland inlet	Jarkus transects for coast of Terschelling and Ameland	Kustgenese 2.0
2019, fall	Singlebeam survey of the ebb tidal delta of Ameland inlet		Kustgenese 2.0
2020, spring	Singlebeam survey of the ebb tidal delta of Ameland inlet	Jarkus transects for coast of Terschelling and Ameland	regular MWTL 'Vakloding'

Multi beam bed surveys

Within Kustgenese 2.0, high-resolution multi beam data was measured along 4 transects or areas, at several intervals, see (Figure 2.5, Table 2.8). These data can be subdivided in 3 categories:

1 Measurements of the Sections A, B and C (5-6 surveys).
2 Repeat surveys of bed forms through the tidal cycle in Section D on 07-09-2017.
3 In addition to the Sections A-D, the direct surroundings of the measurement frames were measured before and after deployment of the frames.

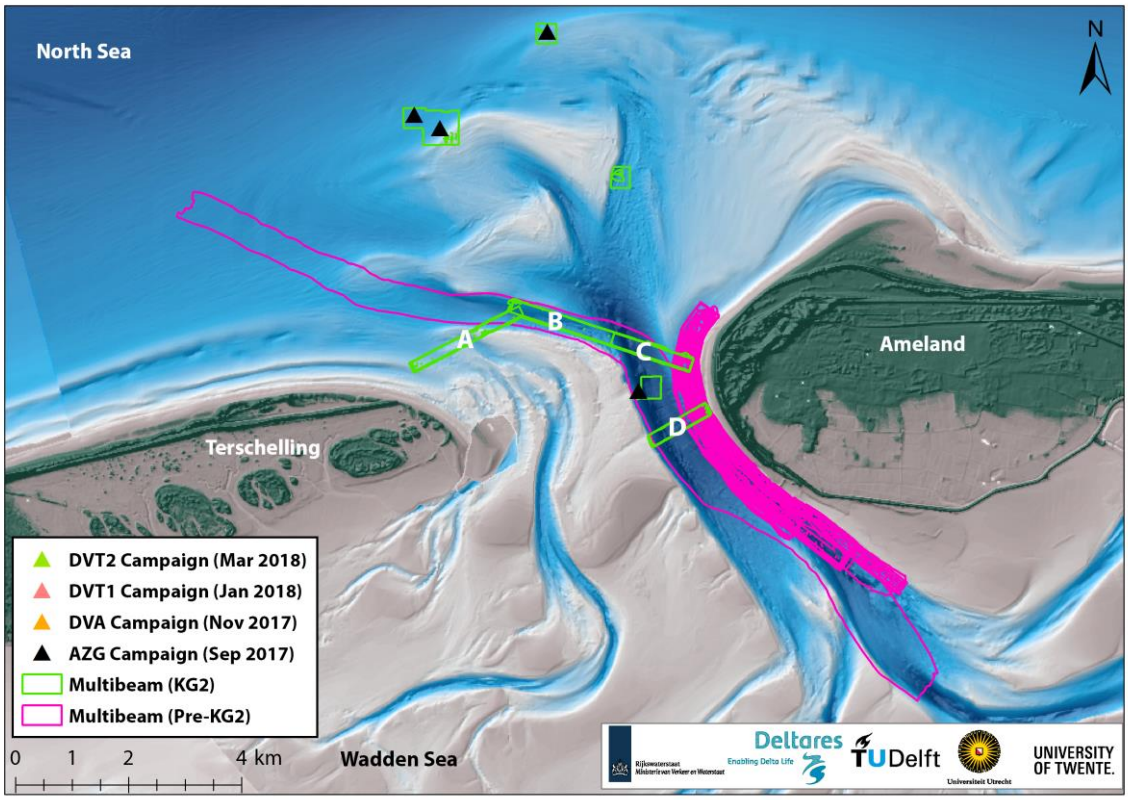

Figure 2.5 Overview of KG2 AZG multibeam measurements. ADCP transect measured were carried out along Sections A, B C and D to determined water fluxes.

Table 2.8 Multibeam measurement periods Ameland Inlet Sections A-D.

Section A	Section B	Section C	Section D
30-08-2017	30-08-2017	30-08-2017	07-09-2017 7:54 - 8:26
31-08-2017	31-08-2017	31-08-2017	07-09-2017 8:36 - 9:27
02-09-2017	02-09-2017	03-09-2017	07-09-2017 9:37 - 10:17
03-09-2017	04-09-2017	04-09-2017	07-09-2017 10:24 - 11:08
04-09-2017	06-09-2017	06-09-2017	07-09-2017 11:13 - 11:52
06-09-2017			07-09-2017 11:57 - 12:31
			07-09-2017 12:37 - 13:14
			07-09-2017 13:18 - 14:13
			07-09-2017 14:15 - 14:55

Bathymetric surveys pilot nourishment Ameland ebb-tidal delta
From March 2018 till February 2019 a pilot nourishment of 5 million m^3 was put in place at the Ameland ebb-tidal delta. The nourishment contour is shown in Figure 2.6.

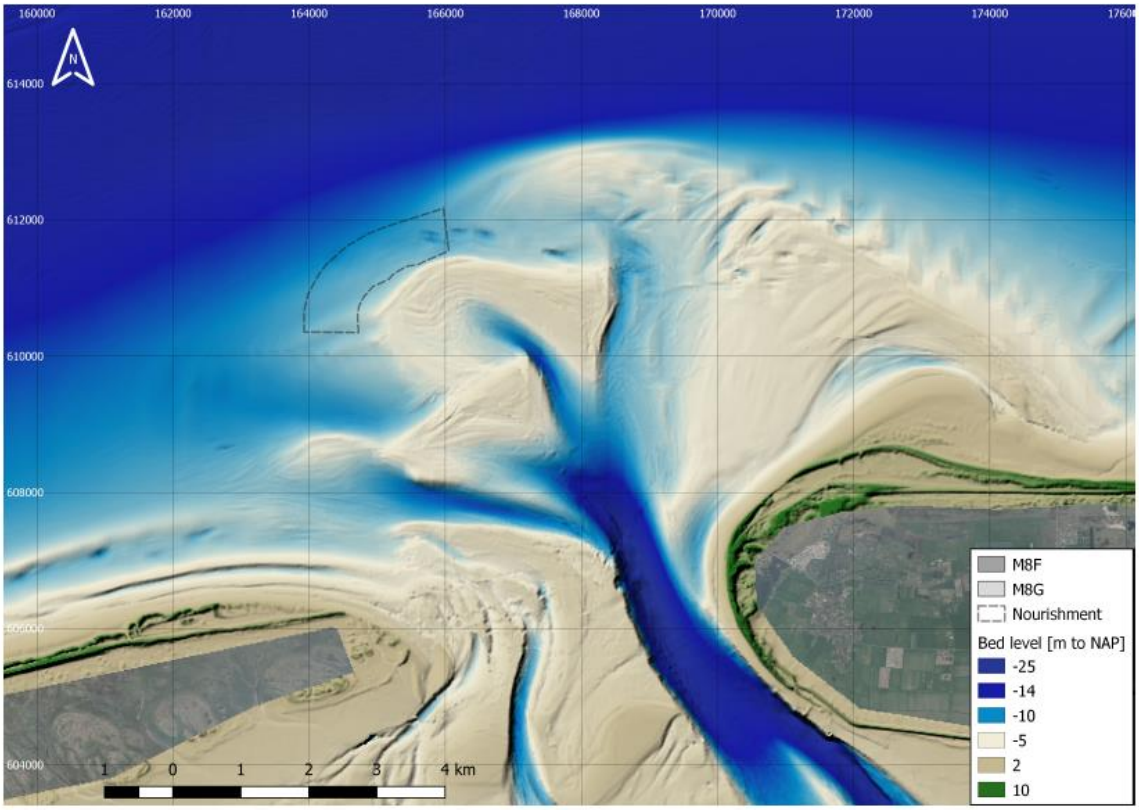

Figure 2.6 Location of the pilot nourishment (dashed contours) on the Ameland ebb-tidal delta. The bathymetry is from fall 2017.

Before and during the execution phase of the nourishment, 10 bathymetric surveys were conducted in the nourishment area and a 500 – 1000 m contour around that area. Figure 2.7 shows the outline of survey #0 (directly before start of the nourishment). The same area will be surveyed every three months from May 2019 until February 2021. Table 2.9 gives an overview of the begin and end dates of the surveys.

Surveys are conducted using both singlebeam and multibeam, see for example Figure 2.8. The survey before nourishment construction (#0) was entirely measured with multibeam echo sounder equipment. This required a large time window with relatively good weather conditions as the transects needed to be sailed close to each other. As the first survey took too long to be completed in this time window it was decided to optimize the survey plan for subsequent measurements. Depending on weather conditions, the multibeam measurements cover the entire nourishment area or are limited to the edges of it and the recent depositional areas. The shallow parts of the ebb delta will be measured using singlebeam, with transects relatively close to each other. The entire seaward side of the nourishment is sailed with 100 m-spaced transects.

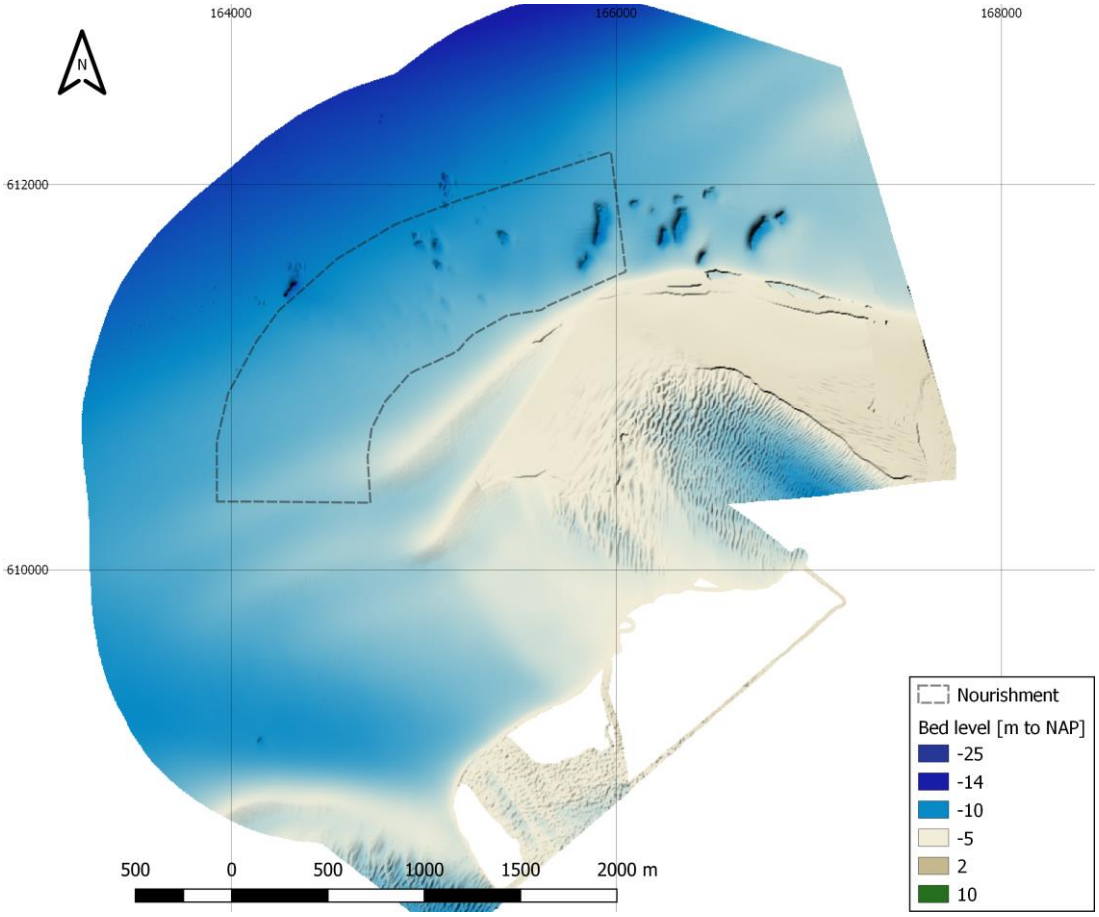

Figure 2.7 Outline of bathymetric survey #0, directly before the start of the nourishment.

Table 2.9 Overview of bathymetric surveys (to be) conducted in the area of the pilot nourishment Ameland ebb-tidal delta. The end date of survey #10 is unknown.

Survey number	Date	Remark
0	8 Feb – 29 Mar 2018	before nourishment construction, entirely with multibeam
1	7 Apr – 2 May 2018	uncomplete due to weather conditions
2	1 – 8 June 2018	
3	15 Jun – 6 Jul 2018	
4	23 Jul – 7 Aug 2018	
5	7 – 27 Sep 2018	
6	8 – 19 Oct 2018	
7	5 Nov – 18 Dec 2018	uncomplete due to weather conditions
8	20 – 24 Jan 2019	
9	20 – 28 Feb 2019	first survey after nourishment construction
10	19 – 22 June 2019	
11	Aug 2019	
12	Nov 2019	
13	Feb 2020	
14	May 2020	
15	Aug 2020	
16	Nov 2020	
17	Feb 2021	

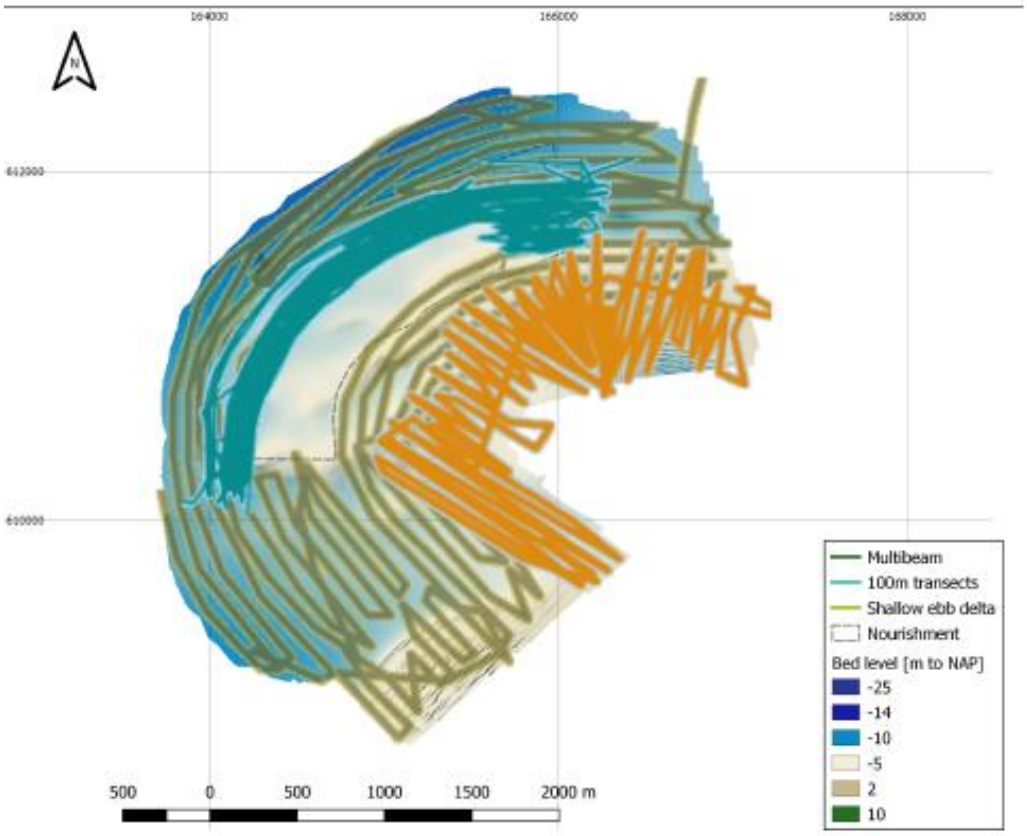

Figure B.1: Survey tracks during survey 8.

Figure 2.8 Singlebeam and multibeam tracks of survey #8.

Boxcores

To determine seabed sediment composition and benthic ecological communities, boxcores were taken across the inlet and ebb-tidal delta. The locations were chosen based on a series of morphological units (16), defined by depth, slope, orientation and morphological activity (Holzhauer, 2017). In such a way, morphologically representative coverage of the entire site was obtained, using a relatively limited (165) number of cores (Figure 2.9). Sampling of shallower locations took place from September 4th-5th, and deeper locations from 20th-21st, 2017. The second survey with 55 samples took place on 24 March 2018.

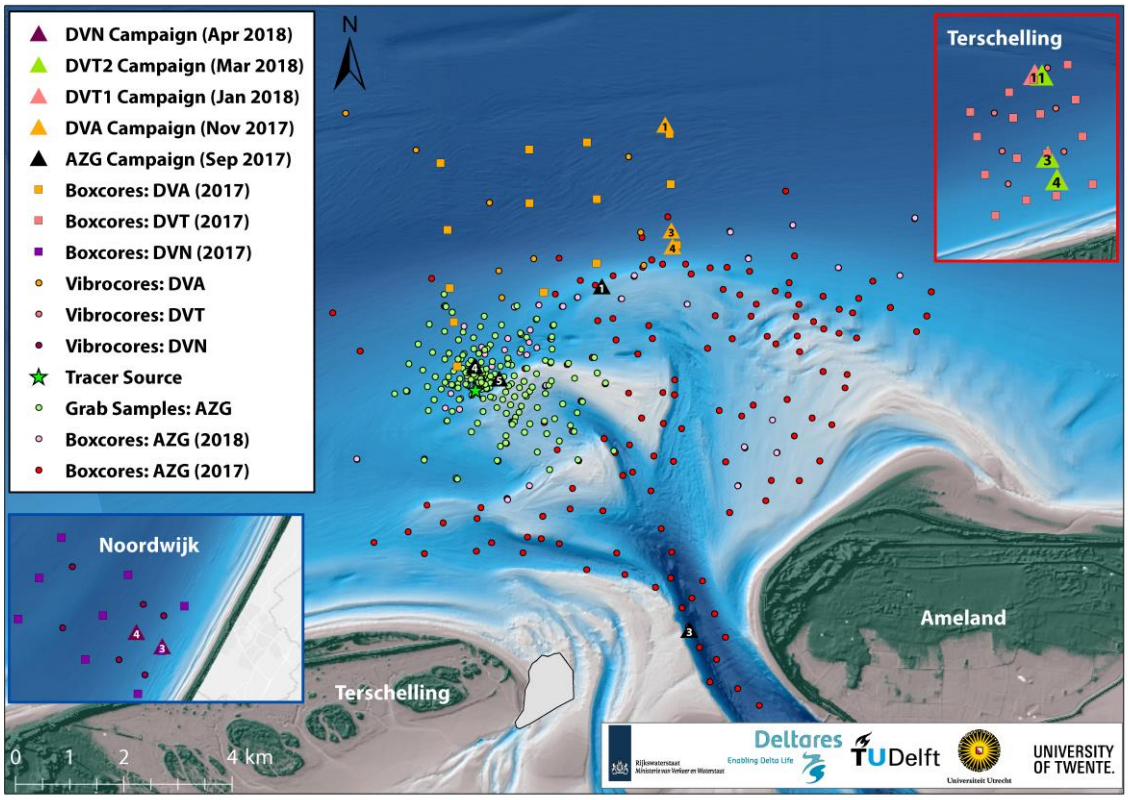

Figure 2.9 Overview of sediment samples taken during Kustgenese 2.0 campaign. The majority of samples were taken as part of the AZG campaign (grab samples and boxcores), and vibrocores were taken as part of each DV campaign. The deployment site for the sediment tracer used in the AZG campaign is indicated by the green star. The grey-filled polygon just east of Terschelling indicates missing bathymetry data.

Fish

Sandeel[3] is currently the most important fish in terms of total fish biomass in the coastal zone and outer deltas of the Wadden Sea. It is an important prey source for seabirds and sea mammals. There is little known about marine life in the (Ameland) Inlet. A modified 1.24 m shellfish dredge with a fixed tooth bar (6" teeth), 10 mm mesh and a 6 mm mesh cod-end liner was used for sampling the sandeels in the Ameland Inlet (Table 2.10, Figure 2.10).

Table 2.10 Specifications of the modified 1.24 m shellfish dredge of Rijkswaterstaat.

Modified 1.24m Shellfish Dredge Specifications	
Towing warp	Steel 14mm main with 24mm extension
Depth: payout ratio	approx. 3/4:1
Net	10mm mesh with 6mm cod end liner and chain mat
Estimated headline height	0.5m
Dredge width	1.24m
Tooth length	6"

[3] *Lesser sandeel: Ammodytes tobianus, Raitt's sandeel: A. marinus and Greater sandeel: Hyperoplus lanceolatus*

Figure 2.10 Modified 1.24 m shellfish dredge of Rijkswaterstaat.

The survey was undertaken from 18 to 22 September 2017 and from 25 to 27 June 2018 at night between 11 pm and 4 am. Due to bad weather conditions, 32 of the 40 planned locations were sampled in 2017 and 20 locations in 2018 (Figure 2.11). The position of the vessel WR82 “Gerdia” was tracked at all times. Dredge start times and positions were recorded when the gear reached the seabed. The recorded times and distances varied between 2 to 7 minutes over distance 95 m to 212 m, respectively, deepening on flow velocities and the sailing speed of the ship.

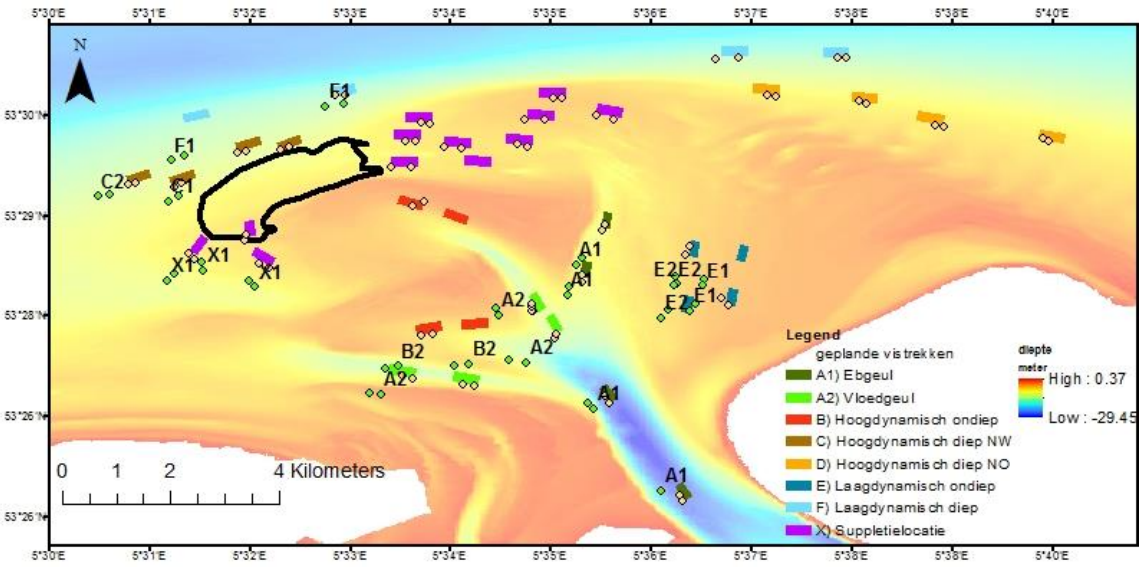

Figure 2.11 Planned (coloured shapes) and actually samples sandeel locations in 2017 (yellow diamond symbols) and 2018 (green diamond symbols).

2.4 Lower shoreface campaigns

The lower shoreface campaigns at Ameland, Terschelling and Noordwijk consists of i) frame measurements, ii) boxcores and vibrocores, and iii) multibeam surveys.

Frame measurements

The frame measurements were carried out at 3 locations in a transect normal to the coast at water depths between 10 and 20 m (Figure 2.1, Table 2.2). The Ameland lower shoreface frame locations were more or less in line with the Ameland Inlet frames 1-3. There were two measurement campaigns at Terschelling, as the wind and wave conditions were considered to be too mild to have sufficient seabed dynamics during the 1st campaign.

Multibeam measurements

Multibeam measurements were done at water depths between ~8 and ~20 m (Figure 2.12). Tracks were taken alongshore, in line with the main tidal current, and with 100% overlap to have a good and complete spatial coverage. The first multibeam measurements were carried out in September 2017 (Ameland), September-November (Noordwijk) and November-December (Terschelling). These surveys were repeated in August (Ameland), September (Noordwijk) and October (Terschelling) 2018.

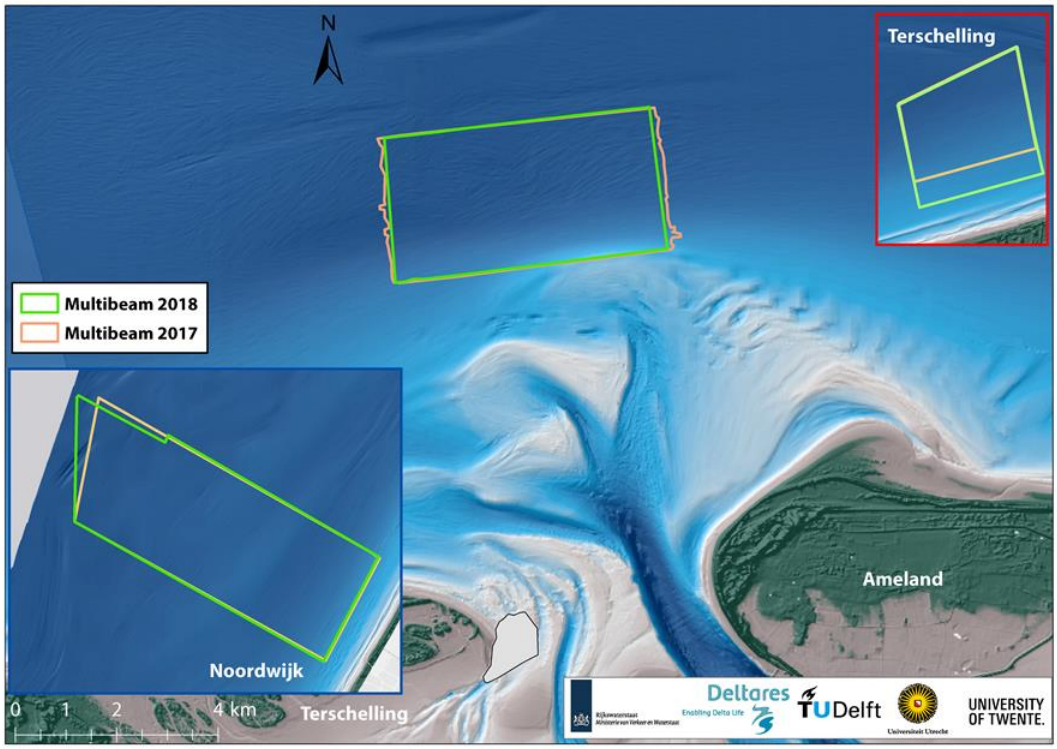

Figure 2.12 Location of the lower shoreface multibeam surveys.

Boxcores and vibrocores

Boxcores (~0.3 m deep) and vibrocores (~5 m deep) were taken to reveal the lower shoreface bed structure (e.g. clay layers), bed composition (grain size) and bed dynamics (e.g. storm deposits). During the July 2017 campaign in total 23 vibrocores and 42 boxcores were taken at the lower shoreface of Ameland, Terschelling and Noordwijk (Figure 2.9). In September 2018 another 48 boxcores were taken. The new locations were based on a first analysis of the 2017 cores and multibeam measurements. In the 2018 campaign rectangular boxcores were used instead of the round ones which were used in 2017. This was done to analyse the stratigraphy.

3 Dataprocessing

3.1 ADCP – Frames

General information

An Acoustical Doppler Current Profiler (ADCP) is an instrument which makes profile measurements of velocity. It sends four acoustic signals with a given strength and frequency towards the different measurement cells. It measures the reflected signals, the time between transmission and reception of a signal determines the velocity cell. The difference in frequency (Doppler shift) of the reflected signals is used to obtain the current velocity. Additionally, the strength of the reflected signal (backscatter) can indicate the amount of suspended particles or other constituents in the water. To know how reliable the velocity estimates are, the correlation between the signals from each of the four beams can be used. In this campaign the ADCP on the frames pointed upwards to analyse the velocity profile above the frame (Figure 3.1, left). The DV Frame 4 measurements included a downward-looking ADCP (Figure 3.1, right). The ADCPs used during the successive campaigns also include an internal pressure sensor (not always functioning, see below).

Figure 3.1 Upward-looking ADCP used on each campaign (left), downward-looking ADCP (right) used on Frame 4 during the DV campaigns.

ADCP type, settings, and position

Teledyne RDI Workhorse Monitor ADCPs were used during the campaigns (Teledyne RD Instruments, 2018a; Teledyne RD Instruments, 2018b). Specifications for the ADCPs are provided in Appendix B.1. The convention for naming the ADCPs is ADC01, ADC02, etc.

The position of the ADCPs on the frame is shown in Figure 3.2. They were mounted on top of the frame at a height of 2.3 m above the sea bed. It should be noted that also one RDI ADCP was used in downward-looking mode on Frame 4 for all DV campaigns.

Throughout the campaigns, different settings have been used for the blanking distance, number of cells and cell size. The exact settings per instrument can be retrieved from the NetCDF files, but the range of values that were used can be found in Appendix B.1.

ADC01, ADC02, ADC03, and ADC05 did not measure pressure and were replaced by ADC06, ADC07, ADC08 and ADC09 during servicing of the frames during the AZG campaign. ADC02

and ADC07 were on the missing Frame 2 during the AZG campaign, and thus did not return any data.

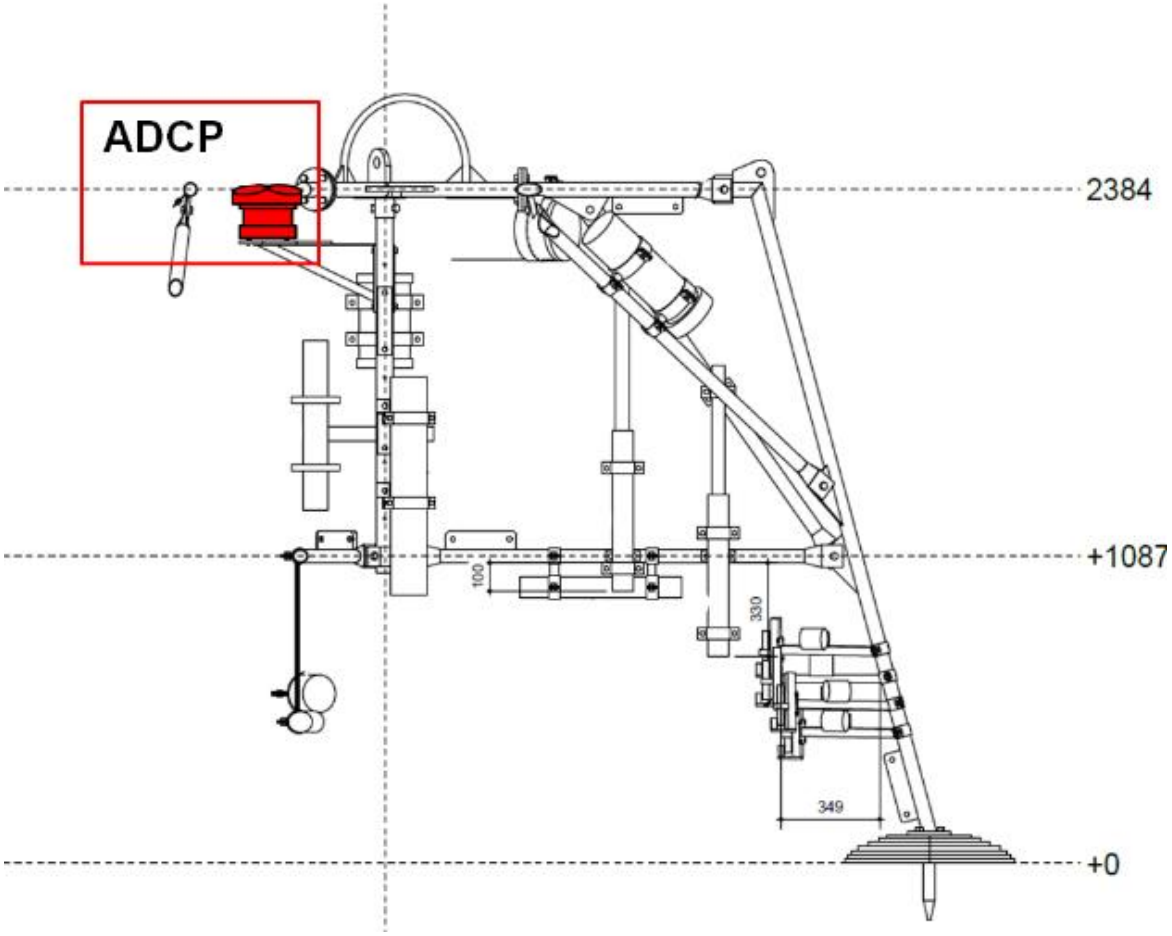

Figure 3.2 Design of frame featuring RDI Workhorse Monitor ADCPs. The instrument (highlighted in red) is mounted near the top of the frame with the sensor pointing upward at a design elevation of 2.3 m above the seabed. Actual height above the seabed varies slightly per frame due to assembly and field conditions.

Data processing

Binary files from the instrument are first read using the RDI ADCP toolbox of Bart Vermeulen (Vermeulen, 2015).

The elevation of the measurement cells with respect to the bed $z_u(n)$, is defined for the center of each cell using the following formula:

$$z_u(n) = z_{instrument} + z_{mid,bin1} + ndz \quad (3.1)$$

in which $z_{instrument}$ is the distance of the instrument from the bed, $z_{mid,bin1}$ is the distance to the center of the first cell measured from the top of the instrument, including the blanking distance where the instrument cannot return data, n is the cell number, and dz is the cell size. The number of cells returning reliable velocities depends on the local water depth at the time of the measurement. Cells located above the water surface return a velocity signal which is unreliable but not easily distinguished based on the velocity magnitude or correlation values. To determine

which cells are dry and should be excluded, we estimate the water depth above the ADCP from the internal pressure sensor. Assuming a hydrostatic pressure distribution, we can define total water depth *h* as:

$$h = z_p + \frac{p}{\rho g} \tag{3.2}$$

with *p* the pressure, z_p the elevation of the internal pressure sensor above the bed, ρ the water density (assumed to be 1025 kg/m^3) and *g* the gravitational constant (9.81 m/s^2). Subsequently every dry cell (defined as $z_u(n) > h$) is masked in order to exclude it from analyses. Note that this procedure can contain errors, as the pressure distribution can deviate from the hydrostatic pressure distribution in case of short surface waves. The velocity values at the upper cell should therefore be considered carefully.

After defining the inundated cells, the velocity signals returned by each beam are converted to an East-North-Up (ENU) coordinate system (Appendix C.1) and then filtered and de-spiked (Appendix C.2), and depth-averaged (Appendix C.3). The raw pressure signal is corrected for air pressure to obtain water pressure (Appendix C.4).

Information on the resulting NetCDF data file can be found in Appendix E.1.

3.2 ADCP HR – Frames

General information
An ADCP HR is an ADCP (Section 3.1) which can be applied in High Resolution mode. High Resolution refers in this case to the small cell size which can be used to get a high spatial resolution (an order of magnitude finer than the “normal” ADCPs). It sends three acoustic signals with a given strength and frequency towards the different measurement cells. Then, it measures the reflected signals, the time between transmission and reception of a signal determines the velocity cell. The difference in frequency (Doppler shift) is used to obtain the velocity. Additionally, the strength of the reflected signal (backscatter) can indicate the amount of suspended particles or other constituents in the water. To know how reliable the velocity estimates are, the correlation between the signals from each of the three beams can be used. In this campaign the ADCP HR pointed downwards to analyse velocities below the frame in the lowest 50 cm above the bed (Figure 3.3). The ADCPs used during the successive campaigns also include an internal pressure sensor.

Type of ADCP, settings, and position
The type of ADCP used here is the Aquadopp Profiler HR from manufacturer Nortek (Nortek AS, 2008b; Nortek, 2017b; Nortek, 2017c). Two different types of head are used for the instruments: downward and side-ward configuration. Apart from the attachment to the frame, there is no difference between the two versions. They are attached to the frame such that the beams look towards the bottom and the cells are at the same height. Figure 3.4 shows the attachment to the frame of both a downward and sideways head configuration Aquadopp Profiler. Specifications for the ADCP-HR instruments are given in Appendix B.2. The convention for naming the ADCP HR instruments is AQD01, AQD02, etc.

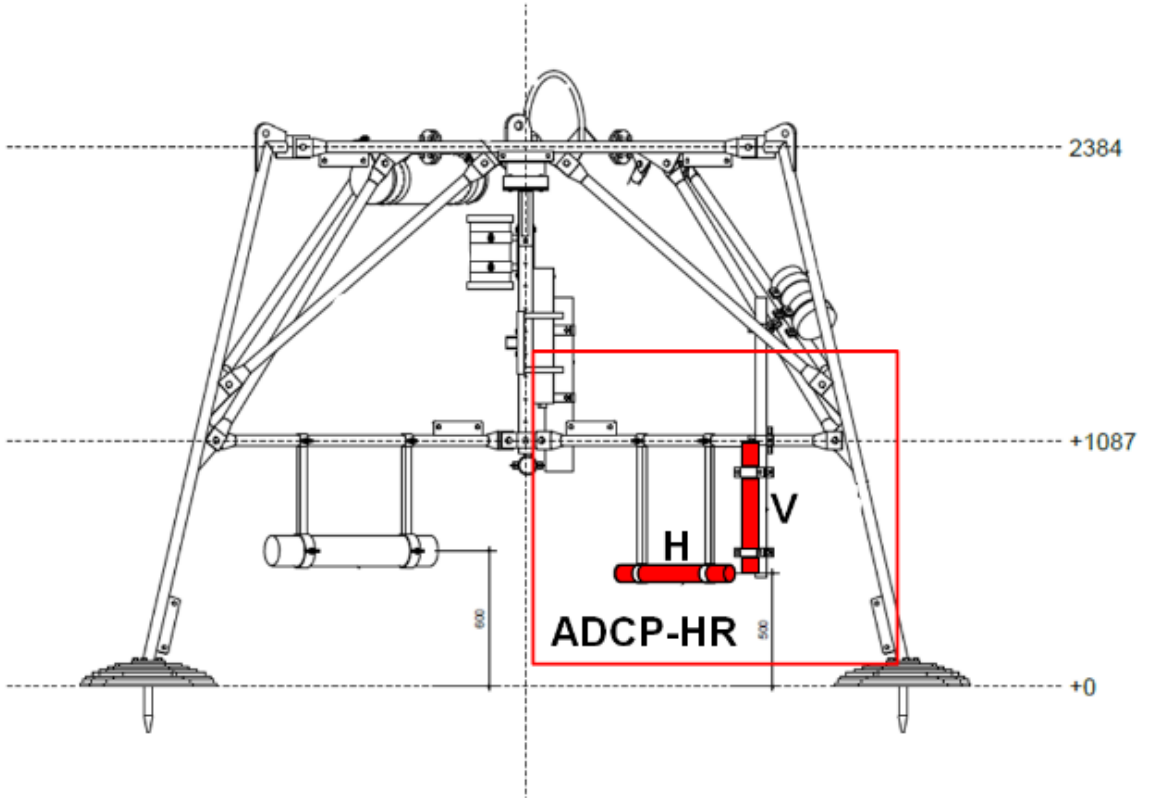

Figure 3.3 Design of frame featuring a Nortek Aquadopp Profiler ADCP HR. The instrument (highlighted in red) is mounted near the bottom of the frame, with the sensor at a design elevation of 0.50 m above the seabed. Actual height above the seabed varies slightly per frame due to assembly and field conditions.

Figure 3.4 Downward looking ADCP-HRs with sideward (left) and downward (right) head configuration.

Data processing

Binary output files of the Nortek Aquadopp Profiler are in .prf format. Nortek AquaPro-HR software is used to convert these binary files into ASCII files. The ADCP-HR data are processed in the same way as the ADCP (see Section 3.1), except for the depth-averaging which was not

carried out. The included data on correlation and amplitude could be used for bed level detection. Information on the resulting NetCDF data file can be found in Appendix E.2.

3.3 ADCP - Watersheds

General information
The ADCPs on the watersheds were placed to measure the water depth and flow velocity profiles there (Figure 3.5). Aquadopp is the brand name of the ADCP manufactured by Nortek and used for this part of the study. Aquadopps can be configured in two modes: Low Resolution or High Resolution. On the watersheds, the Low-Resolution mode was used. In this way, the full water column could be measured, without the restrictions on specific discharge for using the instruments in High Resolution mode. The drawback is that fewer cells can be specified in the vertical direction.

Figure 3.5 ADCPs being prepared for deployment on the watersheds.

Type of ADCP, settings, and position
The type of ADCP used here is the Aquadopp Profiler LR from manufacturer Nortek (Nortek AS, 2008a; Nortek, 2017a; Nortek, 2017c). Instrument settings are given in the Appendix B.3. The instruments are programmed such that they averaged velocities over 1 minute. Thus, they give one vertical velocity profile per minute. The orientation is based on the internal compass.

Six ADCPs were placed on the watersheds: three south of Ameland (AmID4, AmID5, AmID6) and three south of Terschelling (AmID1, AmID2, AmID3) (Figure 2.3). These locations were chosen to be as close as possible to the watersheds, but also low enough so that they were submerged for a significant part of the tidal cycle.

The ADCPs were buried in the bed, with the head pointing upwards, approximately 5 cm above the bed. They were mounted in a protection frame (stainless-steel to reduce effects on the compass). Furthermore, a small buoy was attached to recover the instrument more easily.

The top of the watershed ADCPs was measured by DGPS. The procedure included 10 measurements, which were used to determine the average bed level. The bed level directly next to the instrument was measured and approximately two circles (radius of 1 m and radius of 2 m) were measured with 4 measurements for each circle (Figure 3.6).

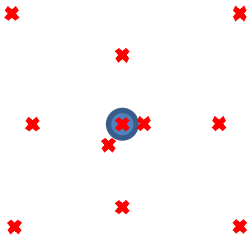

Figure 3.6 Sketch indicating the GPS measurement procedure for the watershed ADCP (blue) and DGPS measurement locations (red crosses).

Data processing

The ADCP watershed data are processed in the same way as the ADCP-HR (see Section 3.2). Information on the resulting NetCDF data file can be found in Appendix E.3.

3.4 ADV

General information

An Acoustic Doppler Velocimeter (ADV) is an instrument which makes high resolution point measurements of velocity (Figure 3.7). It sends a single acoustic signal with a given strength and frequency towards the measurement volume, and it measures the reflected signals in three beams. The difference in frequency (Doppler shift) is used to obtain the velocity. To know how reliable the velocity estimates are, the correlation between the three beams can be used.

Figure 3.7 Nortek (left) and Sontek (right) ADVs mounted on Frames 4 and 5, respectively.

Type of ADV, settings, and position

Twelve ADVs of two different manufacturers were used during the campaigns:

- 3x Sontek Hydra (At frame 5 during the Ameland Inlet Campaign) (Sontek, 2008)
- 9x Nortek Vector (At all other frames and campaigns) (Nortek AS, 2005; Nortek, 2017c; Nortek, 2017d)

Instrument settings are given in the Appendix B.4. The convention for naming the ADVs is ADV01, ADV02, etc.

The position on the frame is shown for the Nortek and Sontek ADVs in Figure 3.8. It should be noted, that depending on the flow direction, velocities might be disturbed by interference with the frame or other instruments nearby. Two ADVs were positioned 0.35 m and 0.65 m above the bed. If a third ADV was available, this was located 1 m above the bed. Pressure sensors were located inside the canister for the Nortek ADVs. For the Sontek ADVs, pressure is measured at 4 Hz by a separate instrument at a height of 1.91 m above the bed. Therefore, in

the data-files different values are given for the velocity height above the bed (z_u) and the pressure height above the bed (z_p).

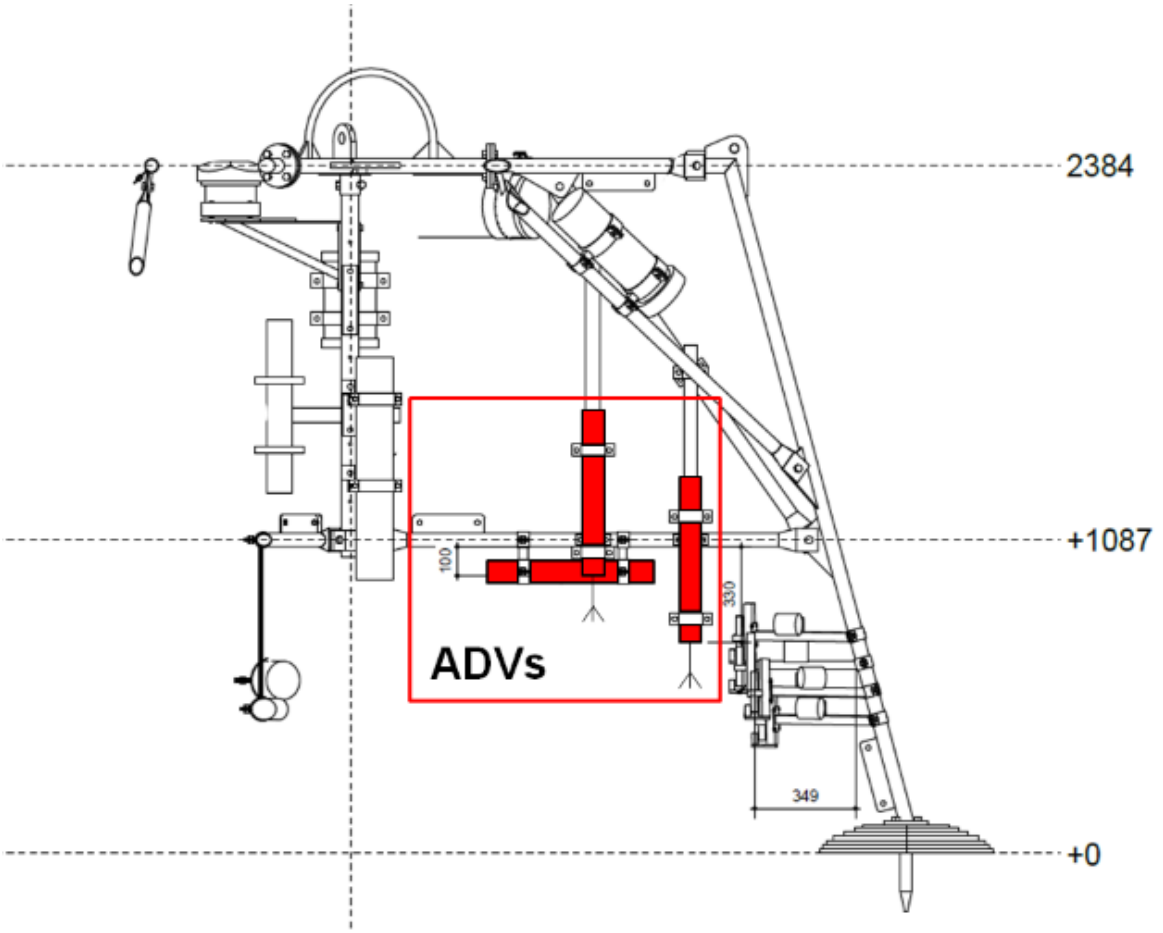

Figure 3.8 Design of frame featuring Nortek Vector ADVs. The instruments (highlighted in red) are mounted near the bottom of the frame, with their sensors at design elevations of 0.35, 0.65, and 1.00 m above the seabed. Actual height above the seabed varies slightly per frame due to assembly and field conditions.

Data processing

Binary output files of the ADV are in .vec format. Nortek Vector software (Nortek, 2017d) is used to convert these binary files into ASCII files. The ADV data are processed in the same way as the ADCP-HR (see Section 3.2). Information on the resulting NetCDF data file can be found in Appendix E.4.

3.5 Moving boat ADCP

Over three (non-consecutive) tides in September 2017, velocities were measured across the Ameland Inlet, such that discharge estimates could be derived. Two vessels (Potvis, also known as AQVPO; and Siege, also known as RWSSI) sailed across the inlet (Figure 3.9). Both were employed with ADCP instruments that measured vertical velocity profiles simultaneously. The ships sailed back and forth along a predefined navigation route for approximately 13 hours, covering a complete tidal cycle. Every 20 minutes, the ships sailed the same track. One additional transect was measured on 18 September 2017. This transect did not cover the full tidal cycle (almost 8 hours) and did not cover the full inlet (see Figure 2.5). An overview of the time frames in which the measurements were executed is given in Table 3.1.

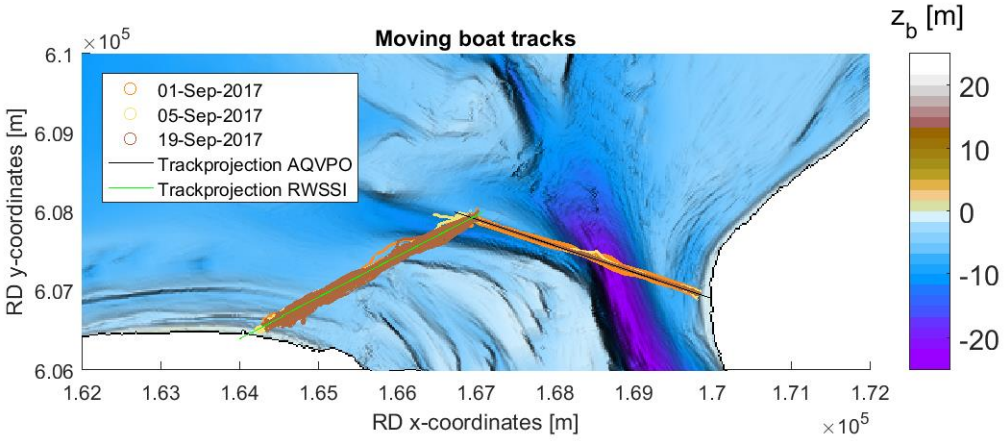

Figure 3.9 Tracks of the ADCP measurements in the Ameland tidal inlet, simultaneously executed by the survey vessels Rijkswaterstaat Siege (RWSSI) and Aquavision Potvis (AQVPO). Every location, where water depth and flow velocity were recorded, is plotted (circles).

Table 3.1 Time frame of the ship-mounted ADCP measurements across the Ameland inlet.

Day	Ship	Start	End	Duration
1 September 2017	AQVPO	05:10:13	18:08:26	12 h 58 min
	RWSSI	05:10:30	18:08:17	12 h 57 min
5 September 2017	AQVPO	05:30:07	18:32:43	13 h 02 min
	RWSSI	05:29:48	18:28:04	12 h 58 min
18 September 2017	RWSSI	10:23:41	18:19:03	7 h 55 min
19 September 2017	AQVPO	04:50:26	18:06:40	13 h 16 min
	RWSSI	04:50:15	18:01:46	13 h 11 min

The measurements were processed by Aquavision to instantaneous discharge through the tidal inlet (Aquavision, 2017a,b). For this purpose, the measurements were projected on a (manually defined) navigation route (Figure 3.9), that was used as the target route during the measurements. For each measurement location, a discharge per unit width ($m^3/m/s$) was determined by integrating the flow velocity over the depth. After integrating the discharge over the width of the defined tracks, the total discharge through the inlet was estimated. Additionally, the total sediment fluxes were computed by multiplying the discharges with sampled sediment concentrations (except for the Section D measured on 18 September 2017). Both the measured velocities as the derived discharges and sediment fluxes are provided on the THREDDS server. In this dataset, the discharge and sediment flux are positive with flow from the Wadden Sea towards the North Sea (i.e., positive in ebb direction). Information on the resulting NetCDF data file can be found in Appendix E.5.

3.6 Drifters

General information

During the AZG campaign, drifter deployments have been performed to obtain more information on spatial variations in velocity, in order to complement the Eulerian measurements at the frames. The concept was to have floating devices which primarily measure the movement of the top water layer (and are as least as possible influenced by wind). These devices were equipped with GPS trackers in order to log their movement.

30 drifters have been developed for this field campaign at TU Delft (Figure 3.10). 6L water tight cans were used with increased weight by a layer of concrete to minimize buoyancy. A bottom plate was added for stability and a flag for visibility.

In cooperation with H-Max (https://www.h-max.nl/) an Android-based GPS-tracking application was developed. This application internally stores its position every second and sends the position every 30 seconds to a web-portal. This enables the drifters to be tracked in the field and more easily retrieved.

Figure 3.10 Drifters in harbour (left) and deployed in the water (right).

Deployments

- 50 small-scale deployments were performed during 6 days at different stages of the tidal cycle.
- 1 large-scale deployment was performed on 9 September 2017 during a full flood and ebb cycle.

Methodology

Output of the GPS trackers is longitude and latitude data with a frequency of 1 Hz. Many duplicate data points were encountered in the time series, as the GPS position was not always updated. All duplicates were removed in order to prevent 0 m/s velocities. Subsequently, a low-pass filter was applied in order to eliminate all small-scale movements. Velocity magnitudes and directions were obtained from the filtered velocities. This resulted in data points non-uniformly distributed in space and time. Finally, in order to make velocity maps from all points, the inverse distance weighting method was used to interpolate the velocity in every cell of a predefined grid. This method gives most weight to points which are close and least weight to points far away.

Data set details

To get more information on the drifter data set, contact Floris de Wit f.p.dewit@tudelft.nl or Marion Tissier m.f.s.tissier@tudelft.nl.

3.7 Pressure sensors

General information

During the AZG campaign, eight pressure sensors surrounded Frames 4 and 5. Unfortunately, sensor 6 did not record any data during the campaign. The location of the sensors with respect to the bigger instrument frames is shown in Figure 2.3.

Type of pressure sensor, settings, and position

The type of sensor used is an OSSI-010-003C-03 Wave Gauge, manufactured by Ocean Sensor Systems (Ocean Sensor Systems, 2015). It is a submersible self-logging, self-powered pressure sensor with a pressure range up to 3 bar. The pressure sensors were attached to small frames, as can be seen in Figure 3.11. Convention for naming the Pressure sensors is PS001, PS002, etc. The instrument settings can be found in Appendix B.5.

Figure 3.11 Pressure sensor frames.

Data processing

Daily data files are generated in .csv format by the instrument. At the end of the day, the file is closed approximately 10 s before the new day begins. This results in about 10 s (or 500 data points) where no data is logged. Since the exact amount of missing points between the bursts varies, NaNs are added at the end of the burst in order to have a vector length of 864 000 (one day at 10 Hz). In this way, all bursts have the same length. The raw pressure signal is corrected for air pressure to obtain water pressure (Appendix C.4). Information on the resulting data files can be found in Appendix E.6.

3.8 LISST

General information

The Laser In-Situ Scattering and Transmissometery (LISST) instrument (Figure 3.12) optically measures the volumetric concentration and size of suspended particles. It uses 32 concentric ring detectors to measure the scattering and transmission of a 670 nm laser beam around suspended particles. This makes it useful for determining both the amount and size characteristics of suspended sediment and organic matter.

Figure 3.12 LISST-100X installed on Frame 3. The sensor is visible in the circular opening on the right side of the instrument.

Type of LISST, settings and position

LISST-100X Particle Size Analyzers (Sequoia Scientific Inc., 2015) were used on multiple frames in each campaign. The instrument was operated in burst mode, taking the average of 5 instantaneous measurements every second for 15 seconds in a row. This 15-second burst was repeated once per minute, with no data being collected for the remaining 45 seconds of every minute. An optical path length (distance between the laser and the sensor) of 0.05 m was used, which is appropriate for moderate turbidity levels. A particle size range of 2.5 to 500 µm was chosen based on typical sediment grain sizes at the measurement sites. The LISST was mounted horizontally, suspended 0.6 m above the seabed (Figure 3.13). The convention for naming the LISSTs is LIS01, LIS02, etc. The LISST specifications can be found in Appendix B.6.

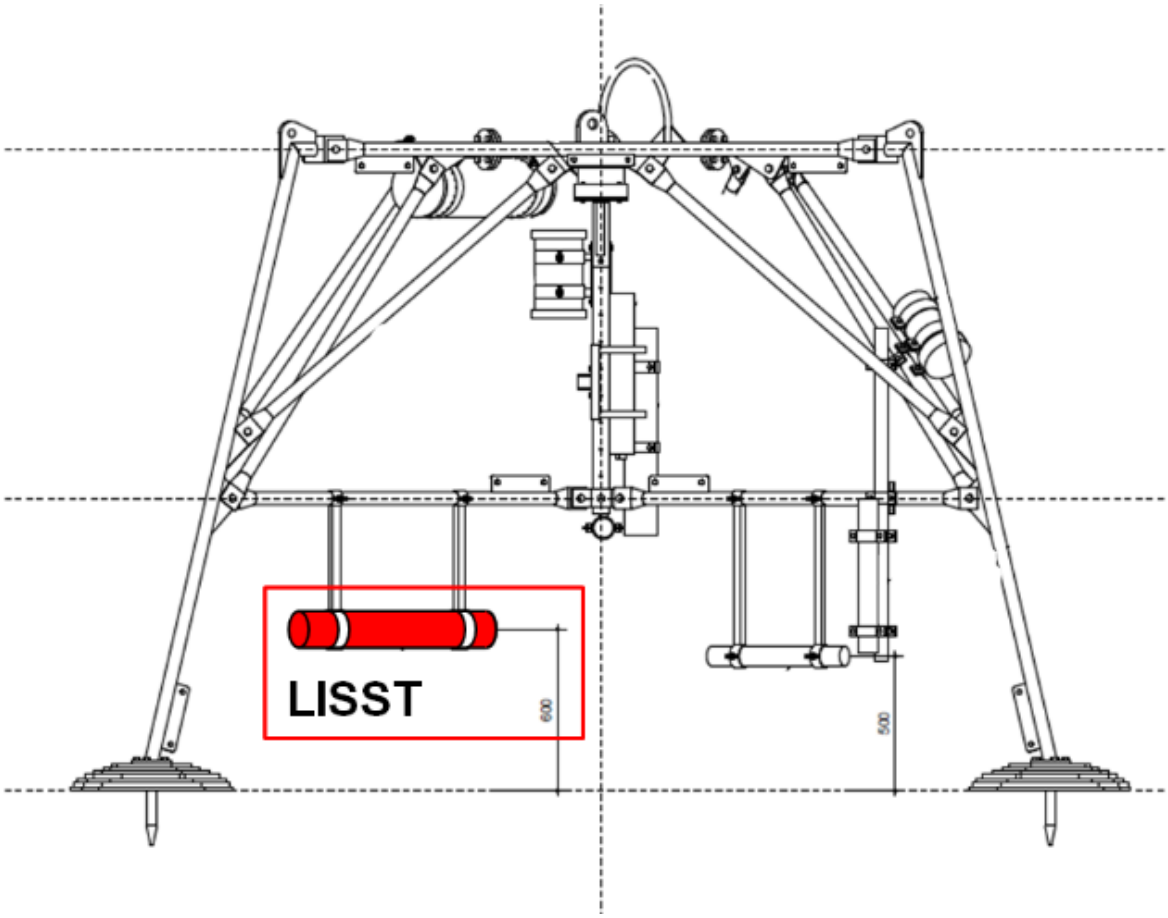

Figure 3.13 Design of frame featuring the LISST-100X. The instrument (highlighted in red) is mounted near the bottom of the frame, with the sensor at a design elevation of 0.60 m above the seabed. Actual height above the seabed varies slightly per frame due to assembly and field conditions.

Calibration

To calibrate the LISST, the background scatter intensity of the laser in clean water must be measured. This procedure was carried out prior to each campaign in accordance with the manufacturer's specifications (Sequoia Scientific Inc., 2015). This calibration stage ensures that the laser detection rings are properly aligned and provides a basis for interpreting the measurements on site. Additional calibration using water samples is necessary to convert the volumetric concentration readings from µg/L to a mass concentration (i.e. mg/L); however, this step was not completed. Suspended particles in Ameland Inlet consist of flocculated fine sediment, organic matter, and sand (Pearson et al., 2019). Due to the varying density of these particles, a direct conversion to mass concentration by assuming uniform grain density (e.g. 2650 kg/m^3) is not possible. This difference in units should be borne in mind when making comparisons with numerical models or other measurements.

Data processing

Upon retrieval of the data from the instrument, raw binary *.dat files were processed using the LISST-SOP Version 5.0.50 software (Sequoia Scientific Inc., 2012). The background scatter intensity files (*.asc) created during the most recent calibration stage were then used to process the data. The ASCII file (*.asc) created by LISST-SOP was then read into MATLAB and converted into NetCDF format. No de-spiking or filtering was carried out on the time series, and no correction for atmospheric pressure has been performed on the depth measurements.

Note on data quality
This section contains a brief discussion of the measurements with respect to the operating limits and accuracy of the sensors (Table 3.2), as well as an overview of datasets flagged as incomplete or featuring significant errors.

Table 3.2 Range, accuracy, and resolution of the sensors on the LISST-100X Particle Size Analyzers (Sequoia Scientific Inc., 2012).

Sensor	Range	Accuracy	Resolution
Solid State Diode Laser (670 nm, 1mW)	-	-	12 bit
Grain Size (Calculated)	2.5 to 500 µm	-	32 log-spaced size classes
Depth	0 to 300 m	+/- 0.12 m	0.08 m
Temperature	-10 to 45 °C	+/- 0.5% of reading + 0.001 mS/cm	0.01 °C

The LISST mounted on Frame 3 (LIS01) functioned during all campaigns, and the LISST on Frame 4 (LIS02) worked in the AZG campaign. However, the LISST mounted on Frame 5 during the AZG campaign and Frame 1 during subsequent campaigns (LIS03) experienced a serious, unexplained malfunction, and did not produce usable data for any of the measurement periods.

Two main quality control checks are suggested by the manufacturer. First, the laser must have sufficient power. Typical laser reference intensity is between 0.5 to 2.0 mW; the data must be discarded if the laser reference is 0 or close to 0, as this indicates that the laser is dead and in need of replacement (Sequoia Scientific, 2015). Secondly, data quality is also highly dependent on the optical transmission. If the optical transmission is too high (>0.995), then the water is too clear and the readings at those timesteps must be discarded since the signal-to-noise ratio is too low (Sequoia Scientific, 2015). Conversely, highly turbid water can decrease optical transmission below optimal levels and result in unreliable data. If the transmission falls between 0.30 and 0.10, then caution must be used when interpreting the measurements (e.g. Chapalain et al., 2018). Readings taken when transmission is below 0.10 must be discarded (Sequoia Scientific, 2015).

Accuracy of the instrument may be affected by variations in particle composition (e.g. solid grains of sand vs. flocs), sharp local gradients in salinity (i.e. Schlieren effect), or particles exceeding the size range of the LISST (Chapalain et al., 2018). Biofouling of the sensor may also affect the reliability of the data.

Information on the resulting data files can be found in Appendix E.9.

3.9 Multi-parameter Probe

General information
The Multi-parameter Probe (Figure 3.14) is an instrument typically used for water quality monitoring and measuring physical oceanographic properties. It uses multiple sensors to measure conductivity, temperature, depth, turbidity, pH, chlorophyll, phycocyanin blue-green

algae (BGA-PC), and dissolved oxygen (DO). From these variables, salinity and density can also be computed.

Hence, its measurements are useful for both ecological monitoring (e.g. physical/chemical conditions affecting benthic and aquatic ecosystems or the presence of organic matter), as well as understanding physical drivers of hydrodynamics (e.g. salinity and density are important for baroclinic flow).

Figure 3.14 YSI 6-Series Multi-parameter Probe (MPP) mounted on Frame 3 (AZG) prior to deployment.

Type of MPP, settings, and position

YSI 6600v2-4 Multi-parameter Water Quality Sondes (YSI Incorporated, 2012) were mounted vertically on the central pole of each frame during all of the measurement campaigns (Figure 3.15). Specifications for the Multi-parameter probe are given in Appendix B.7. The convention for naming the MPPs is MPP01, MPP02, etc.

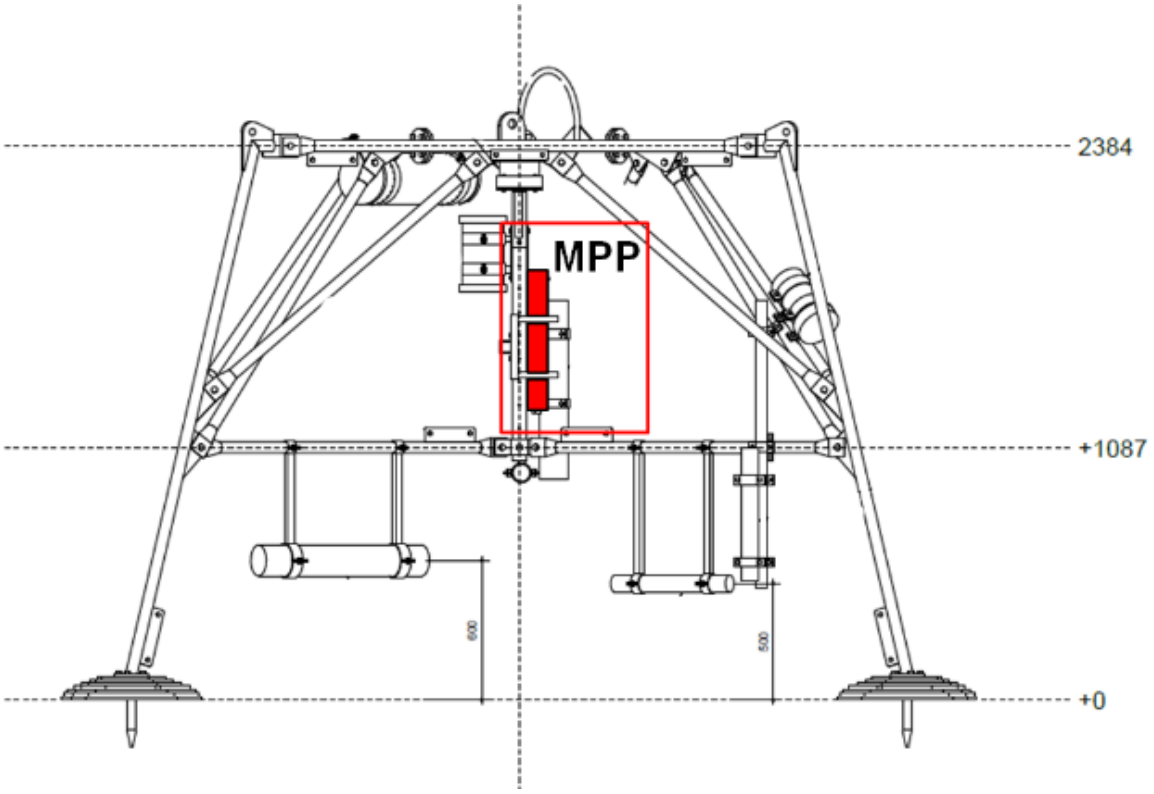

Figure 3.15 Design of frame featuring the YSI 6600v2-4 Multi-parameter Probe (MPP). The instrument (highlighted in red) is mounted along the centre column of the frame with the sensor at a design elevation of 1.265 m above the seabed. Actual height above the seabed varies slightly per frame due to assembly and field conditions.

Calibration

The temperature, conductivity, pH, and DO sensors were calibrated prior to each campaign, following the procedures outlined by YSI Incorporated (2012). The sensors were placed in a container filled with water having known properties, and their readings were compared with the "true" values. Instrument settings were adjusted until measurements were within an acceptable margin. All other sensors used the factory settings.

Data processing

A raw Sonde .dat binary file is converted to ASCII format using the YSI EcoWatch software. This ASCII file is then read into MATLAB and converted into NetCDF format. Depth is directly calculated from pressure internally, so a raw pressure time series was not output by the instrument. It is also not possible to do a straightforward recalculation of the pressure since the internal calculations implicitly account for the fluid temperature/conductivity. Hence, in the conversions to salinity/density, depth is used as 1 m ~1 dbar pressure. Thus, there will likely be a ~2% error in any derived salinity and density quantities. No correction for atmospheric pressure has been performed on the depth measurements, since the calculation is made internally. Practical salinity and water density are computed from the conductivity, temperature, and depth readings using the TEOS MATLAB Toolbox (McDougall & Barker, 2011). No de-spiking or filtering was carried out since the 5-minute sampling interval of the sensors generally led to clean time series without significant noise.

Data quality
Each of the sensors on the Multi-parameter Probe has different operational limits and accuracy (Table 3.3). The validity of the measurements from each frame is discussed in greater detail in Section 4.3. Information on the resulting NetCDF data file can be found in Appendix E.10. The instrument quality flags in Table 2.3 were based on whether there was a time series containing data within the normal operating range for each of the main variables measured. Instruments without measured time series for all variables were flagged as incomplete.

Table 3.3 Range, accuracy, and resolution of the sensors on the YSI 6600v2-4 Multi-parameter Probe (YSI Incorporated, 2012).

Sensor	Type	Range	Accuracy	Resolution	Depth Range	Temperature Range
Temperature	Thermistor	-5 to 50 °C	±0.15 °C	0.01 °C	0 to 200 m	-5 to 50 °C
Depth	Stainless steel strain gauge	0 to 61 m	±0.12 m	0.001 m	0 to 61 m	-5 to 45 °C
Conductivity	4 electrode cells with autoranging	0 to 100 mS/cm	±0.5% of reading +0.001 mS/cm	0.001 – 0.1 mS/cm (range dependent)	0 to 200 m	-5 to 60 °C
pH	Glass combination electrode	0 to 14 units	±0.2 units	0.01 units	0 to 200 m	-5 to 50 °C
Turbidity	Optical, 90° scatter, with mechanical cleaning	0 to 1000 NTU	±2% of the reading or 0.3 NTU (whichever is greater)	0.1 NTU	0 to 61 m	-5 to 50 °C
Chl	Optical, fluorescence, with mechanical cleaning	0 to 400 µg/L Chl	0.1 µg/L Chl detection limit	0.1 µg/L Chl	0 to 61 m	-5 to 50 °C
BGA-PC	Optical, fluorescence, with mechanical cleaning	0-100 RFU	220 cells/mL detection limit	0.1 RFU	0 to 61 m	-5 to 50 °C
ODO	Optical, Luminescence Lifetime	0 to 50 mg/L	0 to 20 mg/L, ±1% of the reading or 0.1 mg/L (whichever is greater)	0.01 mg/L	0 to 61 m	-5 to 50 °C

3.10 OBS

General information
An Optical Backscatter Sensor (OBS) is an instrument which sends a single frequency optical signal and measures the reflected signal (backscatter). The amount of backscatter determines the amount of sediment in the water. However, backscatter is not only influenced by sediment concentration, but also by sediment diameter, bubbles, algae, and more.

Type of OBS, settings and position
Two types of OBSs were used during the campaigns (Figure 3.12):

1 Campbell OBS-3+ Turbidity Sensor (Campbell Scientific, 2017)
2a Seapoint Turbidity Meter -AZG campaign, frame 5 (Seapoint Sensors, 2013)
2b Seapoint Turbidity Meter Array -AZG campaign, frame 5 (Seapoint Sensors, 2013)

Specifications for each of these instruments can be found in Appendix B.8. The convention for naming the OBSs is OBS01, OBS02, etc.

Figure 3.16 Seapoint (left) and Campbell (right) OBSs, installed on frames 5 and 4, respectively.

OBSs are located at the same leg of the frame as the ADVs in order to have synchronized velocity and turbidity measurements (Figure 3.17). At Frame 5 during the AZG campaign, eight OBSs were available of which 5 were in an array at 11, 14, 17, 20, 21, 23, 50, and 80 cm above the bed. At all other frames, four Campbell OBSs were present per frame at 20, 30, 50, and 80 cm above the bed. These OBSs logged data to the ADVs (two OBSs per ADV).

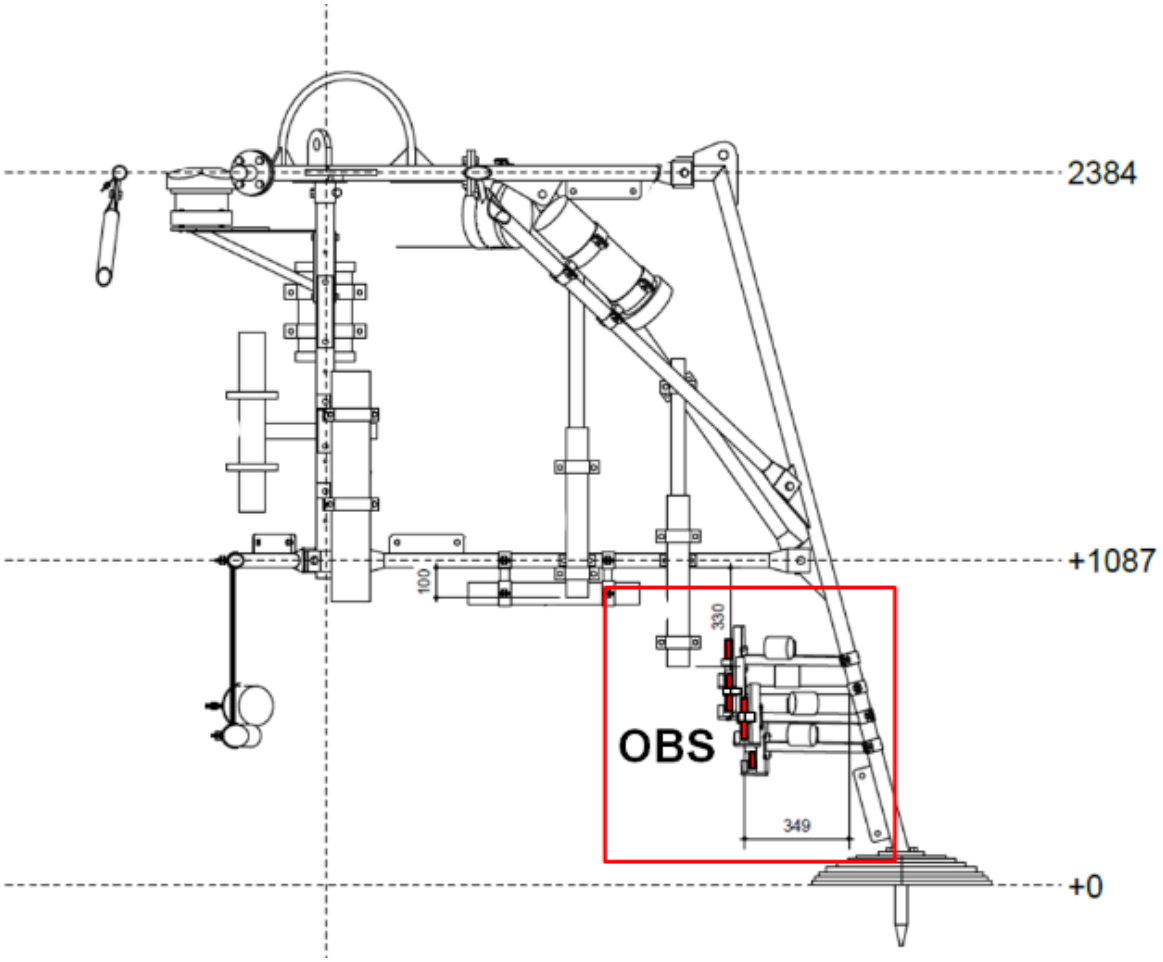

Figure 3.17 Design of frame featuring Campbell OBS-3+ Turbidity Sensors. The instruments (highlighted in red) are mounted near the bottom of the frame, with their sensors at design elevations of 0.20, 0.30, 0.50, and 0.80 m above the seabed. Actual height above the seabed varies slightly per frame due to assembly and field conditions.

Calibration

Calibration of all OBS's was performed at the laboratory facilities of Utrecht University. For calibration, sediment from the seabed near the frames was used. In a mixing tank, a known quantity of this sediment was brought into full suspension. The sediment concentration was slowly increased while the instruments were logging. The output voltage of the instrument was recorded, resulting in voltage as a function of concentration per instrument. To obtain a continuous calibration curve, a linear fit was used between 0 g/L and 10 g/L, and a parabolic fit for concentrations higher than 10 g/L (Figure 3.18). Physically you would expect the suspended concentration to scale linearly with the measured voltage. The better parabolic fit for higher suspended concentrations is an indication that the validity of the calibration curve for higher concentrations is questionable. On the other hand, suspended sediment concentrations larger than 10 g/l are not common in the area of interest.

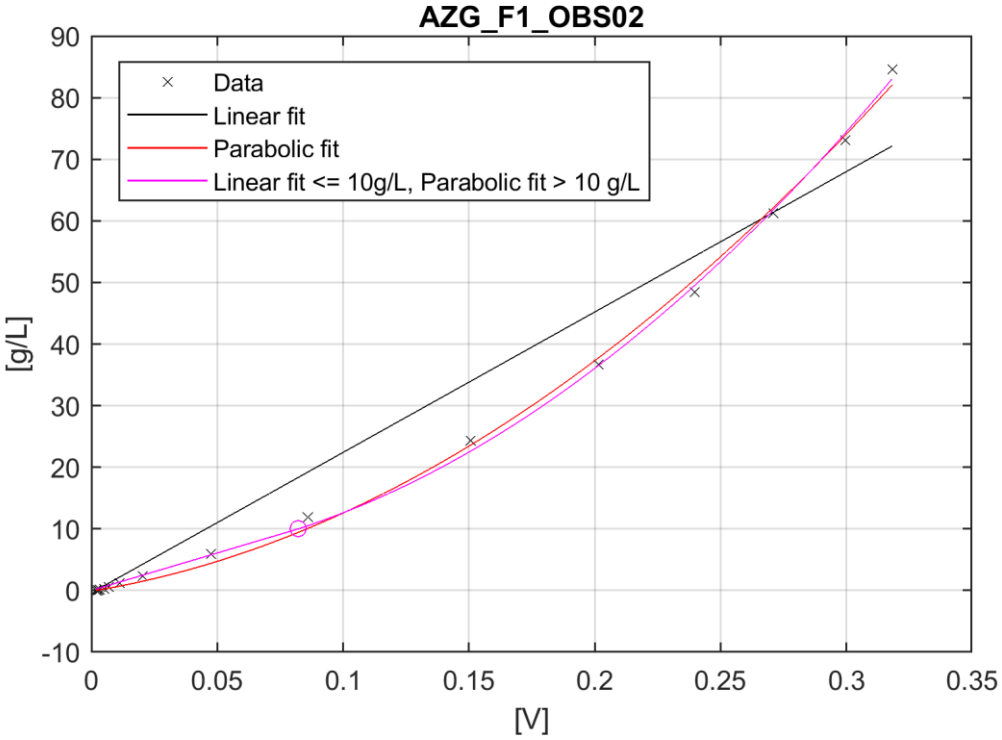

Figure 3.18 Example of a calibration curve for OBS2 during the AZG campaign. The black line indicates a linear fit through the entire dataset, and the red line shows a parabolic fit through the entire dataset. The pink line indicates a hybrid approach, where there is a linear fit for concentrations < 10 g/L, and a parabolic fit for higher concentrations.

Data processing and data quality

Raw voltages recorded by the instrument were de-spiked to remove outliers as per Appendix C.2. It should be noted that data quality of all OBS signals is questionable. Large concentration variations with a tidal timescale are observed in the time series, which cannot be explained by differences in bed shear stress. Based on the LISST (Section 0) it was concluded that fine sediment and flocs were likely encountered by the instrument in the water column. Since the instrument was not calibrated for this type of sediment, and fines lead to much higher backscatter than sand, it is difficult to interpret the data and its validity. For this reason, only the voltages if the OBS signals are provided on the THREDDS server.

Information on the resulting data files can be found in Appendix E.11.

3.11 Water samples

Water samples collected during transects of the inlet were processed in the laboratory in accordance with NF-EN 872:2005 (AFNOR, 2005). Suspended solid concentration was determined by filtration through glass fibre filters. Information on the resulting data files can be found in Appendix E.12.

3.12 Tracers

General information

The tracer experiment involved depositing sediment with a unique signature (fluorescent (Figure 3.19) and magnetic) on the outer ebb-tidal delta and allowing it to be reworked by waves

and currents. The location, quantity, and characteristics of tracer sediment retrieved later from the seabed and water column can be used to give insight into sediment transport pathways and sorting behaviour. The intention was to use the results of this experiment to better understand the potential behaviour of nourishment sand placed on the highly dynamic ebb-tidal delta.

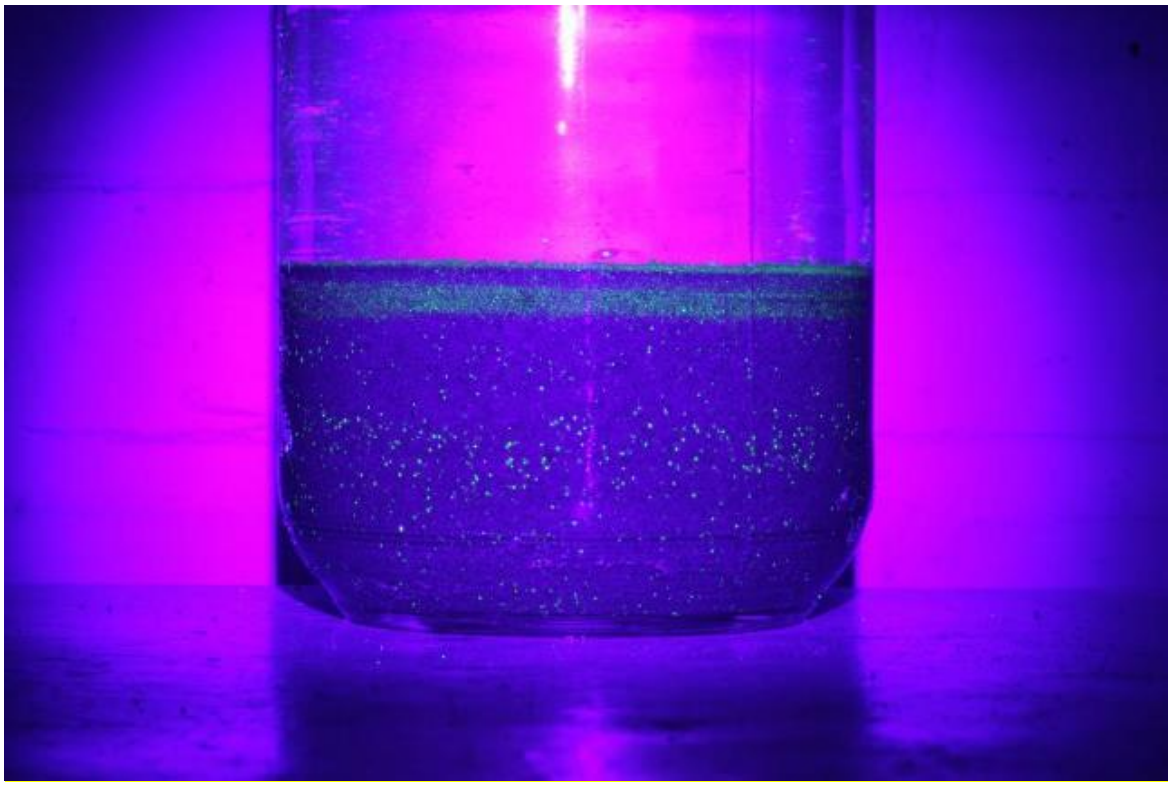

Figure 3.19 Example of tracer sediment recovered from the seabed. The sample is illuminated under ultraviolet light, which causes the tracer particles to appear as green dots, and native sediment as the darker purple matrix surrounding them.

Tracer Manufacture, Deployment, and Retrieval

The tracer particles were manufactured by Partrac Ltd. to have physical and hydraulic properties that closely matched the native sediment at the site (Table 3.4, Figure 3.20). The tracer is fluorescent under ultraviolet light and ferrimagnetic, developed from non-toxic, natural materials (Black et al., 2004).

Table 3.4 Specifications for tracer particles used in this experiment.

Variable	Value
Deposited Tracer Mass	2000 kg
Deployment Latitude:	53.485°N
Deployment Longitude:	5.536°E
Tracer d50	285 µm (Medium Sand)
Tracer Mean Diameter	253 µm (Medium Sand)
Tracer Sorting	2.203 (Poorly Sorted)
Tracer Skewness	-0.546 (Very Fine Skewed)
Tracer Kurtosis	2.640 (Very Leptokurtic)
Tracer Density	2628.0 kg/m3 (+/- 1.5 kg/m^3)

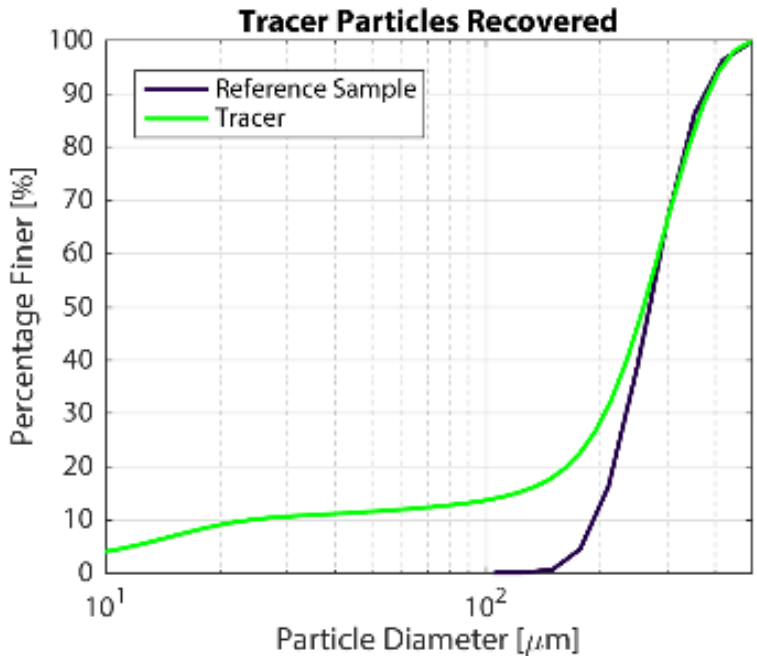

Figure 3.20 Particle size distribution of tracer sediment. The tracer was matched to a reference sample of the native bed sediment to ensure that they would behave similarly. The fine tail of the tracer PSD is due to small particles that make up the fluorescent/magnetic coating that the sand grains are treated with.

2000 kg of the tracer particles were deposited on the ebb-tidal delta from a ship at -6.5 m NAP on August 29th, 2017, after which the material could disperse naturally. After deployment, an extensive sampling campaign was carried out to monitor the distribution of the tracer material in space and time. Over 300 surficial sediment samples (van Veen grab and box core) were collected across the ebb-tidal delta and Ameland Inlet. To capture tracer material suspended in the water column, strong bar magnets were fixed to mooring lines at elevations 1, 2, and 5 m above the bed. These magnets were placed in a perimeter around the tracer deployment site.

Laboratory Analysis

Sediment retrieved from bed samples was dried in an oven at 180°C. Tracer particles were then magnetically separated from the native sediment and counted under UV lights. Samples containing visible tracer particles were then further analysed using a digital microscope (Keyence Corporation, 2014). Particle size analysis of the separated tracer was performed using the microscope's built-in image processing software. The particle size distribution of the native sediment was also determined using a Malvern Mastersizer (Malvern Instruments Limited, 2017).

Note on data quality

As of this writing, laboratory analysis of the tracer data is ongoing, so a review of the data quality is not yet available.

Data File Contents

As of this writing, laboratory analysis of the tracer data is ongoing, so the data is not yet available on the THREDDS server. To get more information on the tracer data set, contact Stuart Pearson s.g.pearson@tudelft.nl or b.c.vanprooijen@tudelft.nl.

3.13 SONAR

General information

All Sonars used in this measurement campaign were of type 2001, produced by Marine Electronics. They were all mounted approximately 1 m above the bed (Figure 3.21). Sonar systems use reflection of sound waves, in this case of 1 MHz, which reflect from 'hard' substances such as the sea bed. Therefore, the reflection can be used to find the bed level.

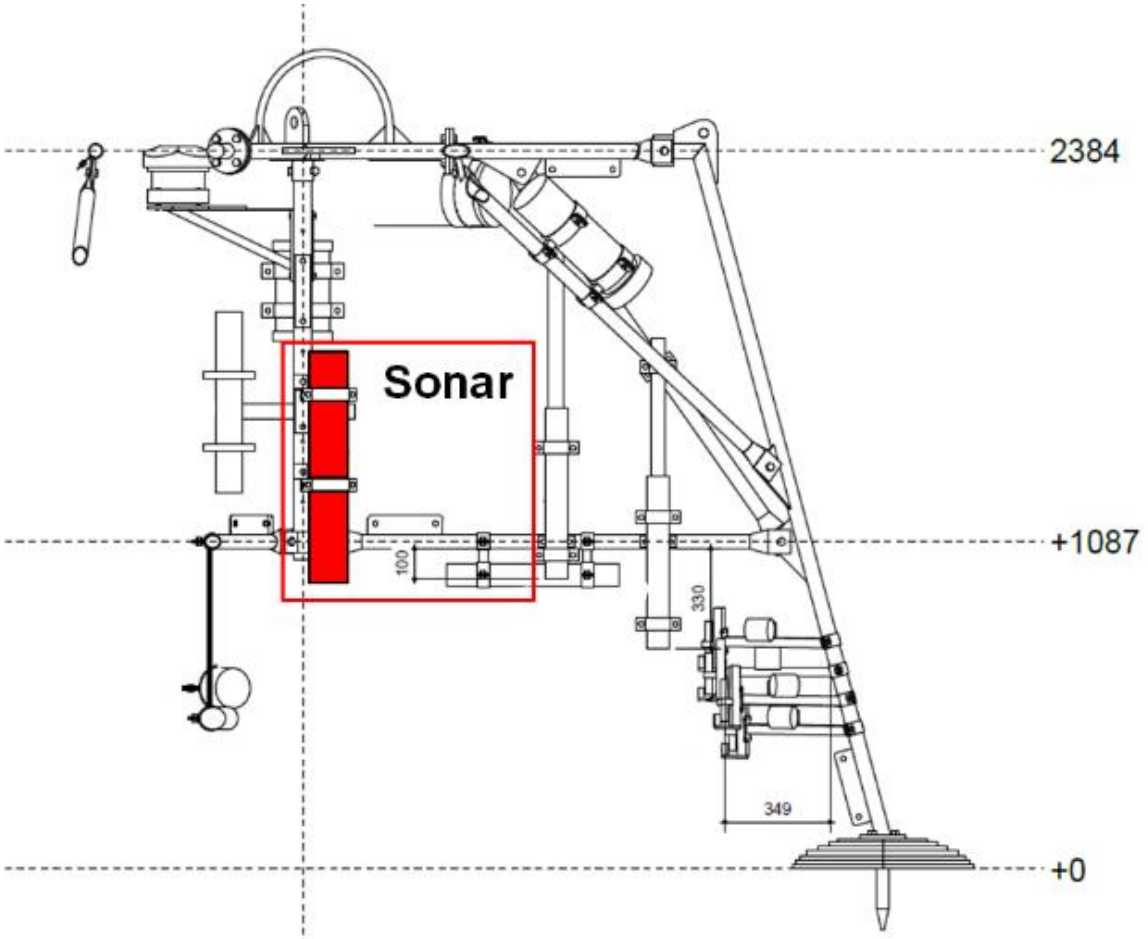

Figure 3.21 Design of frame featuring the 3D Sonar. The instrument (highlighted in red) is mounted on the centre of the frame pointing down, with the sensor at a design elevation of 1.00 m above the seabed. Actual height above the seabed varies slightly per frame due to assembly and field conditions.

All Sonars were set to have a swath arc of 150^{o} which is centred on the vertical axis, so 75^{o} in each horizontal direction (Figure 3.22). A single swath contained 166 vertical backscatter profiles, so the profiles are spaced 0.9^{o} apart. Each profile consists of 842 samples between 0 and 3.7845 m from the Sonar head, therefore the reflection values are 4.5 mm apart. In total 200 swaths were performed to cover a full circle, so the swath step size is 0.9^{o}. The measuring of a full circle takes approximately 15 minutes.

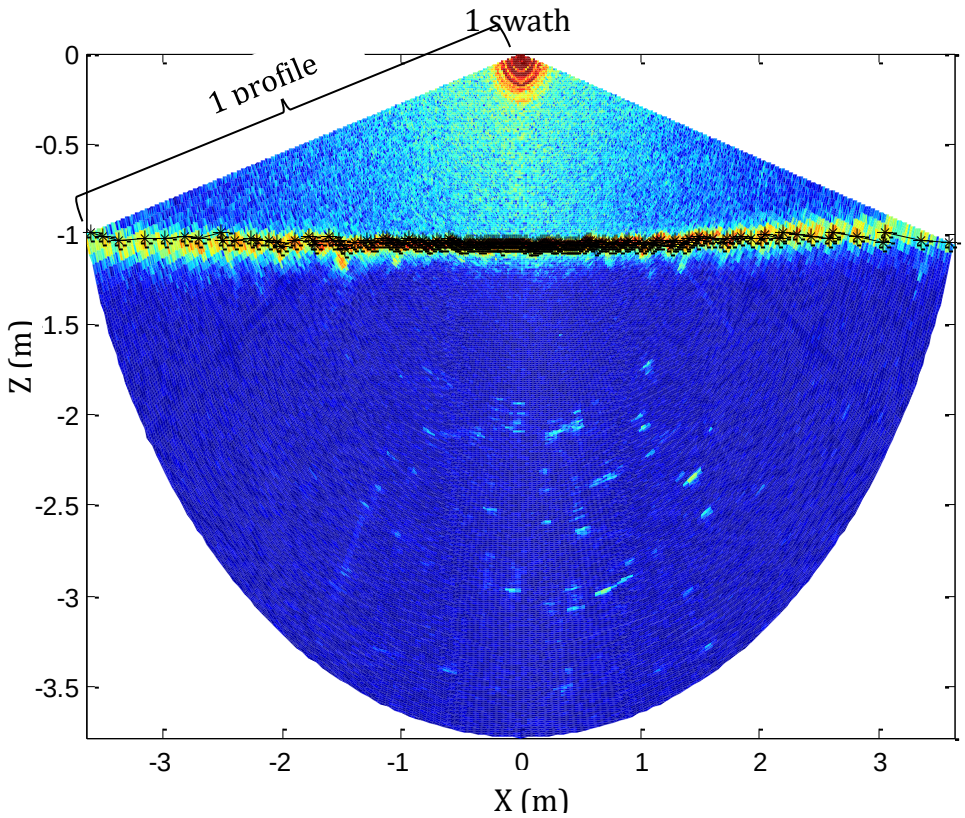

Figure 3.22. Intensity as measured by a Sonar for 1 swath.

Results are stored in one .RW2 file per scan, which contains 27 header lines in asci format, followed by the backscatter data in binary format.

The heading of the Sonar was not measured directly and therefore had to be calculated from other devices on the frame. When the heading of another instrument is known, this heading can be added to the heading of the Sonar. Heading here implies the direction of the '0' mark on the Sonar head and corresponds to the direction of the positive x-coordinate in the Sonar's own x-y-coordinate scheme.

This section discusses the processing steps to transform the raw data into bed levels. All example figures represent the Sonar data of Frame 1 of the Diepe Vooroever Ameland (DVA) campaign on the 9th of November 2017, 07:00. More detailed information can be found in Brakenhoff (2018).

Processing Step 1 – determine bed levels for each swath
Taking into account possible erosion scour holes, it was expected that the bed cannot become lower than twice the sensor height above the bed (~0.9m), so all data points below -1.8 m were considered to be noise. All backscatter data lower than the maximum of this noise area were removed. It was also assumed that the bed will not rise higher than half of the sensor height, so all points above -0.45 m were also removed. This excludes the high reflection around (x,z)=(0,0), which is due to a reflection of the sound waves on the glass Sonar head.

From the data points that remain, the maximum backscatter value was determined for each profile. A second-order polynomial smoothing over the 11 data points around this maximum

was found to lead to a slightly smoother bed level line than the actual maximum, so this smoothed maximum was used (given by the black crosses in Figure 3.22).

Processing Step 2 – conversion to local, Cartesian coordinates
The bed levels for all 200 swaths of one rotation are given in Figure 3.23, which has the same x-axis as Figure 3.22. At this point, the data are still in polar coordinates. These are converted to Cartesian coordinates. Subsequently, all bed elevation data points are put into an (*x*, *y*, *z*) matrix.

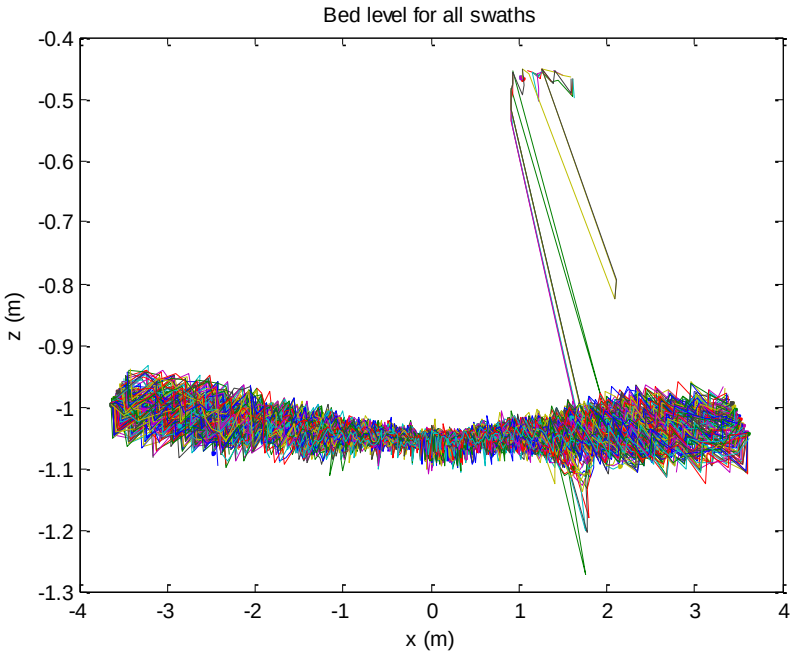

Figure 3.23 Bed levels for all 200 swaths of one rotation.

Processing Step 3 – removal of outliers
Outliers are removed based on a deviation from the median. Windows are created of 25x25 cm, and if a value within this window deviates more than 7 cm from the median, it is removed. This especially removes points from around the legs of the frame (Figure 3.24). The choice of the value of 7 cm (and all other code used in the SONAR data processing) was based on the Bardex II campaign, in which it was found that this 7 cm does not remove any ripples, but only 'true' outliers (Ruessink et al., 2015).

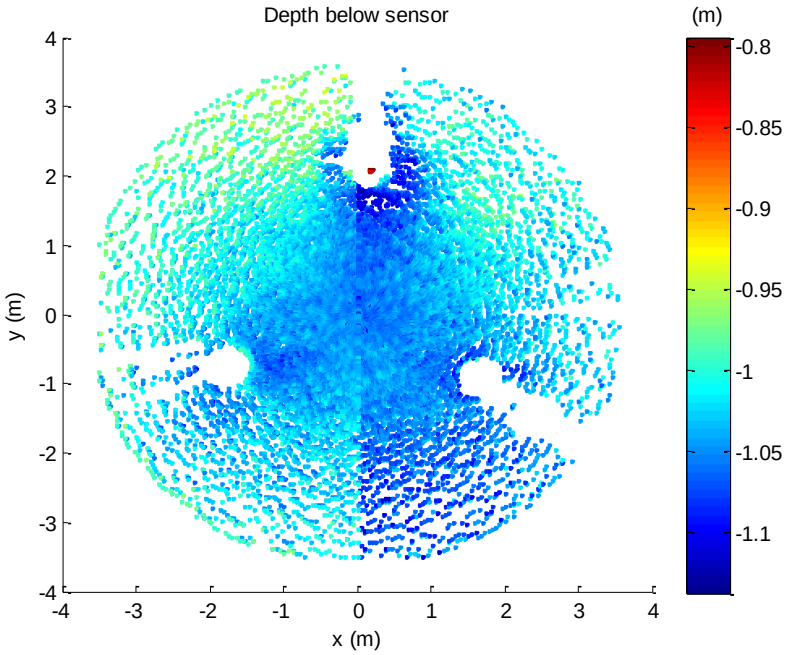

Figure 3.24. Depth without the outliers. The three round white spots correspond to the frame legs.

Processing Step 4 – interpolate to regular grid and remove mean to reveal ripples
The points left after step 3 were interpolated onto a regular grid, from -2.5 to 2.5 m in both *x*- and *y*-direction with a 0.01 m step size. Smoothing was performed with a LOESS filter. This filter uses smoothing length scales *lx* and *ly* (in m) to fill gaps; it removes more than 70% of the bedforms with length scales smaller than l*x*/0.7 and *ly*/0.7. Therefore, the chosen values for *lx* and *ly* should be smaller than the ripple length scale, otherwise ripples are moved as well. The LOESS interpolator also gives an estimation of the root-mean-square error of the interpolated grid. Depth values with a root-mean-square error larger than 0.01 m were removed. This removes points that were extrapolated, which happens when the distance between the measured points is larger than the LOESS length scales. That implies that mainly points at the outer edges of the grid ([x,y]<-2.5 and [x,y]>2.5 m) were removed, and that more points will be removed when a smaller LOESS filer scale is used. After smoothing, the mean was removed to eliminate the larger bed level changes like accretion. This left only the small-scale bedforms.

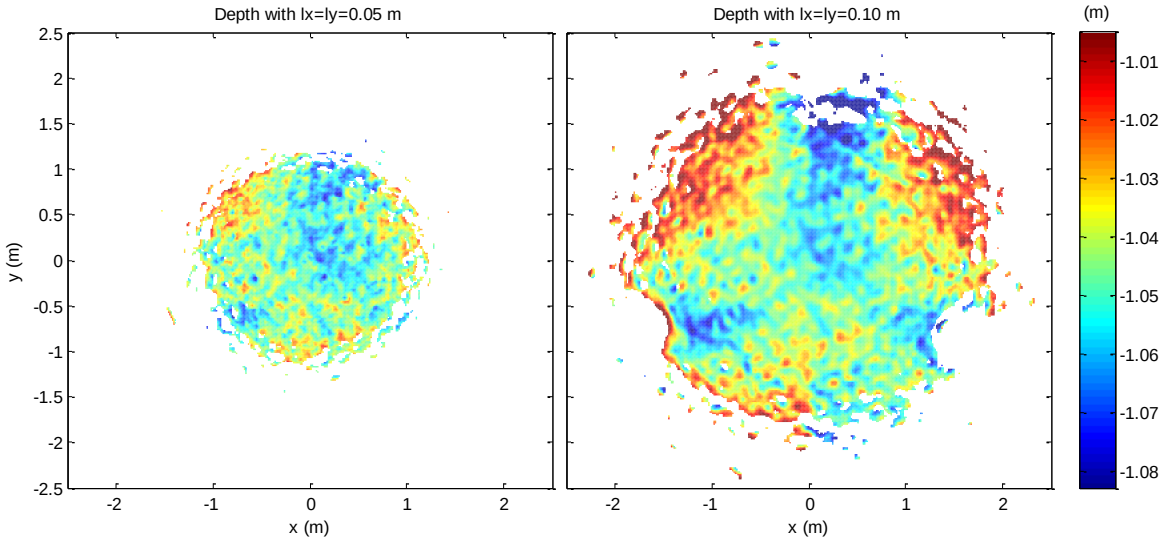

Figure 3.25. Final depth estimations as created with a LOESS filter of 0.05 m (left) and 0.10 m (right).

Processing Step 5 – rotate to ENU
The Sonar coordinate system works with a left-handed coordinate system, analogous to a N-E-S-W coordinate system. The (*x*,*y*) of the Sonar can thus be rotated easily to a N-E-S-W scheme using the rotation angles calculated earlier. No corrections were done for pitch and roll.

Processing Step 6 – saving as .mat and NetCDF, and making figures and movies
For each rotation, two mat-files are stored; one with the depth created with the 0.05 m LOESS filter and one with the depth created with the 0.10 m LOESS filter. File names contain the following elements: campaign name, frame number, position number (redundant), approximate depth of the frame, scale of the loess filter and date in yyyymmddHHMM. As an example, a typical filename looks like this: DVA_F1P1_Depth20_Filter05_201712010000. Information on the resulting data files can be found in Appendix E.13.

3.14 XBand radar

General information
In 2017 an operational system was installed at Ameland, which continuously processes radar images from a navigational X-band radar situated on top of the Ameland light house in order to make an estimate of the local bathymetry. The so called “depth inversion” was done with the XMFit algorithm, which is written in MATLAB code and was developed at Deltares.

The system returns about one estimate per hour, but this depends on the quality of the radar images at that point in time. Over the period October 2017 to September 2018 the system produced about 7000 estimates of which 3500 since the start of the construction of the pilot nourishment in the Ameland outer delta in March 2018. The output files containing the estimates are small enough to reach and transfer via a 4G connection with the local computer. The output files are locally available for 1-2 months after which they are replaced by new estimates, leaving some leeway for (re)analysis in case of system shutdown.

This section provides a concise description of the data-processing of the XBand radar. More detailed information can be found in the Gawehn (2018, in prep).

Workflow of XMFit

XMFit is a depth inversion algorithm (DIA) which exploits the fact that wave characteristics adapt to the local depth and surface currents. Hence, by analysing the waves in their spectral form an estimate can be made for the local depth and surface currents. In this case 256 consecutive images were merged in to a time stack (representative of 12 min) as basis for each estimate. For the purpose of gaining a high spatial resolution, a time stack was divided into smaller computational cubes. Via a 3D-FFT each cube is expressed in terms of a spectrum in wavenumber-frequency space, which directly provides information on the wave characteristics in that part of the radar image. The goal of XMFit is now to find the best match of the data with wave theory in order to estimate which depth and surface currents are most likely. This matching is done by non-linear least squares fitting of the Doppler shifted dispersion cone to the spectral data:

$$\omega = \sqrt{g\,|\boldsymbol{k}|\tanh\left(|\boldsymbol{k}|\,d\right)} + \boldsymbol{U}\cdot\boldsymbol{k} \tag{3.3}$$

Here ω [rad/s] denotes the radian frequency, d [m] the depth, $\boldsymbol{k}$ [rad/m] the wavenumber vector (k_x,k_y), $\boldsymbol{U}$ [m/s] the surface current vector (u,v) and g [m^2/s] the gravitational acceleration.

The process, visualized in Figure 3.26, produces hydrodynamic and morphological information for the time at which the stack of radar images was taken. Here we focus on the morphological results.

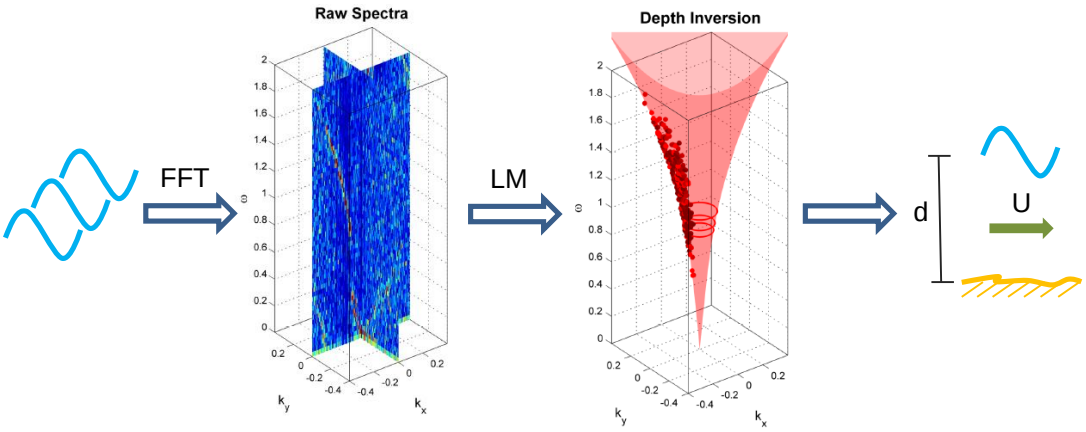

Figure 3.26 Workflow of XMFit. The wave field in a computational cube is first decomposed into a spectrum via 3D-FFT (blue cross sections, 2nd from the left). The energetic parts of the spectrum (red dots in red cone, 3rd from the left) are then fitted to the Doppler shifted dispersion cone (red cone). This is done via a Levenberg-Marquard (LM) minimization. The best fit includes an estimate of the local depth and surface current vector.

Data quality

The quality of the data depends on several factors:

1 The quality of the raw data is determined by the so-called sea clutter, which presents the waves in the radar image. It is caused by the reflection of the radar signal from capillary waves that ride on top of the sea waves. Although capillary waves are omnipresent, there shape and size depend on e.g. wind. An unfavourable shape and size of the capillary waves causes a bad sea clutter.

2 Physics:

a. The wave height is an important indicator for the quality of a depth estimate. If waves are too small (H_s < 0.9 m) they do not “feel” the bottom, which makes an estimate impossible, therefore they are not processed. If waves and/or wind speeds are too high, intensive white capping occurs which has also negative consequences for the estimate.
b. The angle between wave direction and surface current direction also influences the quality of the estimate.

Data selection

For quantification of the shape and behaviour of the pilot ebb shield nourishment at Ameland, a selection was made based on the data quality. This was done by looking at the bias of the depth estimate in the deeper parts of the inlet, where d > 15 m, using in-site measurements. The “bias of the deeper parts” appears to be a good indicator for the quality of an estimate, because the dispersion relationship is more sensitive for larger depths, see Figure 3.27.

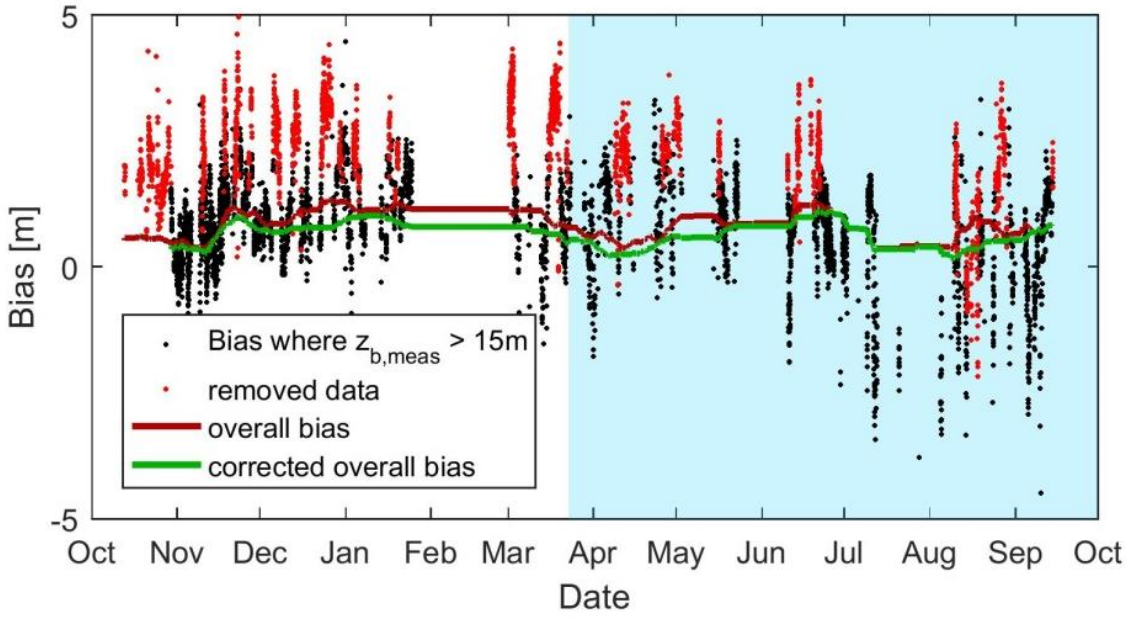

Figure 3.27 The bias as indicator for quality. A positive bias means that the depth is overestimated. For the calculation of the bias, XMFit estimates are compared to in-situ measurements from 2017.The average bias in the deeper parts of the radar domain, $z_{b,meas}$ > 15 m, is a good indicator for the quality of an estimate. Reason for this is the increased sensitivity at these larger depths. The “bias of the deeper parts” is shown for 6800 stacks produced between October 2017 and September 2018 (black scatter). Note that data were neglected based on all data points at depths larger than 15 m (and not just the average). These data are indicated in red. By doing so, also the overall bias improves (from dark red line to dark green line).

If no ground truth data were available, it is not straightforward to judge the quality of the radar estimates. It might be done through intercomparison of radar estimates themselves and/or by looking at confidence intervals of the non-linear fit.

Information on the resulting data files can be found in Appendix E.14.

3.15 Singlebeam bed survey Ameland

The singlebeam bed surveys were gridded by Wim Vissers of Rijkswaterstaat onto a 20m x 20 grid. For the dry beach and dune area LIDAR data was used and for the nearshore, shallow surf zone area, JARKUS data was used, both usually measured in spring of that year. Data was exported as Arc/INFO ascii file (*.asc) and provided to Deltares. Usually, a csv or xlsx file with metadata was provided, including exact dates. Sometimes screenshots of the Rijkswaterstaat MARIA application were provided that show the sailing tracks of the single beam survey. At the moment of writing of this report, the LOL database of Rijkswaterstaat is not accessible for Deltares

At Deltares, the files provided by Rijkswaterstaat with Kustgenese 2.0 single beam gridded bathymetric data are stored in a repository together with all the other Vaklodingen. Note that the raw data are not stored in the Kustgenese 2.0 repository with measurement data for the measurements campaigns, but in the Rijkswaterstaat repository with all other Vaklodingen data: https://svn.oss.deltares.nl/repos/openearthrawdata/trunk/rijkswaterstaat/vaklodingen/raw/grid/

The bathymetric data were then processed by Deltares and split into 10 x 12.5 km 'Kaartbladen' and written to NetCDF files that are available online through an Opendap server. Note that both the Vaklodingen, SBW and Kustgenese 2 data are all stored in the same Vaklodingen NetCDF files, but can be distinguished through the attribute isource.sourec, a 3-digit identifier in which 'VAK' stands for *Vaklodingen*, 'SBW' for *Sterkte en Belastingen Waterkeringen* and 'KG2' for *Kustgenese 2.0*.

Information on the resulting data files can be found in Appendix E.15.

3.16 Multibeam bed survey Ameland

Multi beam output and processed data was provided by Rijkswaterstaat to Deltares including *.pts files with corrected and referenced data. At Deltares, these pts files were interpolated (using inverse distant weighting) to 1m grid resolution for the data of Ameland inlet and to 0.5m for the data of the 'Diepe Vooroever'. Both the raw data provided by Rijkswaterstaat including *.pts files and interpolated grid files are stored in the 'raw' data folder within the Kustgenese 2 repository.

Information on the resulting data files can be found in Appendix E.16.

3.17 Bathymetric surveys pilot nourishment Ameland ebb-tidal delta

The bed surveys were gridded onto a 2 m x 2 m grid (multibeam data) and a 5 m x 5 m grid (singlebeam) by the contractor Van den Herik. Data is available as ASCII data; the metadata is available as CSV files. Data is also available at the LOL (*Landelijk Opslagsysteem Lodingen*) database of Rijkswaterstaat.

Information on the resulting data files can be found in Appendix E.15 and Appendix E.16.

3.18 Multibeam lower shoreface

Multibeam output and processed data was provided by Rijkswaterstaat to Deltares including *.pts files with corrected and referenced data. At Deltares, these pts files were interpolated (using inverse distant weighting) to a raster with 0.5 m resolution, for all six surveys (2 years, three areas). The raw multibeam data was used to create a backscatter-classification map for the 2017 Ameland measurement using algorithms from TU Delft.

Information on the resulting data files can be found in Appendix E.16.

3.19 Boxcores Ameland Inlet

A Reineck Boxcorer with a sample surface of 0.078 m^2 and a depth of 30 cm was used. Two datasets were derived from the boxcores. A sediment sample and a sample of the macro zoobenthic species. A detailed description of the preparation and handling of the samples is given in the field report (Verduin & Engelberts, 2017)

The macrozoobenthos samples were sent to the laboratory of Eurofins Aquasence in Amsterdam. In the laboratory the samples were coloured with Bengal rose 24 hours prior to the determination. First, excess sand and silt were washed away. Hereafter all organisms were handpicked from the sample and sorted into groups of worms, crustacea, bivalves or other species. Finally, the species were identified up to species level if possible. Abundance, Ash-free dry weight was determined of each species per sample. For the bivalves, the length of the shell is measured.

The sediment samples of the top 8 cm of the boxcore were frozen on board of the research vessel and sent to Gent University. The grainsize distribution was determined using a Malvern Mastersizer. The organic matter and calcium particles were not removed from the sample. Organic matter was determined at 550 and 800 degrees Celsius.

Information on the resulting data files can be found Appendices E.17 and E.18.

3.20 Vibrocores and boxcores lower shoreface

Both the vibrocores and the boxcores from 2017 were taken at specified coordinates in the three study areas by Marine Sampling Holland and delivered to Deltares in pvc-liners. These liners were opened, photographed, sampled and described in the lab. Sediment samples were analysed with a Malvern analysis.

The 2018 boxcores were processed by Deltares onboard the sampling vessel Arca. The cores were photographed, sampled and described, for a subset of the cores a lacquer peel was made. Sediment samples were analysed with a Malvern analysis.

Information on the resulting data files can be found Appendices E.19 and E.20.

3.21 Fish

The catch on vessel from each tow was emptied into a bucket, photographed and any sandeels present were retained. The sandeels from each dredge were removed from the sample, put into a polythene bag labelled with station, date and survey type, sealed with cable ties and frozen for subsequent onshore species identification, otoliths for age determination, numeration, length and biomass analysis by Wageningen Marine Research. All bycatch species were identified, counted, measured and returned to the sea. A CTD probe was used to record temperature and salinity depth profiles at approximately every tenth tow location. The logbook of the 2017 sampling is shown in Table 3.5. All fish data (e.g. location, number, length weight, otoliths, bycatch, benthos, shells) are stored.

Table 3.5 Logbook of the September 2017 sandeel sampling campaign. (in Dutch)

Locatie	dag	tijd	y_start	x_start	y_eind	x_eind	lat_s	long_s	lat_e	long_e	Bevist	diepte	temp_b	cond_b
A1_1	18	2054	53.482888	5.5922184	53.480197	5.5919662	53.48083	5.5919	53.48188	5.59225	120	8.9	16.3	5.1
A1_2	18	1955	53.474762	5.5887991	53.472070	5.5885472	53.47235	5.58855	53.47338	5.58843	120	8.8	15.97	5.09
A1_3	19	2137	53.454024	5.5914757	53.451538	5.5932214	53.45343	5.59235	53.45228	5.59312	176	23.2	15.79	5.12
A1_4	19	2219	53.437801	5.6039700	53.435315	5.6057144	53.4369	5.60462	53.43595	5.60513	132	22.8	16.04	5.08
A2_1	19	1856	53.456680	5.5559111	53.456082	5.5603145	53.45617	5.56022	53.4567	5.55855	133	12.6	16.32	5.11
A2_2	19	1824	53.455529	5.5664435	53.454931	5.5708467	53.45502	5.57062	53.4553	5.56873	136	12.3	16.23	5.07
A2_3	18	1922	53.469141	5.5797775	53.466634	5.5814365	53.4675	5.5801	53.46857	5.58005	100	10.4	16.37	5.1
A2_3	18	1933					53.46735	5.58033	53.46825	5.58012	103	10.5	16.39	5.1
A2_4	18	1828	53.465552	5.5824491	53.463045	5.5841078	53.46283	5.584	53.46375	5.58417	110	11.1	16.11	5.07
B1_1	18	2245	53.484832	5.5574525	53.483845	5.5616575	53.4848	5.56032	53.48563	5.56213	153	2.7	16.09	5.04
B1_2			53.482708	5.5651480	53.481293	5.5689940								
B2_1	19	1932	53.463151	5.5603767	53.463956	5.5646872	53.4636	5.56373	53.46337	5.56182	157	7.4	16.43	5.14
B2_2			53.464098	5.5681031	53.464382	5.5725949								
C1_1	21	2225	53.493543	5.5374412	53.494973	5.5412723	53.49478	5.53982	53.49425	5.53843	115	11		
C1_2	21	2318	53.487837	5.5196206	53.489165	5.5235533	53.48862	5.5219	53.4881	5.52065	106	10.5		
C2_1	21	2250	53.493493	5.5305104	53.494775	5.5344864	53.49405	5.53265	53.49373	5.53123	103	11		
C2_2	21	2345	53.487937	5.5123811	53.489305	5.5162749	53.4884	5.51298	53.4888	5.51432	107	11		
D1_1	21	1904	53.501876	5.6327712	53.501577	5.6372642	53.50178	5.63565	53.50227	5.63455	95	8.3	16.31	5.11
D1_2	21	2023	53.503361	5.6163454	53.503063	5.6208386	53.5031	5.62072	53.50325	5.61922	117	8.5		
D2_1	21	1840	53.498697	5.6437027	53.498131	5.6481223	53.49802	5.64852	53.49813	5.6471	120	16.2	16.24	5.08
D2_2	21	1820	53.495752	5.6638328	53.494928	5.6681369	53.49555	5.66598	53.49617	5.66515	106	7.2	16.19	5
E1_1	18	2136	53.467364	5.6125390	53.470044	5.6130295	53.46837	5.61288	53.46967	5.61168	147	3.7	15.81	4.96
E1_2			53.474674	5.6143847	53.477354	5.6148755								
E2_1	18	2114	53.475345	5.6064515	53.478025	5.6069418	53.4767	5.60573	53.47822	5.60645	186	5.5	16.16	5.07
E2_2			53.466159	5.6051475	53.468838	5.6056376								
F1_1	21	2157	53.502660	5.5460236	53.503414	5.5503644	53.50337	5.54905	53.50322	5.54742	113	15		
F1_2			53.498371	5.5217263	53.499307	5.5259654								
F2_1	19	142	53.509404	5.6112312	53.509460	5.6157518	53.50942	5.61453	53.50928	5.6106	262	12.5	16.12	5.11
F2_2	21	1943	53.509289	5.6279974	53.509345	5.6325180	53.50953	5.6324	53.50955	5.63093	106	14.4	16.4	5.14
X1_1	19	2021	53.478676	5.5328817	53.481369	5.5327172	53.4792	5.5324	53.4802	5.54925	162	7.1	16.56	5.18
X1_2	19	2008	53.474517	5.5367284	53.476411	5.5335151	53.47467	5.5365	53.47545	5.53492	244	6.8	16.52	5.16
X1_3	19	2038	53.476204	5.5234630	53.478696	5.5251859	53.47605	5.52403	53.47712	5.52318	155	7.9	16.57	5.18
X2_1	18	2340	53.495557	5.5614096	53.495657	5.5568925	53.49567	5.56077	53.49568	5.55903	218	6.3	16.06	5.05
X2_2	18	2300	53.491082	5.5608889	53.491086	5.5563692	53.49123	5.5601	53.49127	5.5567	225	6.4	16.08	5.03
X2_3	21	2117	53.498573	5.5632218	53.498576	5.5587013	53.49858	5.56313	53.49878	5.56165	107	8		
X3_1	18	2205	53.495022	5.5753741	53.494667	5.5798548	53.49477	5.57948	53.49503	5.5777	130	5.7	15.92	5.03
X3_2	18	2220	53.494494	5.5651070	53.494140	5.5695878	53.49447	5.56852	53.49462	5.56565	183	6	15.81	5
X3_3			53.491314	5.5684248	53.491077	5.5729269								
X4_1	19	58	53.498963	5.5789081	53.498885	5.5834268	53.4991	5.5822	53.4991	5.57898	214	3.7	15.48	4.93
X4_2	19	118	53.499945	5.5903779	53.499278	5.5947579	53.49928	5.59385	53.49993	5.59077	220	3.4	15.66	4.93
X4_3	21	2057	53.502668	5.5809462	53.502700	5.5854668	53.50275	5.58522	53.50275	5.58368	105	5.5		

4 Results

4.1 Introduction

The chapter contains example measurement results. The figures are aimed to illustrate the occurring hydrodynamic conditions, and the data richness and quality. The following plots will be shown:

- 1 time-series plot of depth-averaged velocities (based on ADCP data) per measurement campaign and water depth as function of wind and wave conditions
- at least 1 time-series plot per instrument

4.2 Hydrodynamics

ADCP

Figure 4.1 - Figure 4.5 shows the depth-averaged velocities and water depths based on the ADCP measurements at Frame 3 (AZG) and Frame 1 (DVA, DVT1, DVT2, DVN), as well as the wind and wave conditions from a nearby station. Only wave data of stations part of the KG2 project were visualized. These figures show the following:

- AZG-F3. The ADCP functioned well during most of the measurement period. The pressure sensor did not function between 11 and 18 September 2017. The frame was serviced on 19 September 2017, and the frame was put back again in more shallow water. There was a westerly storm on 13 September 2017 with wind velocities of ~20 m/s (Beaufort scale 8/9), and offshore wave heights of ~6 m.
- DVA-F1. The ADCP functioned well during the measurement period. Wind velocities were lower than 17 m/s (Beaufort scale 7 and lower). Yet, there were multiple high wave events (H_s > 5 m), most notably on 18/19 November and 8/9 December 2017.
- DVT1-F1. The ADCP functioned well during the measurement period. There were no storms and significant wave heights remained below 4 m. Therefore, a second Terschelling campaign was carried out.
- DVT2-F1. This 2-week measurement campaign was relatively short compared to the others. The ADCP functioned well. An easterly storm with wind velocities up to 20 m/s occurred on 17 March 2018, with offshore wave heights of ~5 m.
- DVN-F1. The ADCP functioned well. There was a westerly storm on 1 May 2018 with wind velocities up to 20 m/s.

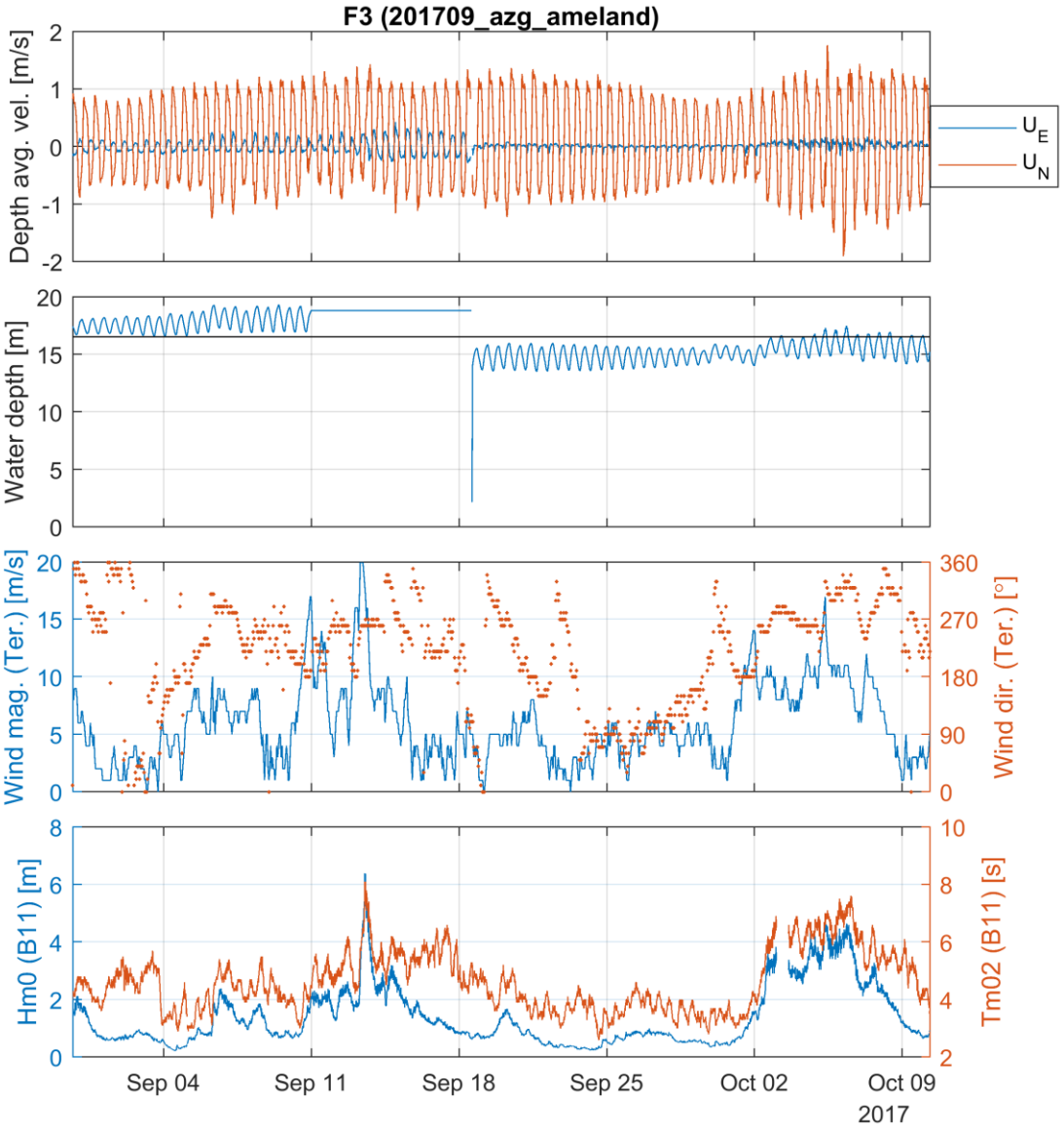

Figure 4.1 Measured hydrodynamics during the AZG campaign at Frame 3. The top panel shows the depth-averaged velocities measured by the ADCP directed to the East (UE) and North (UN). Periods of without measurements (half an hour each hour), are simply interpolated to enhance readability. The second panel shows the related water depths (relative to the bed), with the mean water depth indicated by the solid line. The third panel indicates the wind velocities and directions (in degrees from north, indicating where the wind is originating from) measured at the nearby KNMI station (Ter. is an abbreviation for Terschelling). The fourth panel show the wave height and direction measured at the nearby station AZB11 (see Figure 2.3).

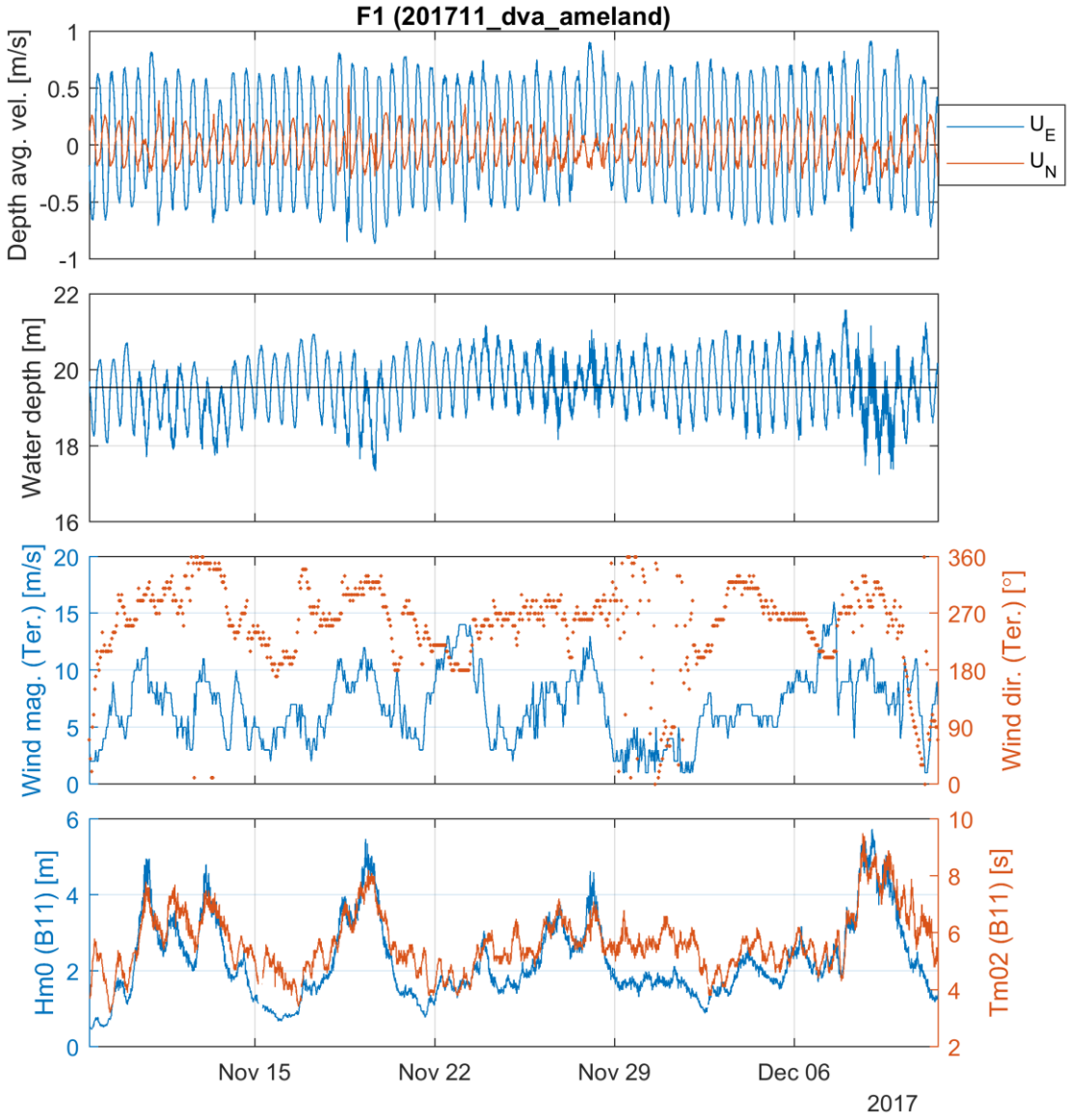

Figure 4.2 Measured hydrodynamics during the DVA campaign at Frame 1. The top panel shows the depth-averaged velocities measured by the ADCP directed to the East (UE) and North (UN). Periods of without measurements (half an hour each hour), are simply interpolated to enhance readability. The second panel shows the related water depths (relative to the bed), with the mean water depth indicated by the solid line. The third panel indicates the wind velocities and directions (in degrees from north, indicating where the wind is originating from) measured at the nearby KNMI station (Ter. is an abbreviation for Terschelling). The fourth panel show the wave height and direction measured at the nearby station AZB11 (see Figure 2.3).

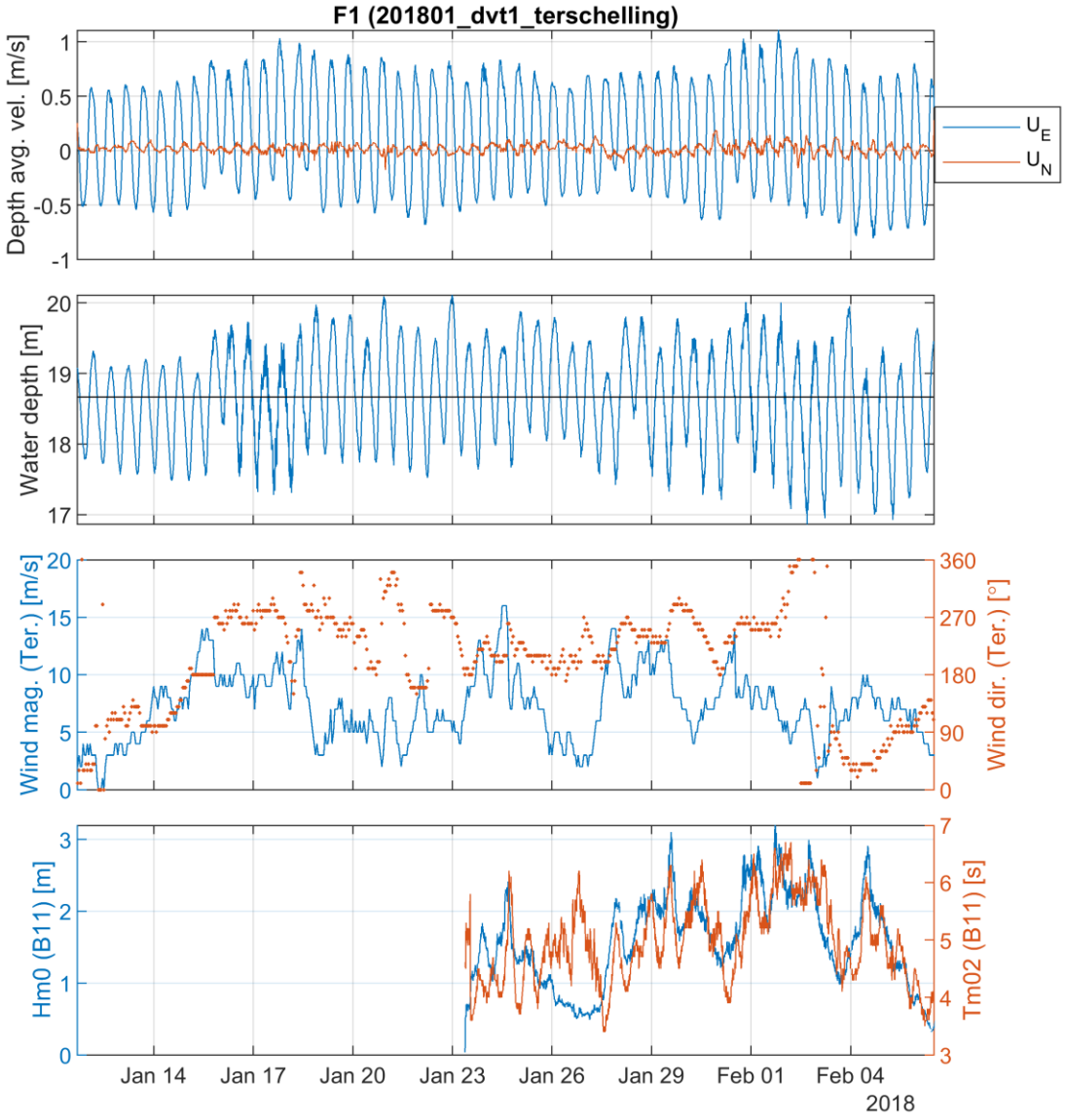

Figure 4.3 Measured hydrodynamics during the DVT1 campaign at Frame 1. The top panel shows the depth-averaged velocities measured by the ADCP directed to the East (UE) and North (UN). Periods of without measurements (half an hour each hour), are simply interpolated to enhance readability. The second panel shows the related water depths (relative to the bed), with the mean water depth indicated by the solid line. The third panel indicates the wind velocities and directions (in degrees from north, indicating where the wind is originating from) measured at the nearby KNMI station (Ter. is an abbreviation for Terschelling). The fourth panel show the wave height and direction measured at the nearby station AZB11 (see Figure 2.3).

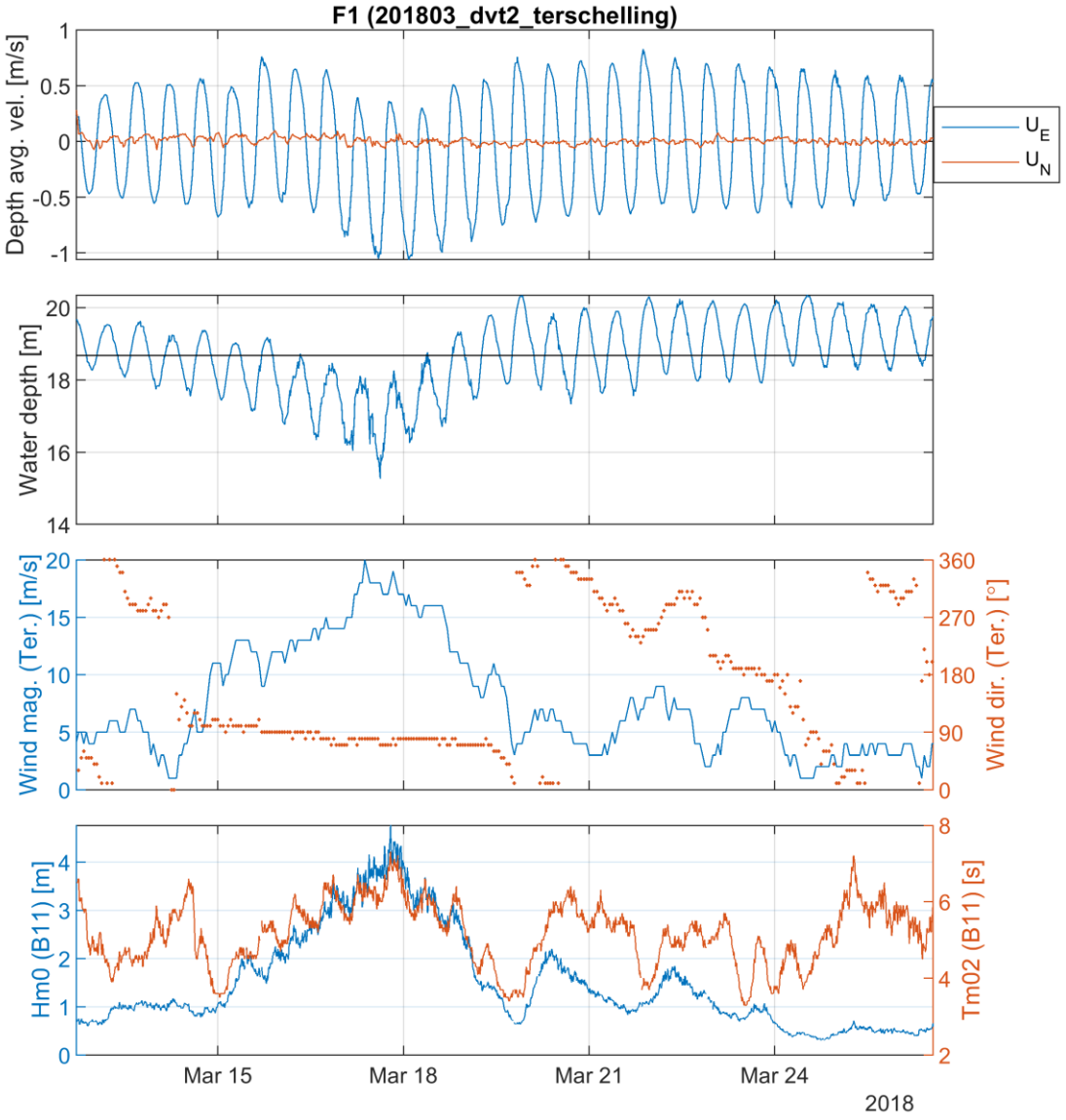

Figure 4.4 Measured hydrodynamics during the DVT2 campaign at Frame 1. The top panel shows the depth-averaged velocities measured by the ADCP directed to the East (UE) and North (UN). Periods of without measurements (half an hour each hour), are simply interpolated to enhance readability. The second panel shows the related water depths (relative to the bed), with the mean water depth indicated by the solid line. The third panel indicates the wind velocities and directions (in degrees from north, indicating where the wind is originating from) measured at the nearby KNMI station (Ter. is an abbreviation for Terschelling). The fourth panel show the wave height and direction measured at the nearby station AZB11 (see Figure 2.3).

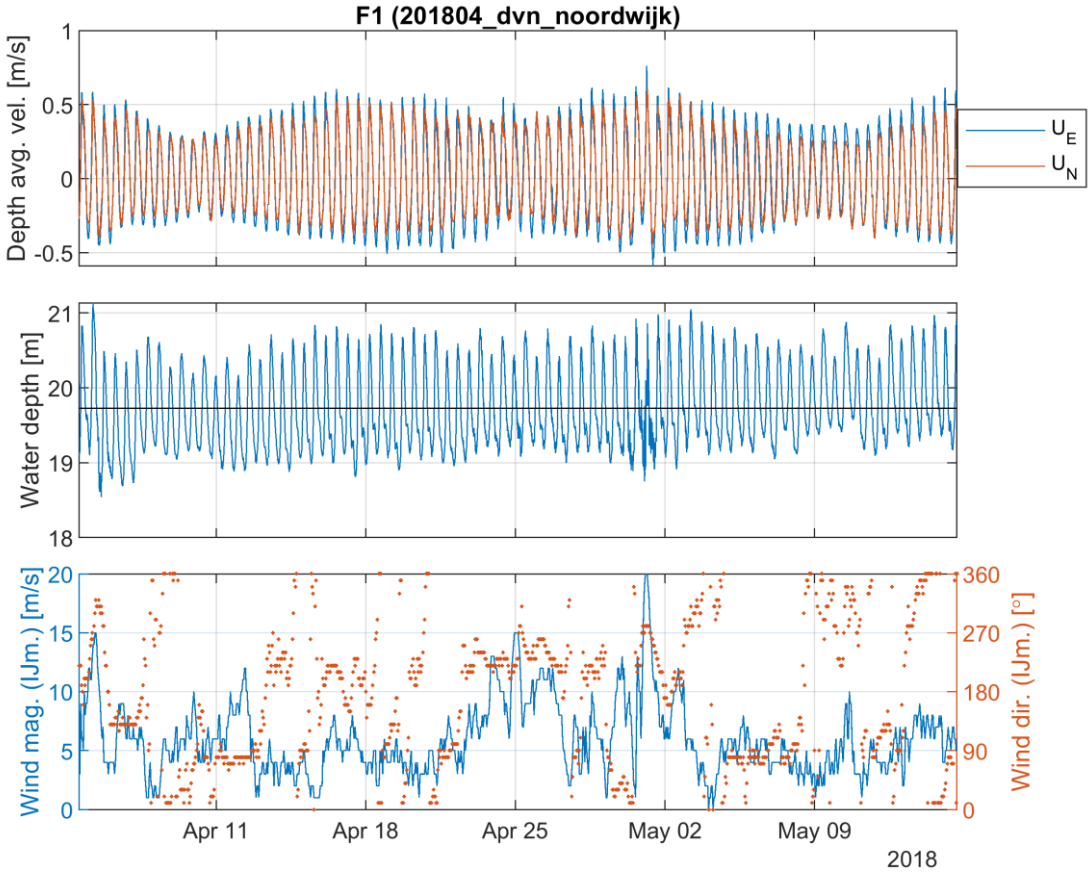

Figure 4.5 Measured hydrodynamics during the DVN campaign at Frame 1. The top panel shows the depth-averaged velocities measured by the ADCP directed to the East (UE) and North (UN). Periods of without measurements (half an hour each hour), are simply interpolated to enhance readability. The second panel shows the related water depths (relative to the bed), with the mean water depth indicated by the solid line. The third panel indicates the wind velocities and directions (in degrees from north, indicating where the wind is originating from) measured at the nearby KNMI station (Ter. is an abbreviation for IJmuiden). Wave data has not been measured at a nearby wave gauge, within this project.

ADCP HR - Frames

Figure 4.6 shows velocity profiles measured by the ADCP (upper part of the water column) and ADCP-HR (near the bed) at AZG Frame 1 at four instants on 4 September 2017 during an average tide with calm conditions (see Figure 4.1). It shows that peak ebb velocities are in WNW direction and peak flood velocities are in ESE direction. The near-bed ADCP-HR velocities are generally smaller than the ADCP velocities measured higher in the water column due to bed friction. Furthermore, this figure shows that the ADCP-HR and ADCP velocity profiles align nicely.

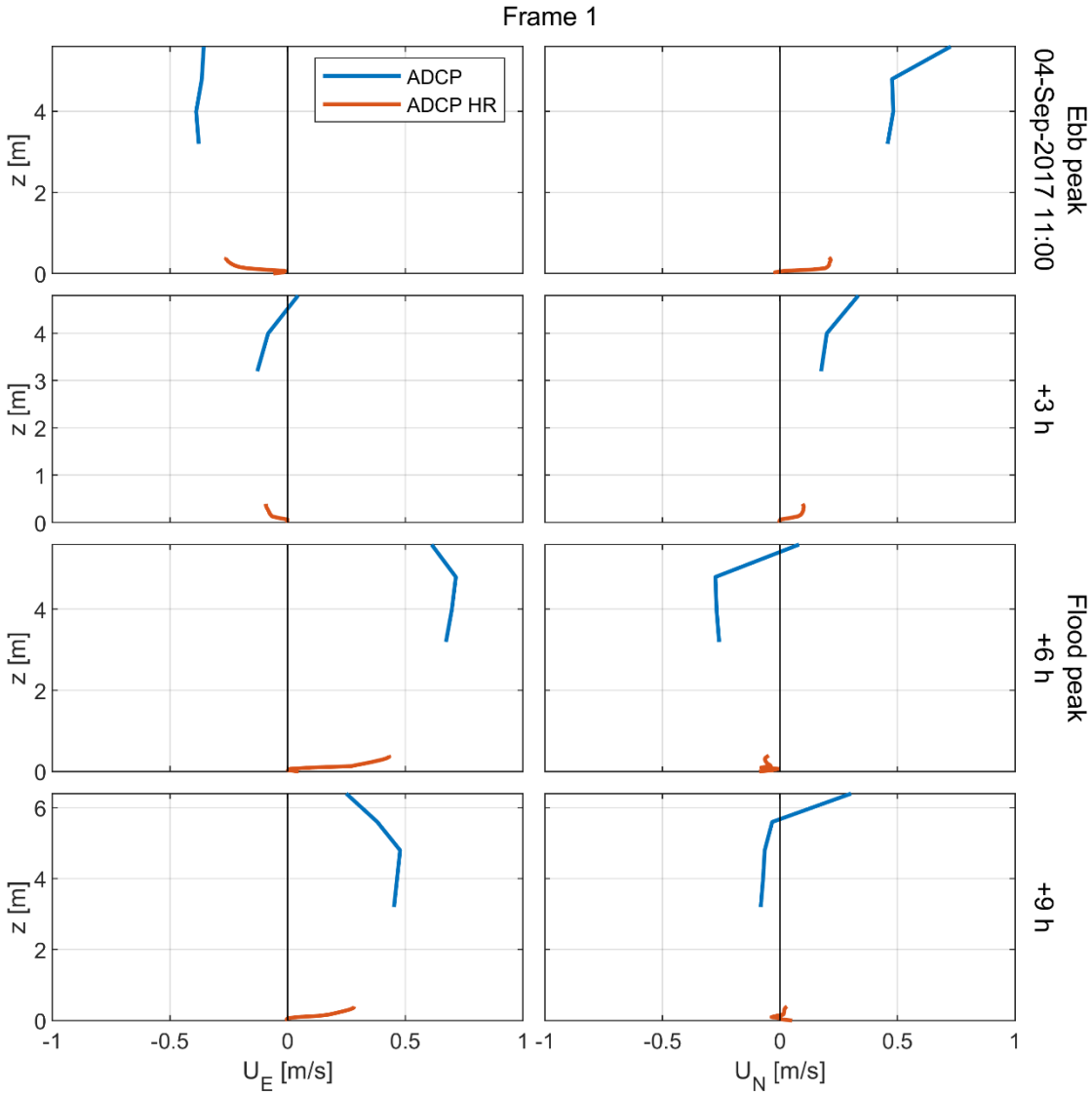

Figure 4.6 Flow velocity profiles over the water column measured with the ADCP (top part of the water column) and the ADCP-HR (bottom part of the water column) at Frame 1 of the AZG campaign. The left panels show the velocity in eastward direction, the right panels show the velocity in northward direction. The top panels show the velocities during an ebb peak (date and time are indicated on the right). Every successive row is 3 hours later in time.

ADCP - Watersheds

An example of a typical velocity signal from an upward looking ADCP mounted on the watershed is shown in Figure 4.7. The ADCPs capture regular tidal fluctuations as well as storm events where water levels and velocities on the watersheds increase (e.g. on 13 September).

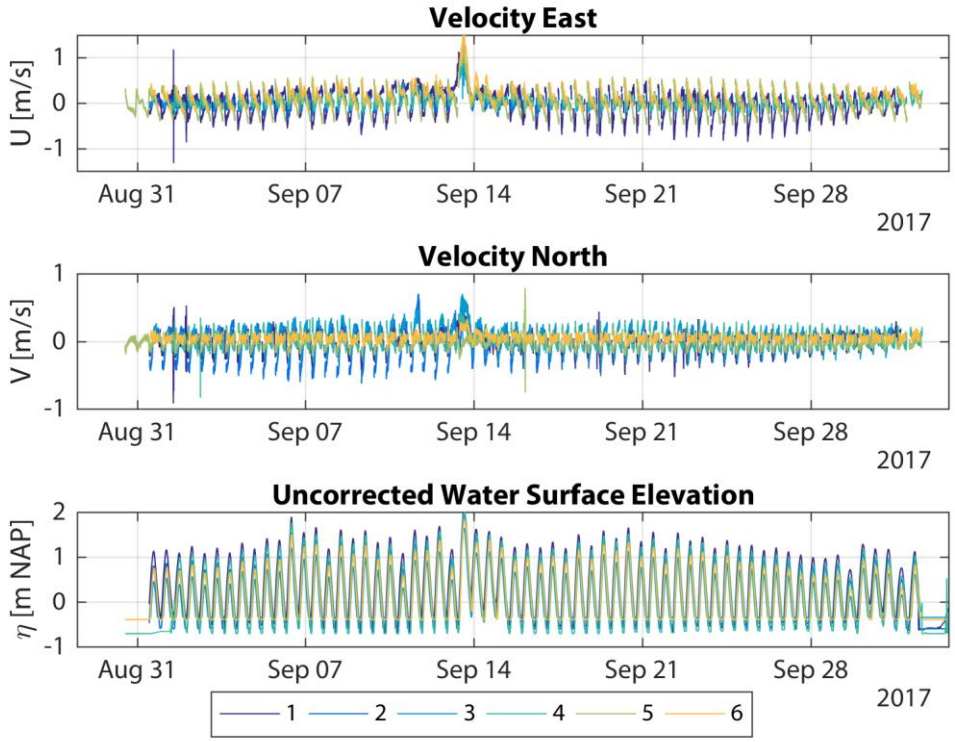

Figure 4.7 Example output from the ADCP-HR instruments installed on the tidal watersheds. The despiked east and north velocity components for each location (AmID1-6) are shown in the upper and middle plot. The lower panel indicates the water surface elevation relative to NAP, as determined from the pressure sensor but uncorrected for atmospheric pressure signal.

ADV

Figure 4.8 shows ADV01 velocities measured at DVT1 Frame 1. This ADV was positioned about 0.65 m above the initial bed. The top panel shows the complete time-series, the middle panel zooms in on 1 day, and the lower panel zooms in on 30 s during that day. The figures show that the velocities have a dominant E-W direction with peak velocities up to ~2 m/s during the storm on 18th of January.

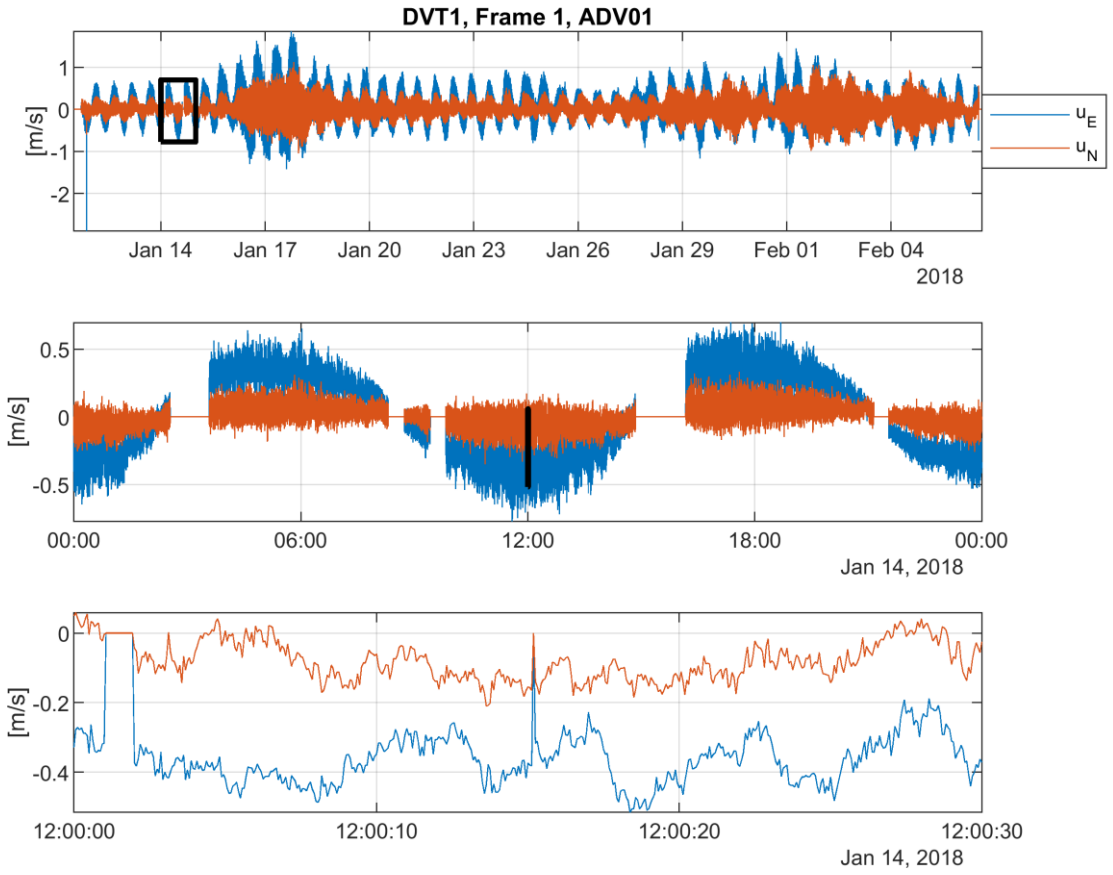

Figure 4.8 ADV01 velocity measurement at Frame 1 during the DVT1 campaign. This ADV was positioned about 0.65 m above the initial bed. The top panel shows the complete time-series, the middle panel zooms in on 1 day, and the lower panel zooms in on 30 s during that day.

Moving boat ADCPs

Discharge and sediment flux measurements, derived from the ADCPs on the moving boats (see Section 3.5), are presented in Figure 4.9. The 1st of September 2017 was representative for a neap tide, the 18th/19th of September 2017 for a spring tide, and the 5th of September 2017 had a tidal range in between the tidal range of the two other measurement days (see Figure 4.1). This also appears from the differences in measured discharges (peak discharges were in the order of 20–30 x 10^3 m^3/s) and even more in the sediment fluxes (with peaks values of 500-1200 kg/s).

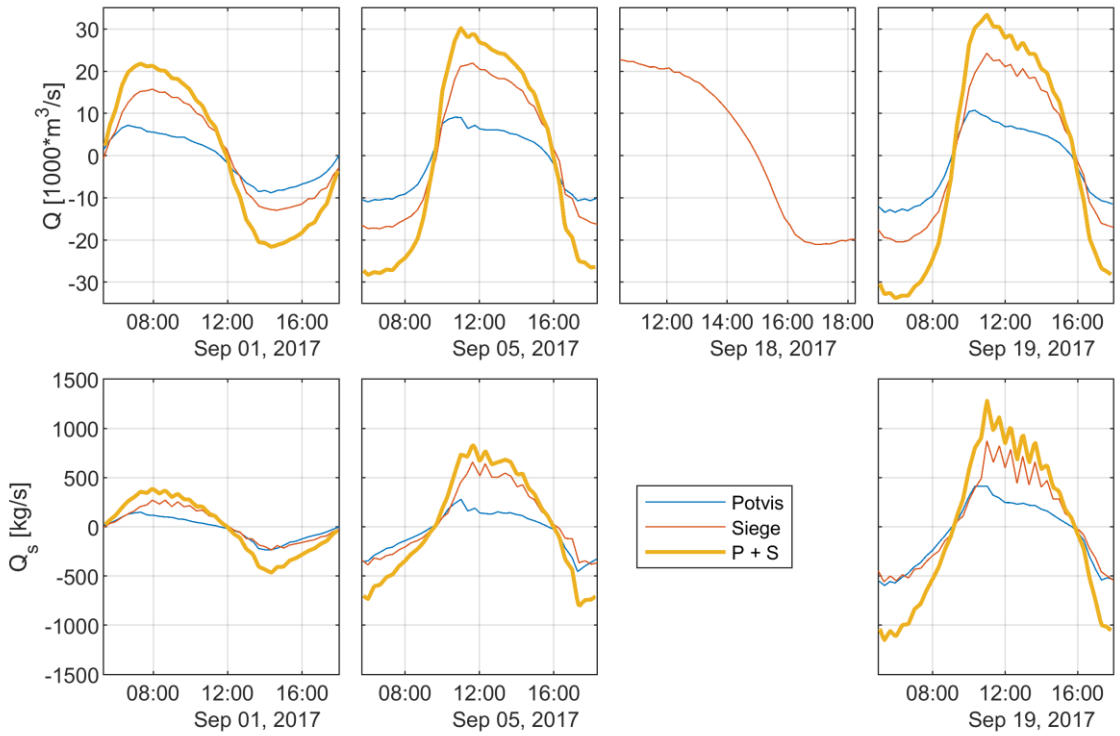

Figure 4.9 Discharge and sediment flux measurement data. Every measurement day (September 1st, 5th, 18th and 19th) is indicated in an individual window. On September 18 Section D was sailed, and on the other dates Section A-C (see Figure 2.5). The discharges and sediment fluxes for Section A-C are presented for each of the two parts of the transect, sailed by either the Potvis (AQVPO in Figure 3.9) or the Siege (RWSS1 in Figure 3.9). Also, the total discharges are indicated (P + S), as the sum of both measurements. The discharge is positive with flow from the Wadden Sea towards the North Sea (i.e., positive in ebb direction). There were no sediment fluxes determined for Section D.

Drifters

Two types of drifter deployments were performed during the AZG campaign, of which the results are shown in Figure 4.10 and Figure 4.11.

- For the large-scale deployment on 9 September (Figure 4.10), it can be seen that the drifters are able to follow the tidal flow for a full tidal cycle going in the basin and out of the inlet again. This can be used to analyse large-scale flow patterns.
- For the small-scale deployments (Figure 4.11), the tidal flow at the outside of the ebb channel is studied in small spatial and temporal scales. It is observed that drifters are a useful tool to visualise spatial and temporal changes in current magnitude (colour) and direction (arrows).

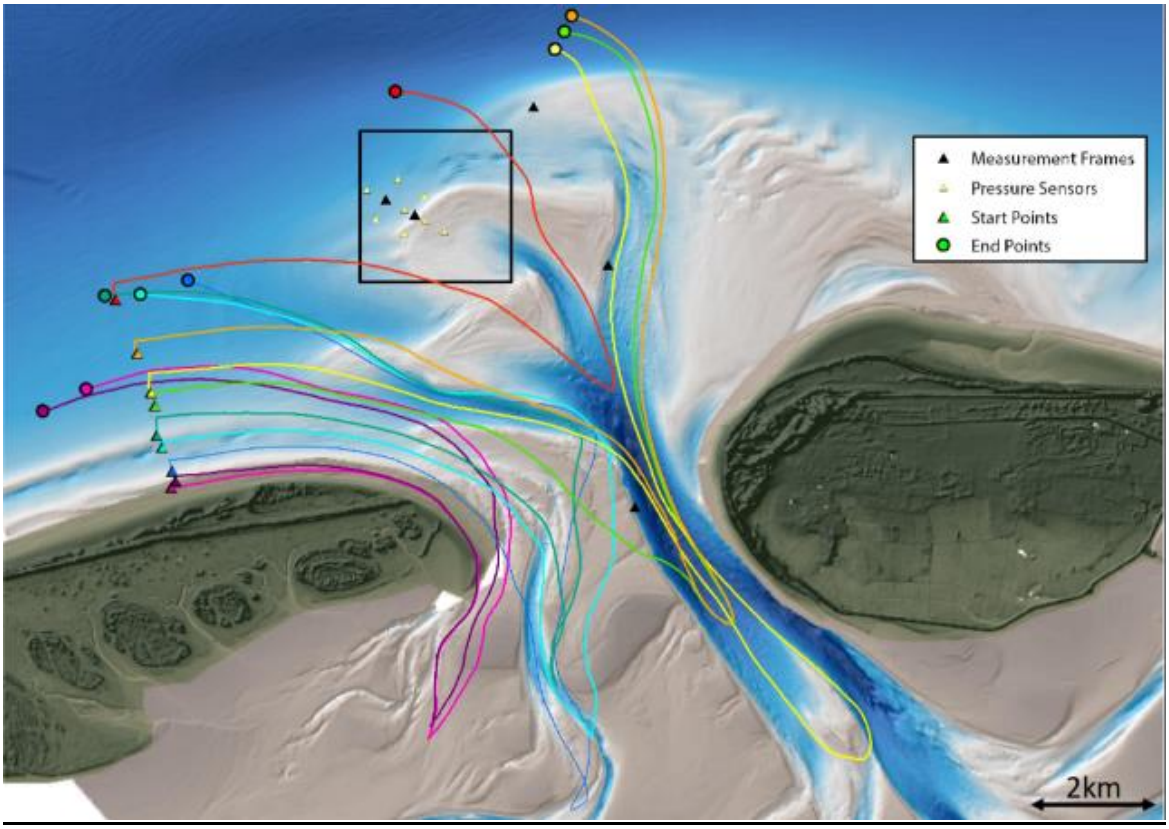

Figure 4.10 Large scale drifter data results. GPS tracks of the large-scale deployment on 9 September 2017 are shown. They are deployed in a 3km long line north of Terschelling (triangles) and retrieved at different locations (circles).

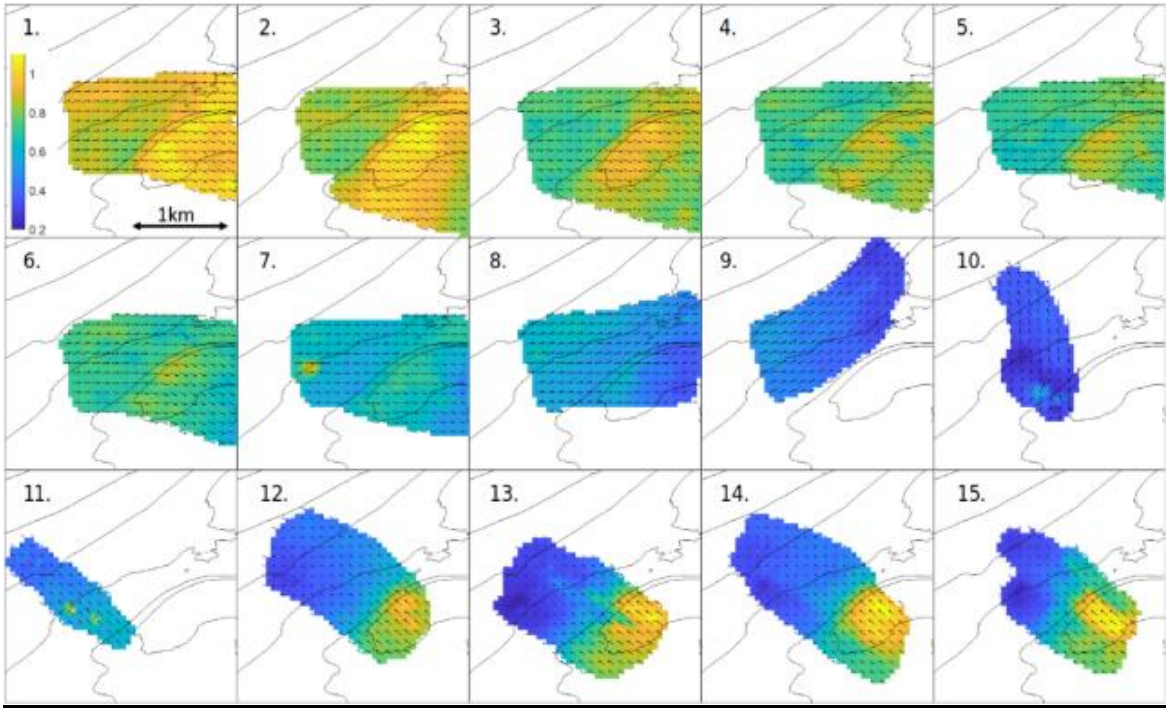

Figure 4.11 Small scale drifter data results. Velocity magnitude (colours) and directions (arrows) of 15 subsequent drifter deployments on 9 September 2017 are shown in the different panels.

Pressure sensors

Figure 4.12 shows an example time series of one of the stand-alone pressure sensors. The pressure was measured by PS05, deployed 30 cm above the bed during the AZG campaign.

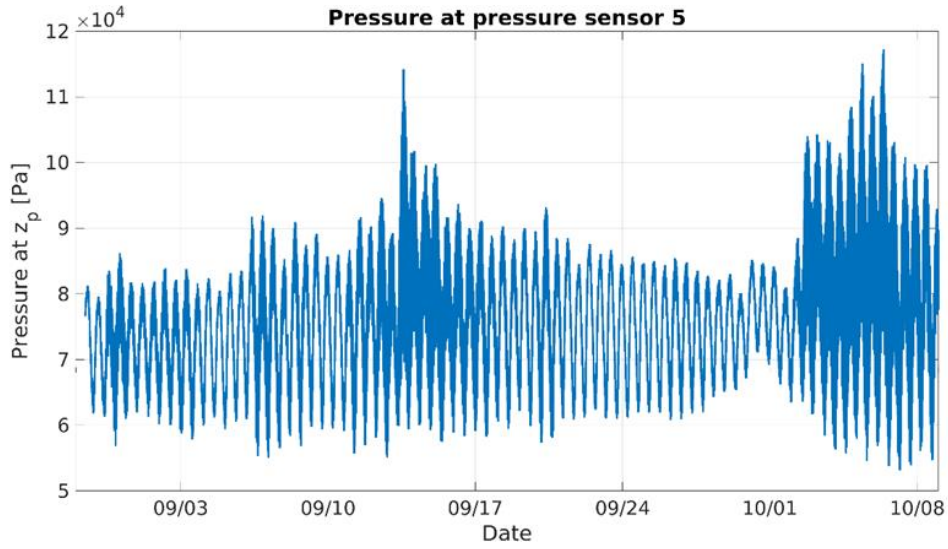

Figure 4.12 Pressure signal (sensor 5, 0.3 m from the bed) during the AZG campaign, 29 August – 8 October 2017.

4.3 Suspended matter

This section does not include OBS data results, as concentrations are too spiky (Section 3.10).

LISST

An example of the output from the LISST at Frame 4 AZG is given in Figure 4.13. This figure shows the total volumetric concentration, the concentration as a function of grain size, the Laser transmission, the battery voltage, the Laser reference sensor, the pressure, the temperature, the optical transmission over path, and the beam attenuation.

The critical thresholds for optical transmission specified in Section 0 indicate whether the LISST data is usable for a given time step. The fraction of the total recorded time when each LISST had an optical transmission value exceeding those thresholds is presented in Table 4.1.

Table 4.1 Fraction of total LISST time series with Optical Transmission exceed acceptable thresholds. Data points when transmission < 0.3 are unreliable, and those with transmission >0.995 or <0.1 must be discarded. Entries marked with a dash (-) indicate that the instrument was not functioning.

		Fraction of Time when Optical Transmission Exceeds Threshold		
Campaign	**Frame**	**>0.995**	**<0.30**	**<0.10**
AZG	3	0.00	0.416	0.242
	4	0.00	0.112	0.031
	5	-	-	-
DVA	1	-	-	-
	3	0.00	0.201	0.142
DVT1	1	-	-	-
	3	0.00	0.072	0.027
DVT2	1	-	-	-
	3	0.00	0.521	0.339
DVN	1	-	-	-
	3	0.00	0.068	0.020

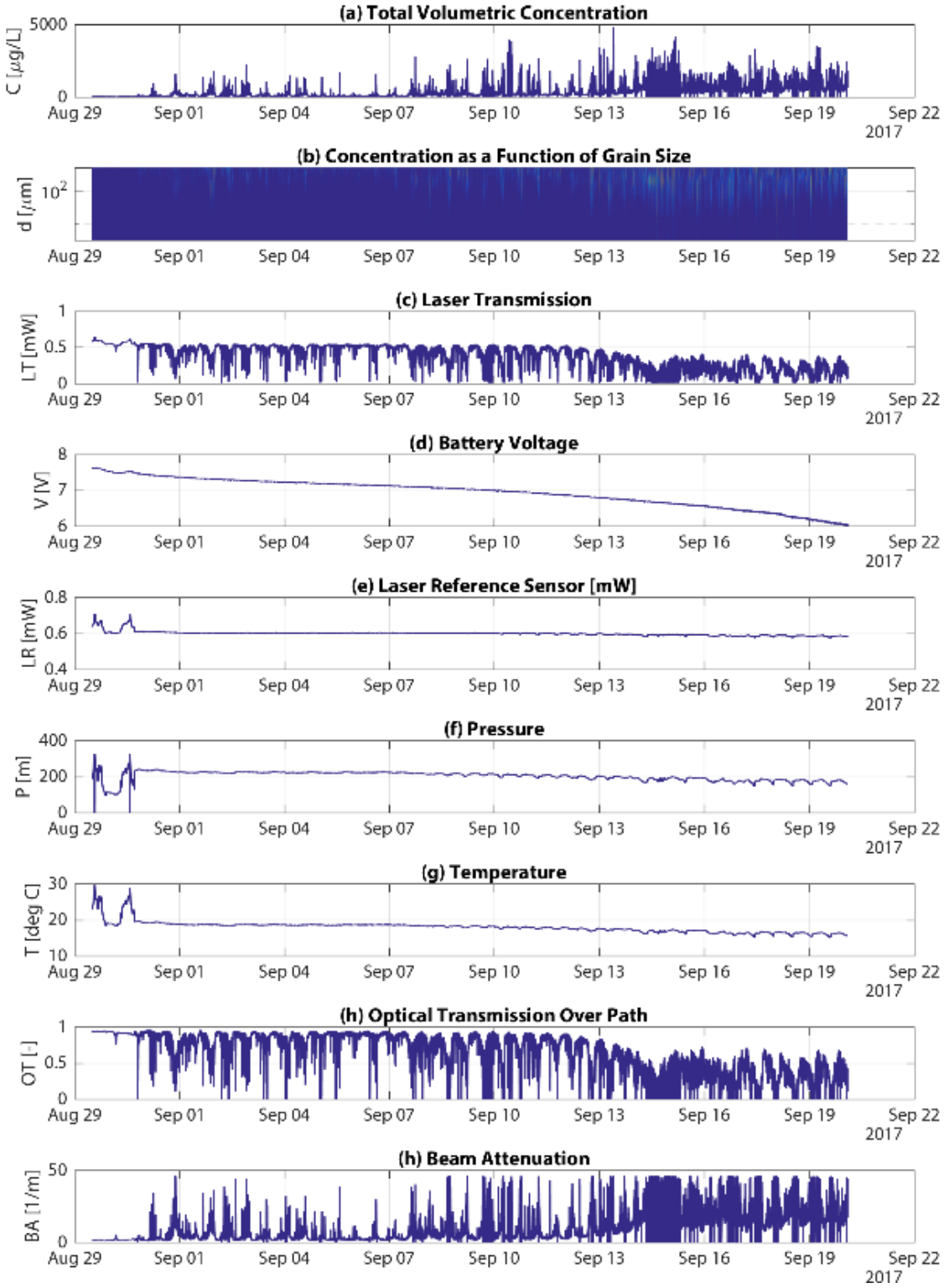

Figure 4.13 Example of LISST signal (at Frame 4 AZG). (a) Total volumetric concentration, (b) Concentration as a function of grain size, (c) Laser transmission, (d) Battery voltage, (e) Laser Reference Sensor, (f) Pressure, (g) Temperature. (h) Optical transmission over path, and (i) Beam attenuation.

MPP

An example of the output from a Multi-parameter Probe is given in Figure 4.14. In most cases, visual inspection of the multi-parameter probe records suggests that quality of the measurements is acceptable. This section contains a brief discussion of the measurements with respect to the operating limits and accuracy of the sensors, as well as an overview of datasets flagged as incomplete or featuring significant errors.

Depth readings tend to fluctuate around the known frame depths, and all sensors were operating within their depth range (Appendix B.7). The sampling interval of 5 minutes (0.0033 Hz) and accuracy of +/- 0.12 m are insufficient to resolve wind waves with frequency of O(0.01-1 Hz) and lengths of O(0.1-10 m), but are adequate for coarse examination of tidal and subtidal water level variations of O($2x10^{-5}$ Hz) and O(0.1-1 m). The 5-minute sampling interval is sufficient to capture relevant temporal variations for all other variables. Note that mean sensor depth sometimes changed when frames were repositioned after the service interval, particularly at locations with relatively steep seabed slopes.

Salinity varies between 20 to 35 PSU, which is similar to the range of 22 to 35 PSU observed by Van Aken (2008a) on the Dutch coast at Texel from 1976 to 2003. Temperature varies between 3 to 20°C depending on the time of year, well within the instrument's operating ranges (Appendix B.7) and historical values observed by van Aken (2008b) at Texel. The sensors are sufficiently precise to measure typical semidiurnal and diurnal variations in both salinity and temperature (Appendix B.7).

The turbidity sensor is capable of measuring turbidity of up to 1000 NTU (Nephelometric Turbidity Units). This appears to be sufficient to capture natural variability for most of the deployments. However, in several cases (AZG-F3, DVA-F1, DVN-F1), this threshold is exceeded, and measured values are cut off above it. Unusually high or jumpy readings may be in some cases attributed to the presence of bubbles (YSI Incorporated, 2012). Furthermore, the instrument is sensitive to variations in suspended particle size, so the presence of flocs may influence the readings. Lastly, biofouling (e.g. macroalgae observed on the frame and sensors when AZG-F3 was serviced) may obscure the sensor. Calibration using water samples is necessary to convert the turbidity readings from NTU to a mass concentration (i.e. mg/L); however, this step was not completed as explained in Section 0.

DVN-F4 salinity readings have occasional negative spikes throughout its deployment. The turbidity sensor on DVN-F3 abruptly stopped working on April 13th, but the rest of the sensors on that instrument appeared to continue functioning normally. DVN-F1 has bizarre cut-offs in Chlorophyll readings.

Several instruments yielded incomplete measurements due to loss of power or other malfunctions. DVA-F4 stopped working on December 6th. This instrument (CIB30523) was taken out of service and repaired. It was replaced with another instrument (CIB19165) for the DVT1 campaign. CIB19165 stopped working on approximately January 20th after a series of unexplained temperature fluctuations. The repaired CIB30523 was then returned to F4 for the DVT2 campaign.

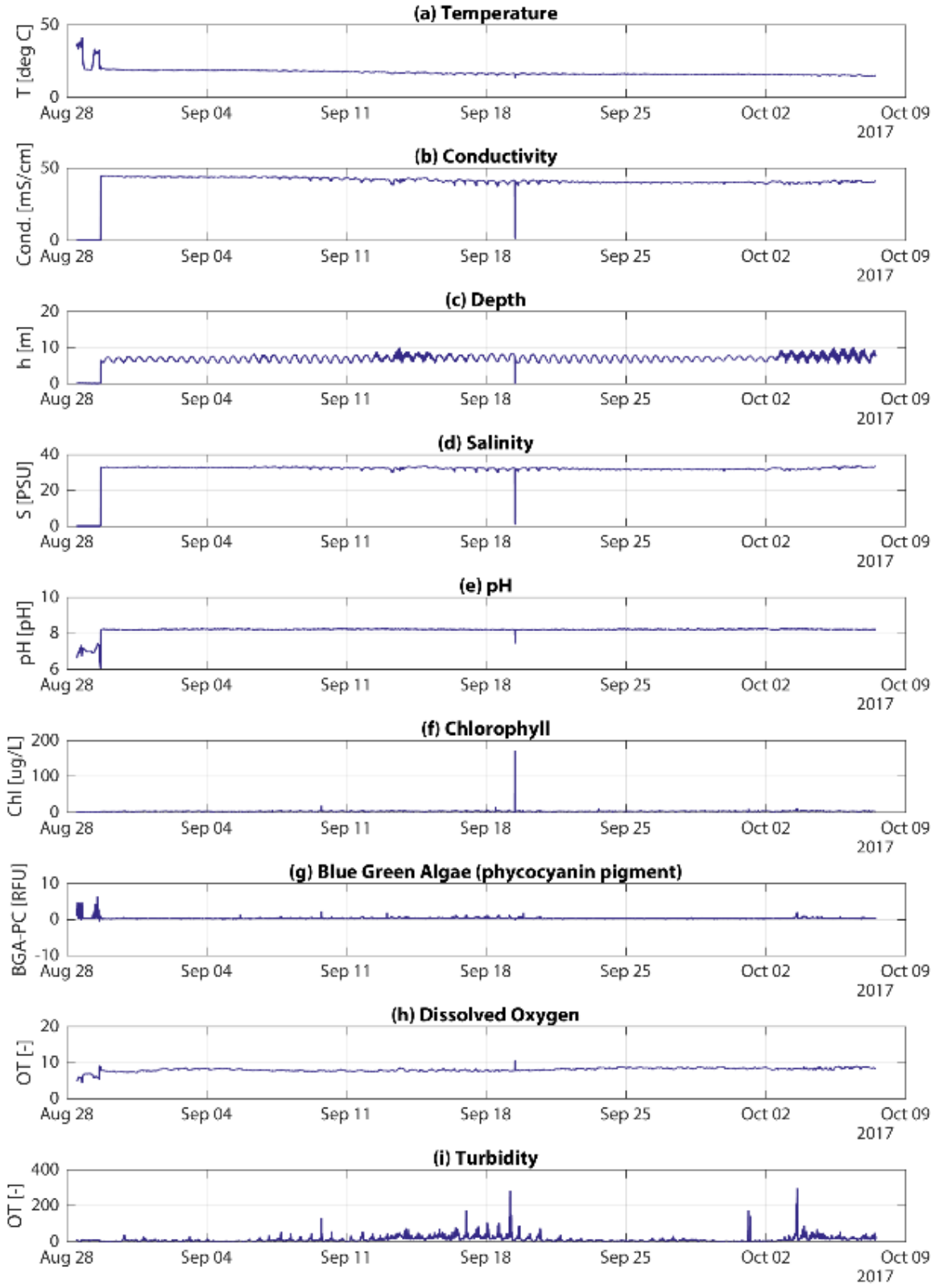

Figure 4.14 Example of Multiprobe signals (at Frame 4 AZG). (a) Temperature, (b) Conductivity, (c) Depth, (d) Salinity, (e) pH, (f)Chlorophyll, (g) Blue Green Algae (Phycocyanin Pigment). (h) Dissolved Oxygen, and (i) Turbidity.

Water samples Ameland Inlet

Figure 4.15 shows the locations and suspended sediment concentrations of water samples taken during 13-hour ADCP transect measurements on September 1st and 5th, 2017. The observed suspended sediment concentrations ranged from 2.5 to 79.0 mg/l.

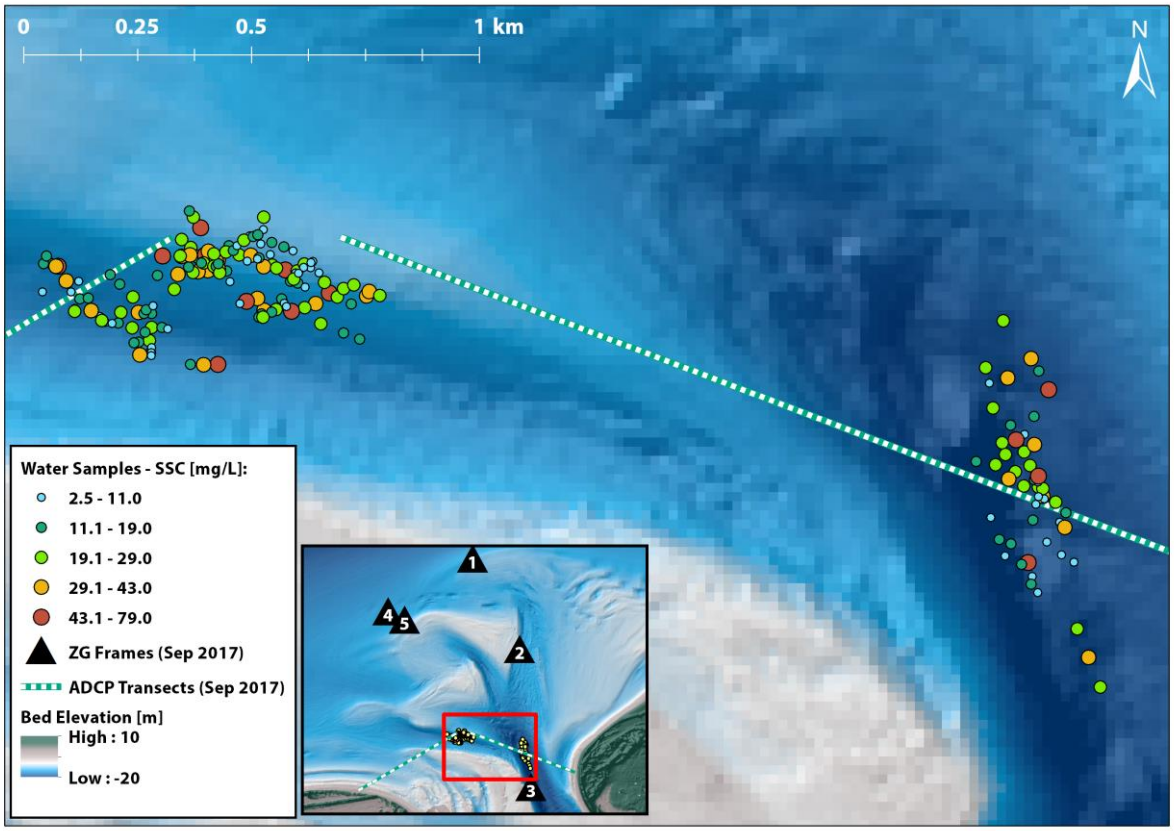

Figure 4.15 Locations and suspended sediment concentrations of water samples taken during 13-hour ADCP transect measurements on September 1st and 5th, 2017.

4.4 Sediment tracers

As of this writing, laboratory analysis of the tracer data is ongoing, so a review of the tracer study results is not yet available.

4.5 SONAR

Figure 4.16 shows an example of the SONAR data at the Ameland lower shoreface (DVA-F1, water depth ~20 m) on 9 November 2017. The three blue spots with lower bed levels indicate scour around the three legs of the frame, and this sand is deposited next to it, shown by the warmer colours. Beside these large-scale undulations, smaller-scale (~0.1 m) bedforms can be observed.

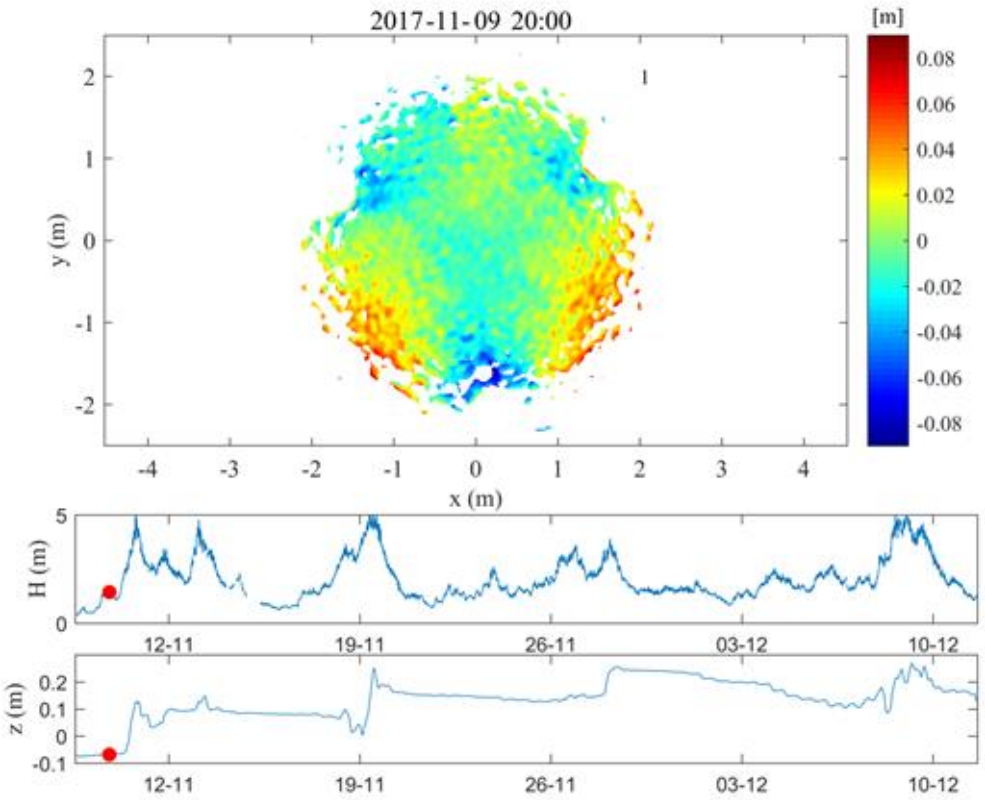

Figure 4.16 Snapshot of the movie of Sonar data of DVA Frame 1 (~20 m water depth) filtered with lx=ly=0.10 m. Upper plot: bed level with the mean removed, with data-quality flag at (x,y) = (2,2) m ("1" indicating that the data is of good quality). Middle plot: wave height as measured by wave buoy AZG12 during the entire DVA campaign (line) and during the time of the measurement of the upper plot (red dot). Lower plot: bed level (mean bed level – original distance between bed and Sonar head) during the entire DVA campaign (line) and during the time of the measurement of the upper plot (red dot).

4.6 XBand radar

Figure 4.17 and Figure 4.18 show an example of the information returned by applying XMFit to the XBand radar data at 22 March 2018, the day when the construction of the nourishment commenced. Results include an estimate of depth, which was used for the analysis of the nourishment evolution. But also, information on wave direction and surface currents is returned. Note that this example result does not fully cover the radar domain. In blank regions, XMFit was not able to get a good estimate, but these regions were and will be covered at other points in time.

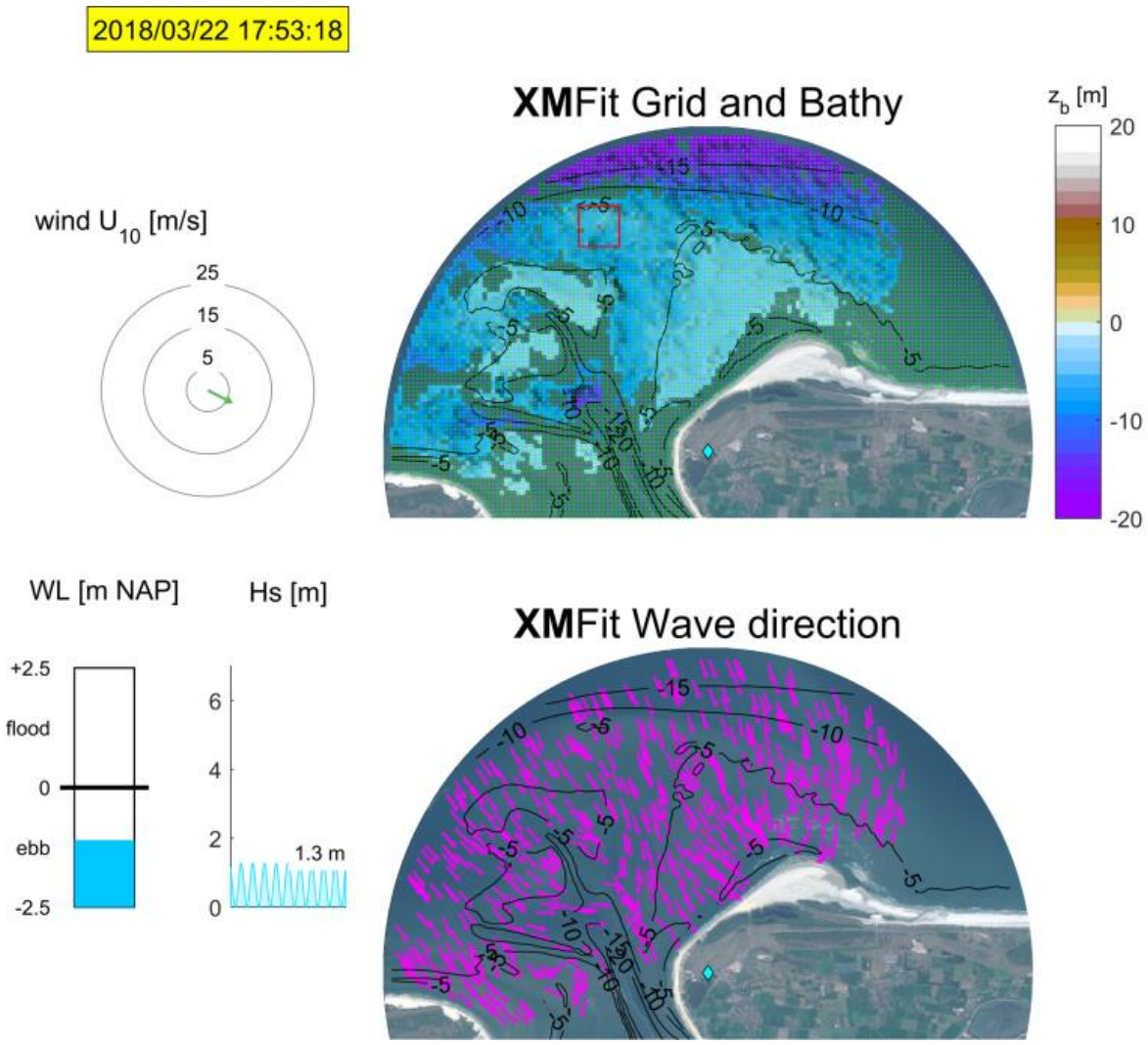

Figure 4.17 Example result of processing XBand radar (using XMFit) just before the start of construction of the pilot nourishment, 22 March 2018. The first panel shows the water depth, the second panel the wave directions. Along the left side (top), information is added on the occurring wind, water level and wave height.

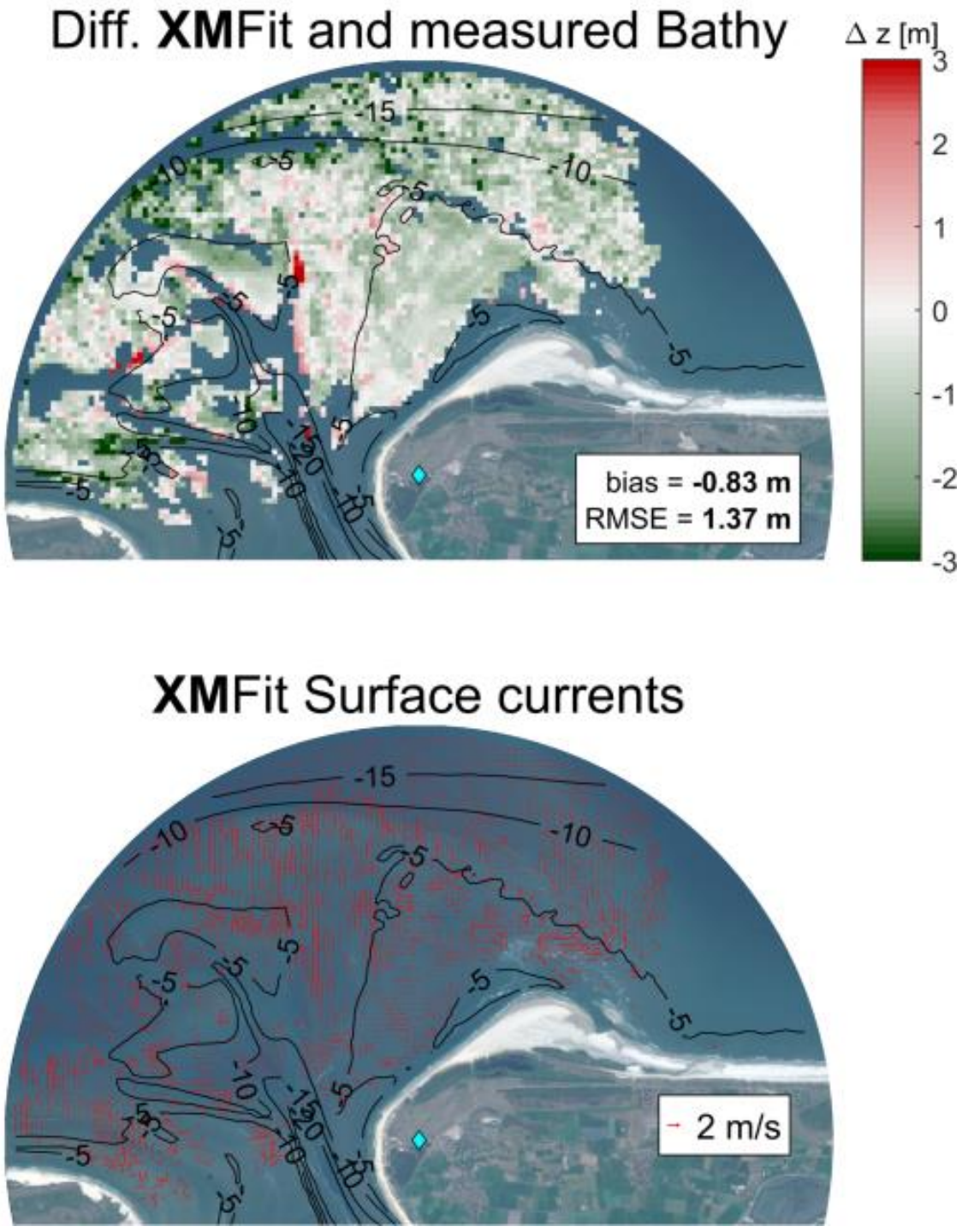

Figure 4.18 Example result of processing XBand radar (using XMFit) just before the start of construction of the pilot nourishment, 22 March 2018. The first panel shows difference with the in-situ measurements (combination of February and August 2017 surveys), and second panel shows surface current patterns. Occurring wind, water level and wave height can be found in Figure 4.17.

4.7 Singlebeam bed survey Ameland ebb-tidal delta

Figure 4.19 shows bed levels and difference maps for the fall 2016 – spring 2017 period. The overall net change is +0.9 mcm (million m^3), which is small compared to the gross changes of 18-19 mcm. More data-analysis and interpretation can be found in Elias (2018).

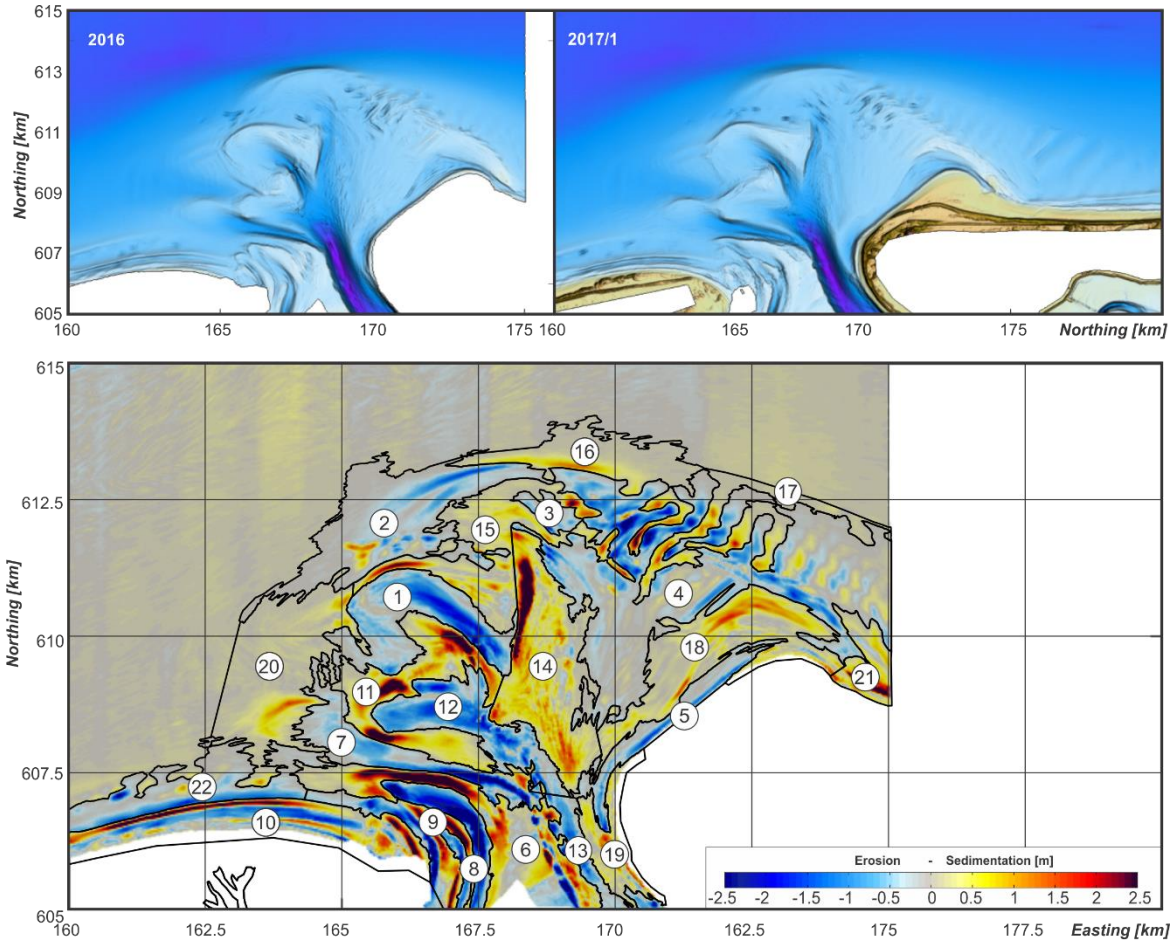

Polygons	Volume change *[mcm]*			Polygons	Volume change *[mcm]*		
	Pos.	Neg.	Total		Pos.	Neg.	Total
1	0.01	-1.95	-1.94	12	0.02	-1.95	-1.93
2	0.13	-1.11	-0.97	13	0.01	-0.63	-0.62
3	0	-0.15	-0.14	14	3.42	-0.05	3.37
4	0.48	-3.82	-3.34	15	1.31	-0.19	1.11
5	0.01	-0.55	-0.54	16	0.72	0	0.72
6	2.71	-0.61	2.1	17	0.60	0	0.6
7	0.1	-1.4	-1.31	18	1.46	-0.04	1.41
8	0.01	-2.07	-2.06	19	0.49	-0.02	0.47
9	0.97	-0.74	0.24	20	0.87	-0.01	0.86
10	1.86	-1.13	0.73	21	0.74	-0.02	0.72
11	2.76	-0.02	2.74	22	0.04	-1.37	-1.33
				Total :	18.72	-17.83	0.89

Figure 4.19 Observed sedimentation-erosion patterns and volume changes over the time period fall 2016 – spring 2017. Tables show the values for the individual polygons. [mcm] is [million m^3]. Positive numbers indicate sedimentation. Figure taken from Elias (2018).

4.8 Multibeam surveys Boschgat, Westgat, Borndiep

Figure 4.20 provides a summary of the migration of the bedforms in Borndiep, based on Section A – Profile 6. The sedimentation-erosion map illustrates that migration occurs uniformly over the bedform field and the selected profile seems representative for these changes. Bedform length is ~7 m and the height 0.3-0.4 m. More information can be found in Elias (2018).

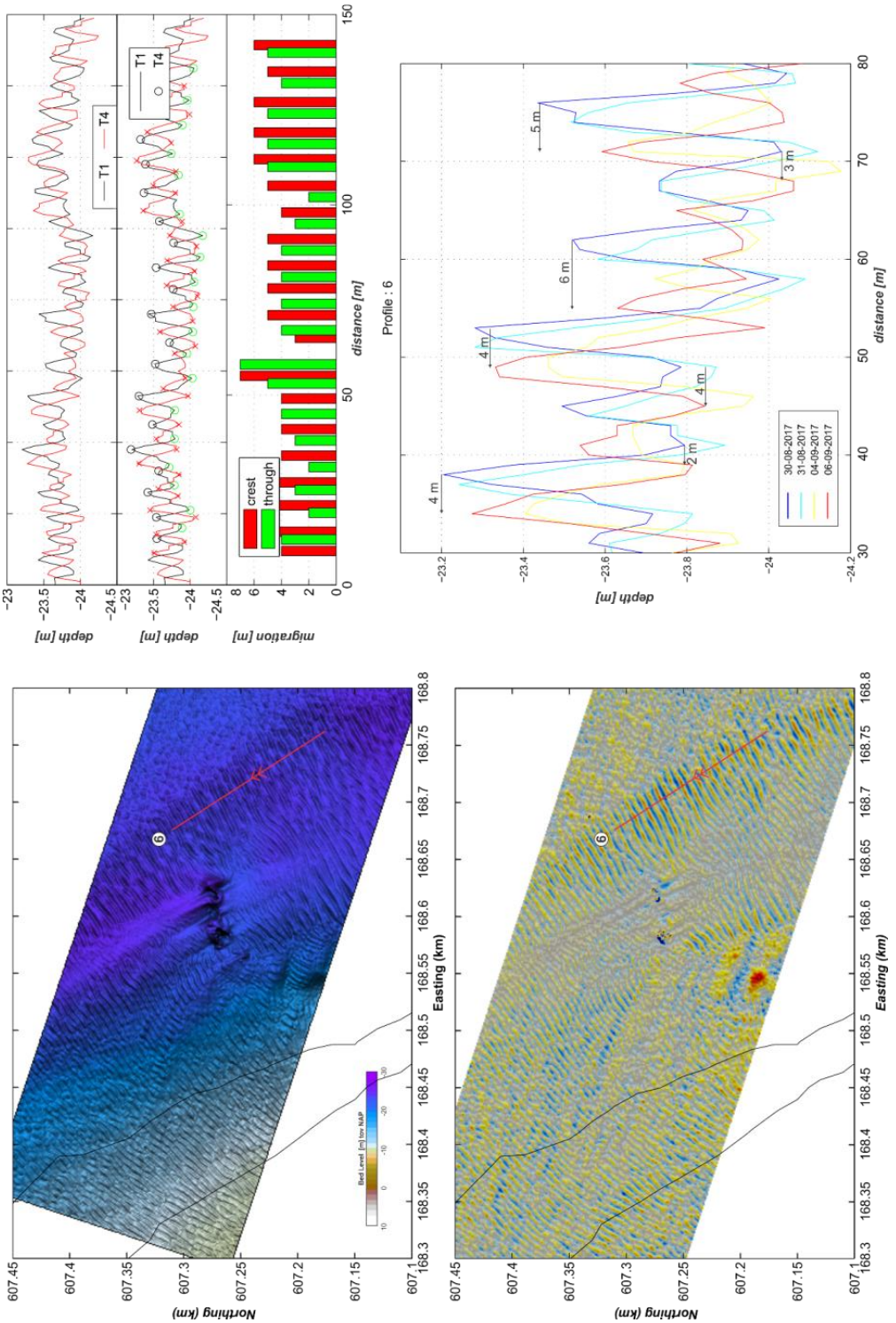

Figure 4.20 Bedforms along Section A-Profile 6. Lower left panel: initial bed level (30 Aug 2017, T1), lower right panel: sedimentation (in red) and erosion (in blue) between T4 (6 Sep 2017) and T1. Figure taken from Elias (2018).

4.9 Bathymetric surveys pilot nourishment Ameland ebb-tidal delta

Van Rhijn (2019) analyzed the subsequent surveys of the Ameland ebb-tidal delta thus providing insight in the development of the nourishment and the surrounding area over time. Figure 4.21 shows the difference between bathymetric survey #8 (January 2019) and survey #0 (February-March 2018, before nourishment construction). This figure shows a bed level increase within the nourishment contour with a maximum of 6 m. The bed level changes of a few meters eastward of the nourishment are the result of the autonomous ebb-tidal delta development.

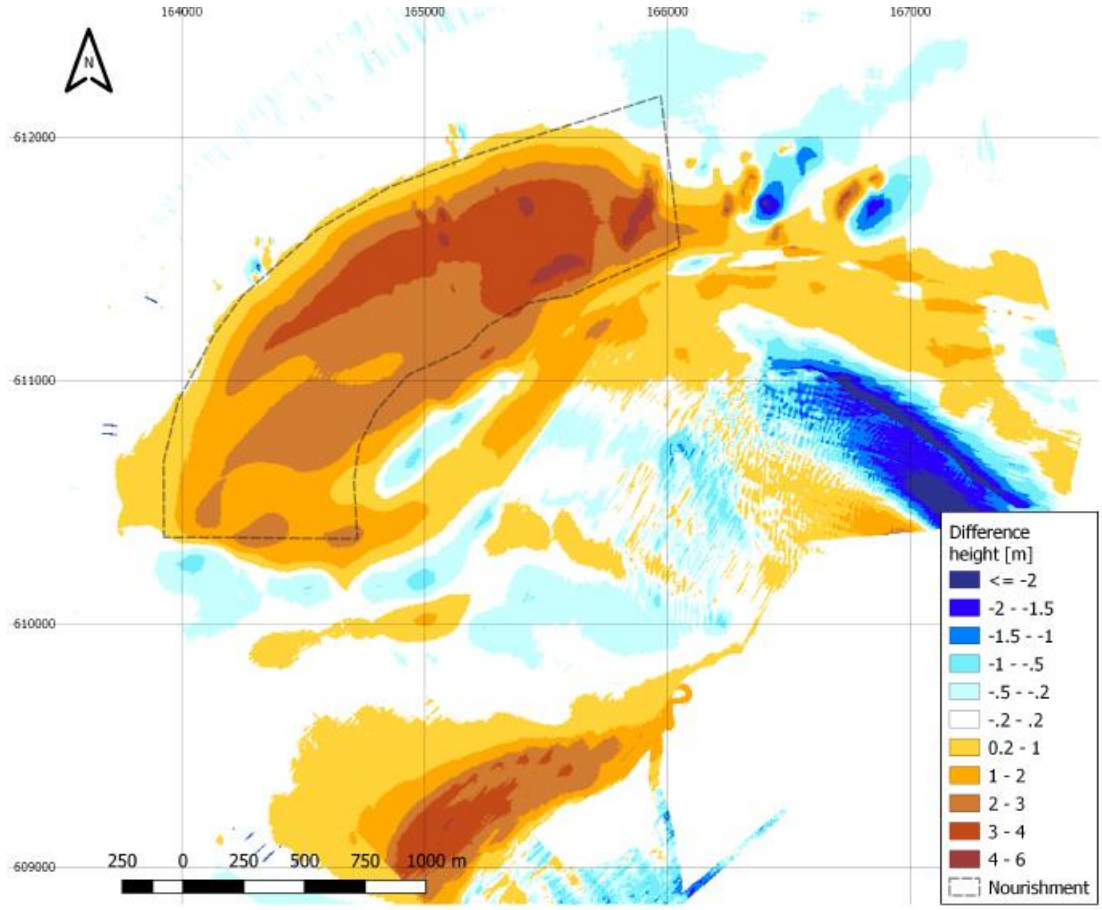

Figure 4.21 Difference between bathymetric survey #8 (January 2019) and survey #0 (February-March 2018, before nourishment construction). The nourishment contour is indicated with the dashed line.

4.10 Multibeam lower shoreface

The high resolution multibeam data resulted in posters displaying the morphology at the three study areas, which is described by Oost et al. (2019, in prep). The morphology gives information on the processes playing a role at different depths, and also reveals remarkable patterns.

For example, at Ameland we can see the transition from large, linear tidal ripples at deeper water to a more wave-dominated flat bed at shallower depths (Figure 4.22). Figure 4.23 shows local erosional features at Noordwijk at water depths between ~11 and 14 m, possibly due to storm waves.

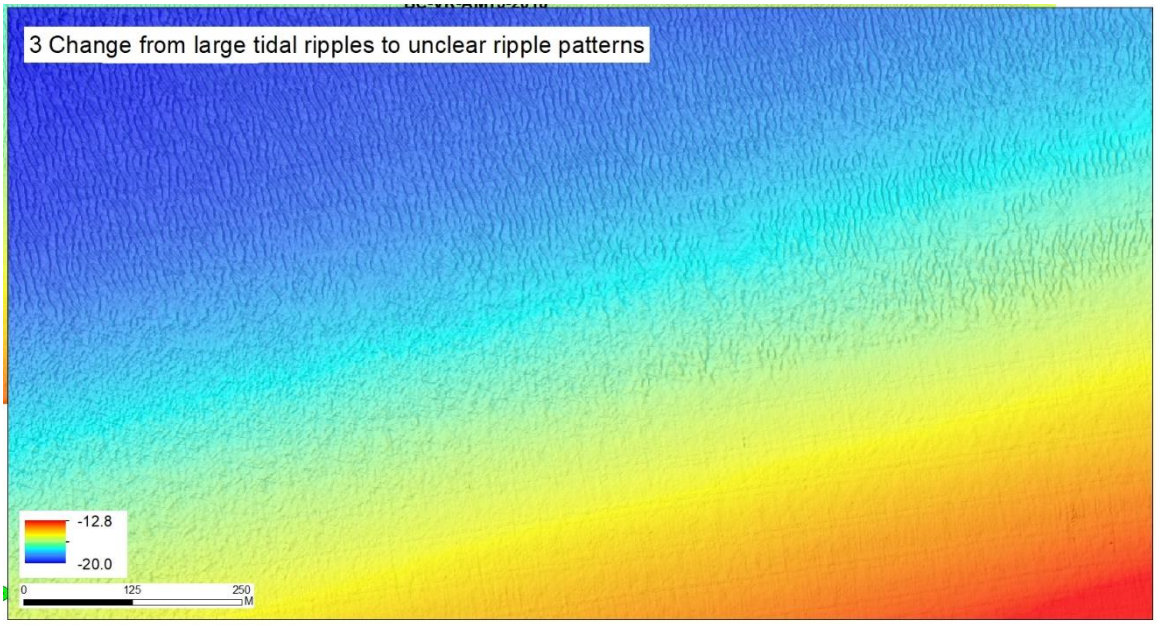

Figure 4.22 Detail of Ameland 2017 morphology.

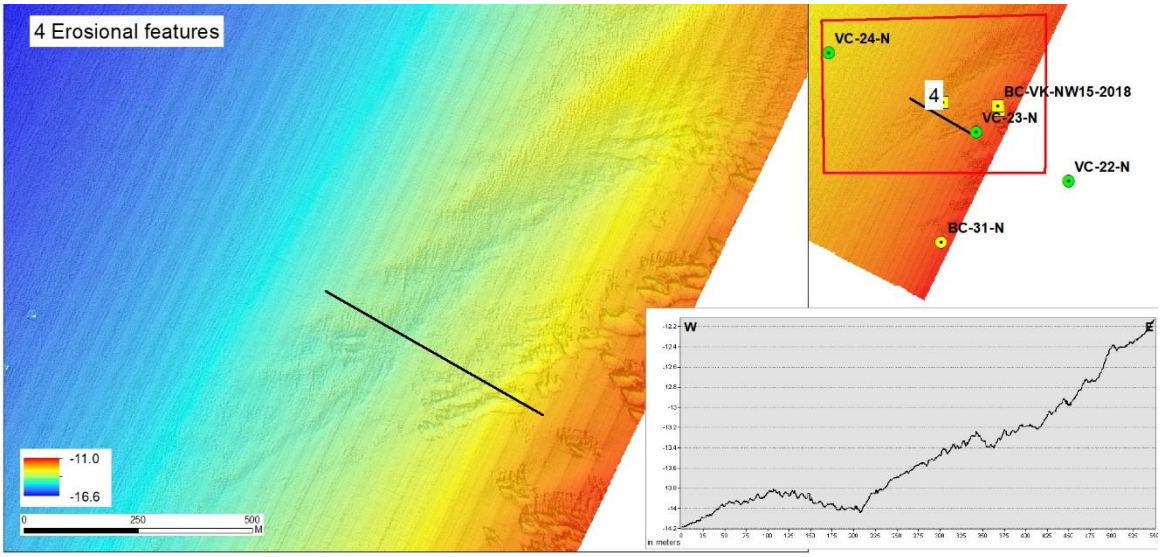

Figure 4.23 Detail of Noordwijk 2017 morphology.

4.11 Boxcores Ameland Inlet

Macrobenthos

Figure 4.24 shows the density and number of species at 165 locations based on boxcores taken in September 2017. In total 96 types of species were found at the ebb tidal delta, of which 71 species were unique. The species were divided into 24 species of worms, 29 Crustacea, 9 bivalve and snails, and 2 Echinodermata. On average there were 9 types of species present in a sample. The number of individuals range between less than 100 up to more than 2000 individuals.

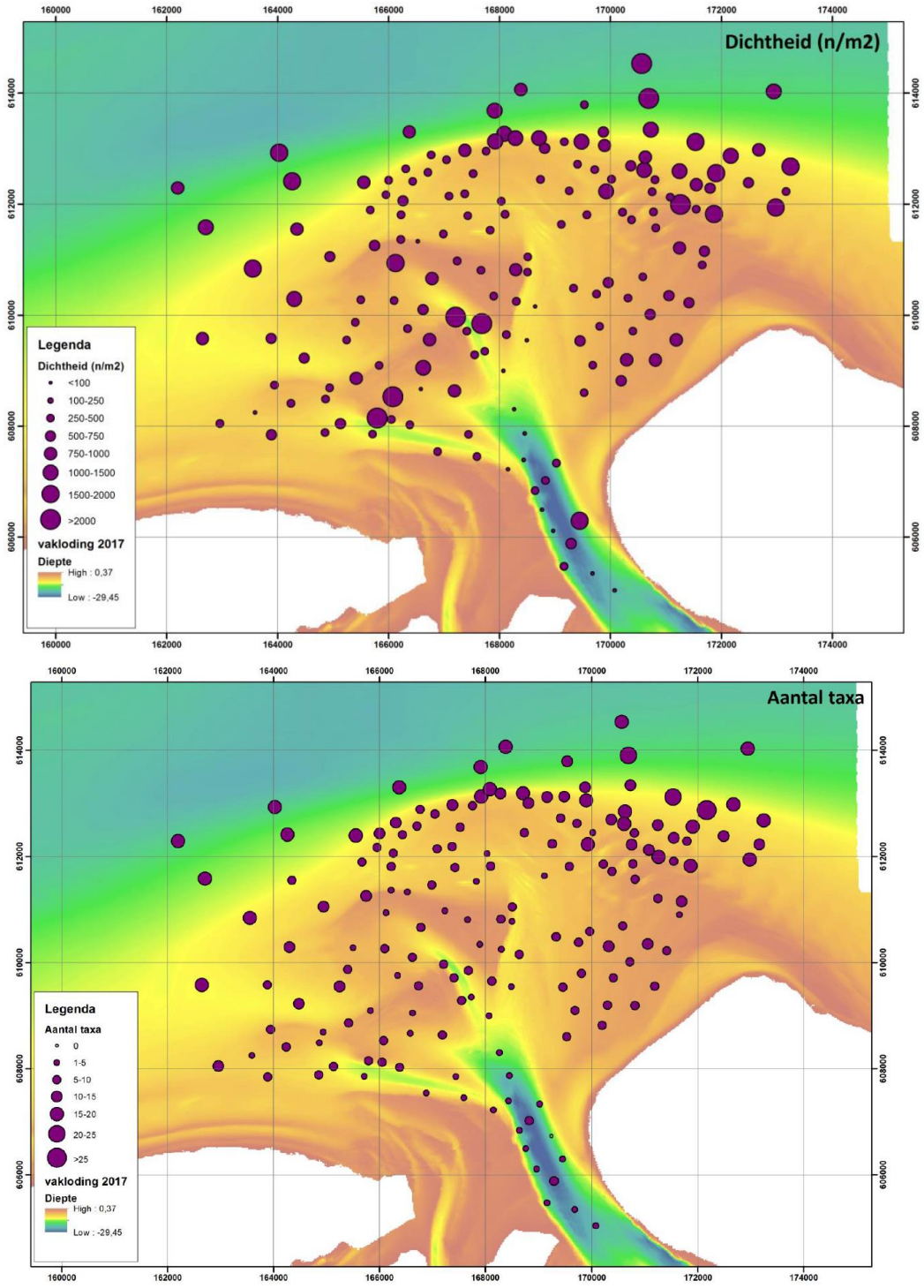

Figure 4.24 Density (top) and number of species (bottom) derived from the 165 boxcores taken in September 2017.

Sediment

Figure 4.25 shows the median grain size derived from the 165 boxcores taken in September 2017. The sediment of the ebb tidal delta mainly consists of fine to medium sand. The sediment in the channel between Ameland and Terschelling is relatively coarse with more than 60% of sediment samples with a D_{50} > 250 um. In the eastern part of the ebb tidal delta the sediment

is less coarse and even contains some silt. The organic matter is very low (<1%) for the whole ebb tidal delta (Verduin and Leewis, 2018).

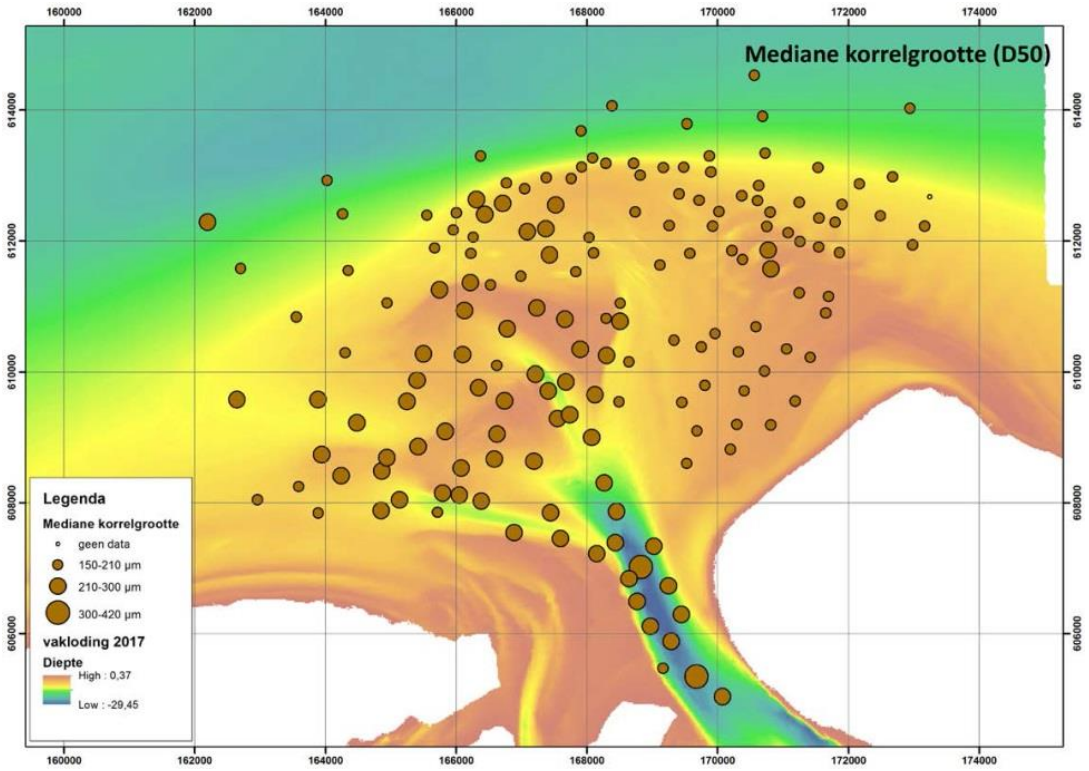

Figure 4.25 Median grain size derived from the 165 boxcores taken in September 2017.

4.12 Vibrocores and boxcores lower shoreface

The vibrocores and boxcores give information on the characteristics of the sediments and depositional structures of the three study areas. They are described by Oost et al. (2019). Examples of vibrocores and lacquer peels are given in Figure 4.26 and Figure 4.27.

The vibrocore VC-11-A contains 0.4 m of yellow-brown shoreface sand that overlies ebb-shield deposits with convoluted sand and clay layers. Below 1.6 m depth the core is formed by tidal channel deposits with sand and intercalated clay laminae. In VC-19-A lower shoreface sandy deposits directly overlie tidal channel deposits (boundary at 0.5 m depth).

The lacquer peel shows foresets in two directions caused by bidirectional currents in the lower and the upper part of the core. A doublet of a horizontally lying dead American jack-knife is present just below the erosion surface in the shell lag, pointing to sudden sediment removal and the formation of a shell lag which was washed out. The somewhat swaly upper deposits directly above it fill up the erosional surface.

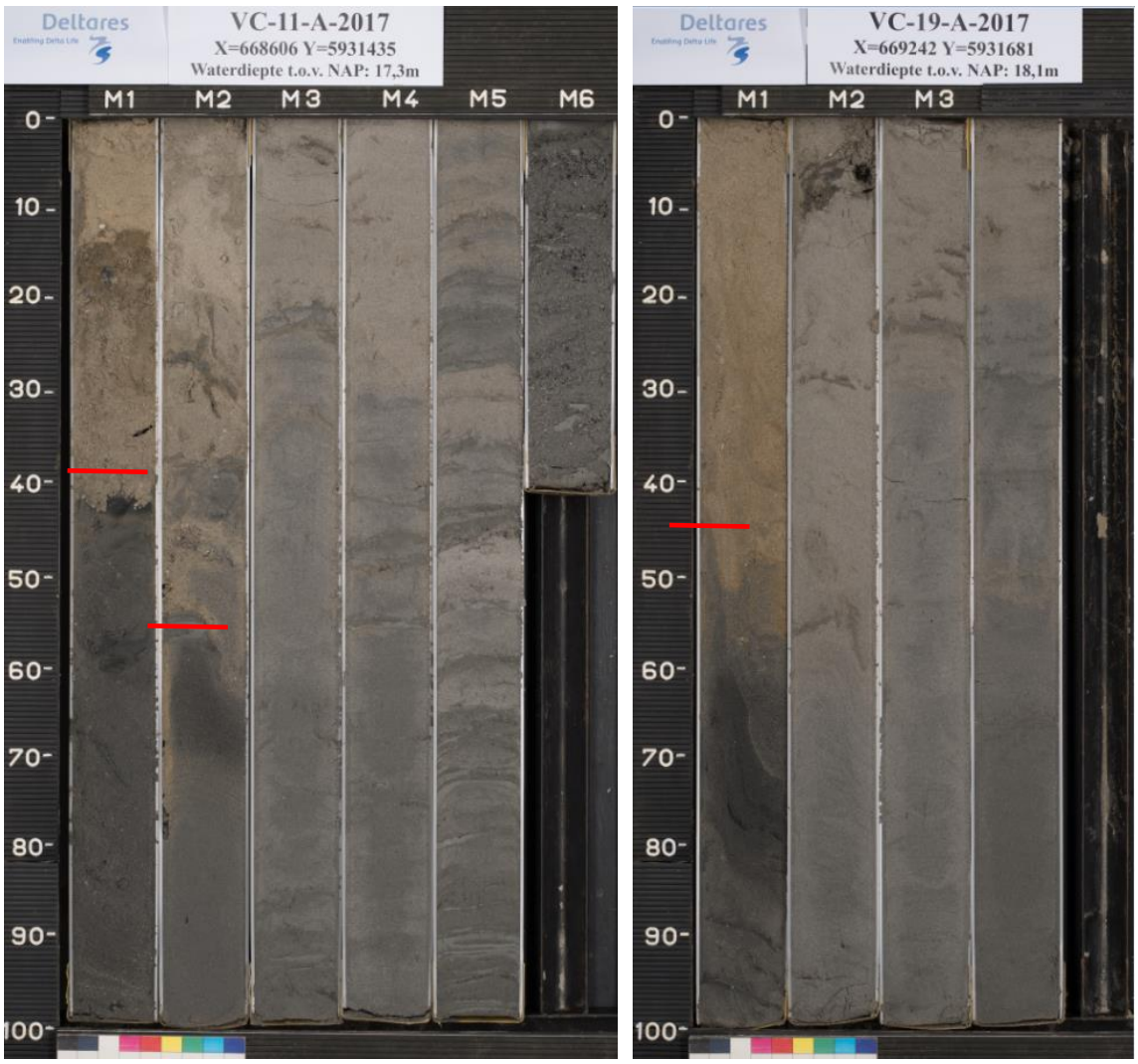

Figure 4.26 Picture of the boreholes VC-11-A (left) and VC-19-A (right) in the Ameland research area.

Figure 4.27 Lacquer peel of boxcore AM05, Ameland lower shoreface.

4.13 Fish

Figure 4.28 shows the results of the catchments in 2017 and 2018 at Ameland Inlet (for the locations see Figure 2.11). The total number of individuals caught by species and sampling area is given in Table 4.2. The results of the 2017 survey indicate large aggregations of juvenile sandeels in certain well-defined areas in the originally planned pilot nourishment location. However, the juveniles were not found in 2018. Sandeels were caught in varying numbers, with a maximum of 23 individuals caught at a single station.

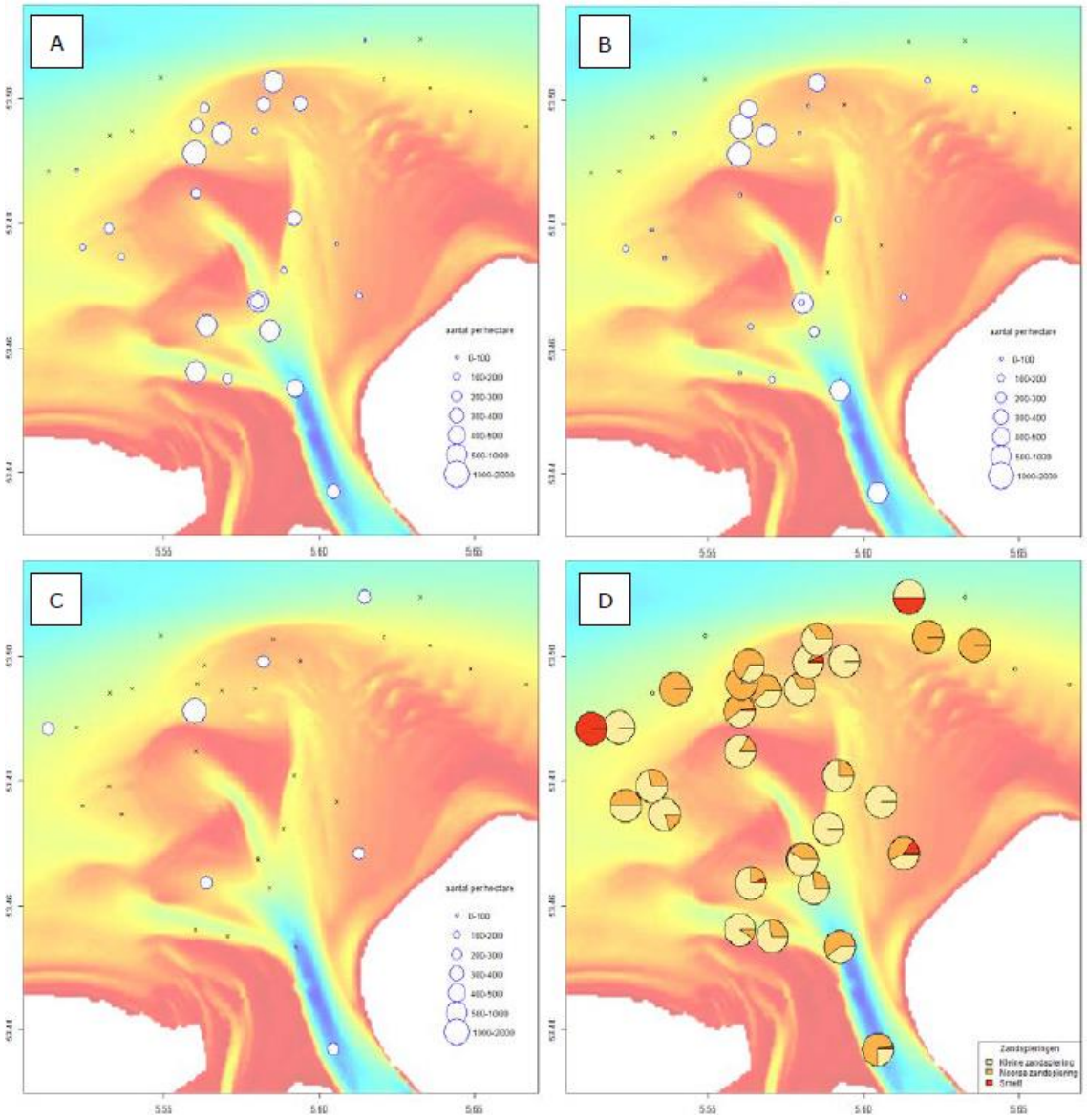

Figure 4.28 Number of sandeels per hectare: A) Letter sandeel; B) Raitt's sandeel; C) Greater sandeel. The locations marked with an X indicate locations where monitoring was planned for, but has not been carried out. D) the ratio of number of species per location.

Table 4.2 Catch rate (number) of sandeels in 2017 and 2018 in the Ameland Inlet.

Sandeel Species	September 2017	June 2018
Lesser sandeel/ 'kleine zandspiering':*Ammodytes tobianus*	204	107
Raitt's sandeel/ 'Noorse zandspiering':*A. marinus*	197	9
Greater sandeel/ 'smelt' :*Hyperoplus lanceolatus*	9	0

5 Conclusions

The Kustgenese 2.0 (KG2) data set is presented, containing bathymetric data, hydrodynamic data, sediment data and benthic species distributions. The data was collected on the ebb-tidal delta of the Ameland Inlet and the lower shoreface offshore Ameland Inlet, Terschelling and Noordwijk, The Netherlands. This data set is unique, because of (i) the large number of measuring locations, including 14 different frame positions, (ii) the large number of advanced instrumentation (20 different devices, including 3D SONARs), (iii) the versatility of the measurements including hydrodynamics, suspended matter, sediment composition, bedforms, bed levels and macrobenthos.

This dataset will help to increase the understanding and modelling of fundamental processes over complex bathymetries under the combined influence of waves and tidal currents. For example, the KG2 data set allows for:

- Analysis of small-scale processes, such as the influence of tidal currents on wave transformation (e.g. De Wit et al., in prep) and the contribution of intra-wave processes on the net sediment transport (e.g. Schrijvershof et al., 2019).
- Analysis and understanding of the spatial variation of the flow, waves and sediment transport on the Ameland ebb-tidal delta, and the morphological feedback resulting from these processes.
- Development of (conceptual) models that describe the interaction between biotic and abiotic processes.
- Validation and improvement of both intra-wave and wave-averaged numerical models for waves, currents, sediment transport and morphological development (e.g. Grasmeijer et al., 2019; Nederhoff et al., 2019).

This data is used within the joint SEAWAD and KustGenese2.0 program to analyse the Ameland ebb-tidal delta as representative of the other Wadden Sea ebb-tidal deltas, as well as the lower shoreface sediment dynamics. Ultimately, the results will be used for in the process of (i) defining the offshore boundary of the Coastal Foundation, (ii) determining the yearly nourishment volume, and (iii) designing large nourishments on the Wadden ebb-tidal deltas.

The data is publicly available at *Waterinfo Extra*, http://waterinfo-extra.rws.nl/, and at 4TU Centre for Research Data at two partly overlapping repositories: https://data.4tu.nl/repository/collection:kustgenese2 and https://data.4tu.nl/repository/collection:seawad.

The work is submitted as journal publication in *Earth System Science Data* (Van Prooijen et al, submitted).

6 References

AFNOR (2005). NF EN 872 Water quality - Determination of suspended solids - Method by filtration through glass fibre filters.

Aqua Vision (2008). Project Sterkte en Belasting Waterkeringen (SBW). Report AV_DOC_080406, Aqua Vision, The Netherlands. (in Dutch)

Aqua Vision (2012). Verwerking ADCP data Amelander Zeegat Stormseizoen 2011/2012. Report AV_DOC_120132, Aqua Vision, The Netherlands. (in Dutch)

Aqua Vision (2017a). Stromingsmetingen Amelander Zeegat 2017, Raai AB. Rapport AV170154_Amelander_Zeegat_RaaiAB definitief_v01, Aqua Vision, Nederland. (in Dutch)

Aqua Vision (2017b). Stromingsmetingen Amelander Zeegat 2017, Raai C. Rapport AV170154_Amelander_Zeegat_RaaiAB definitief_v01, Aqua Vision, Nederland. (in Dutch)

Bot, P.V.M., Colijn, F. (1996). A method for estimating primary production from chlorophyll concentrations with results showing trends in the Irish Sea and the Dutch coastal zone. ICES Journal of Marine Science, 53(6), pp.945–950.

Black, K., S. Athey, P. Wilson, and D. Evans (2004), Particle Tracking: a new tool for coastal zone sediment management, in Littoral, pp. 1–6, Aberdeen, UK.

Brakenhoff, L. (2018). Data quality report Sonar measurements Amelander Zeegat (AZG), Diepe Vooroever Ameland (DVA), Diepe Vooroever Noordwijk (DVN), Diepe Vooroever Terschelling 1 (DVT1), Diepe Vooroever Terschelling 2 (DVT2). Utrecht University, The Netherlands.

Campbell Scientific (2017). OBS-3+ and OBS300 Suspended Solids and Turbidity Monitors: Instruction Manual. Logan, UT: Campbell Scientific, Inc.

Chapalain, M., Verney, R., Fettweis, M., Jacquet, M., Le Berre, D., & Le Hir, P. (2018). Investigating suspended particulate matter in coastal waters using the fractal theory. Ocean Dynamics, 1-23.

Deltaprogramma (2015). Werk aan de delta. De beslissingen om Nederland veilig en leefbaar te maken. (in Dutch)

De Wit, F., Tissier, M., and Reniers, A (in prep). Characterizing wave shape evolution on an ebb-tidal shoal. To be submitted to *Journal of Marine Science and Engineering*.

Duran-Matute, M., Gerkema, T. (2015). Calculating residual flows through a multiple-inlet system: the conundrum of the tidal period. Ocean Dynamics, 65(11), 1461-1475.

Elias, E.P.L. (2018). Understanding the present-day morphodynamics of Ameland Inlet - part 2. Kustgenese 2.0, product ZG-B04. Deltares report 1220339-007-ZKS-0007, December 2018, Final.

Elgar, S., Raubenheimer, B., Guza, R. T. (2005). Quality control of acoustic Doppler velocimeter data in the surfzone. Measurement Science and Technology, 16(10), 1889.

Gawehn, M, (2018). Eindrapportage Kustgenese 2 ZG_B03 Radar 2018: Morfologische Analyse Pilotsuppletie. Report1220339-007-ZKS-0005, Deltares. (In Dutch)

Gawehn, M (2019). Using a new radar-based depth inversion method to monitor the evolution of nourishments on complex coasts, *in prep*.

Goring, D.G., Nikora, V. I. (2002). Despiking acoustic Doppler velocimeter data. Journal of Hydraulic Engineering, 128(1), 117-126.

Grasmeijer, B.T., Van Rijn, L.C., Van der Werf, J.J., Zijl, F., Huisman, B.J.A., Luijendijk, A.P., Wilmink, R.J.A., De Looff, A.P. (2019a). Method for calculating annual sand transports on the Dutch lower shoreface to assess the offshore boundary of the Dutch coastal foundation. Coastal Sediments conference, St. Petersburg, USA.

Grasmeijer, B.T., Schrijvershof, R., Van der Werf, J.J. (2019b). Modelling Dutch Lower Shoreface Sand Transport. Report 1220339-005-ZKS-0008, Deltares, The Netherlands.
Holzhauer, H. (2017). Meetlocaties benthos bemonstering van de buitendelta van Ameland in September 2017 voorafgaand aan de proefsuppletie. Univeristy of Twente, The Netherlands. (in Dutch)
Keyence Corporation (2014), VHX-5000 Digital Microscope User's Manual, Osaka, Japan.
Malvern Instruments Limited (2017), Mastersizer 3000 User Manual, Worcestershire, UK.
McDougall, T.J. and P.M. Barker, 2011: Getting started with TEOS-10 and the Gibbs Seawater (GSW) Oceanographic Toolbox, 28pp., SCOR/IAPSO WG127, ISBN 978-0-646-55621-5.
Mori, N., Suzuki, T., & Kakuno, S. (2007). Noise of acoustic Doppler velocimeter data in bubbly flows. Journal of engineering mechanics, 133(1), 122-125.
Nederhoff, C.M., Schrijvershof, R., Tonnon, P.K., Van der Werf, J.J. (2019a). The Coastal Genesis II Terschelling - Ameland inlet (CGII-TA) model: Model setup, calibration and validation of a hydrodynamic-wave model. Report 1220339-008-ZKS-0004, Deltares, The Netherlands.
Nederhoff, C.M., Schrijvershof, R.A., Tonnon, P.K., Van der Werf, J.J., Elias, E.P.L. (2019b). Modelling hydrodynamics in the Ameland Inlet as a basis for studying sand transport. Coastal Sediments conference, St. Petersburg, USA.
Nortek AS (2005). Vector Current Meter: User Manual. Rud, Norway: Nortek.
Nortek (2017b). HR Profiler: Nortek Quick Guide. Rud, Norway: Nortek.
Nortek (2017c). System Integrator Manual. Rud, Norway: Nortek.
Nortek (2017d). Vector Velocimeter: Nortek Quick Guide. Rud, Norway: Nortek.
Nortek. (2018). How is a coordinate transformation done? Retrieved December 7, 2018 from https://www.nortekgroup.com/faq/how-is-a-coordinate-transformation-done
Nortek AS (2008b). Aquadopp High Resolution: User Guide. Rud, Norway: Nortek.
Ocean Sensor Systems (2015). OSSI-010-003 Wave Gauge: User Manual. Coral Springs, FL: Ocean Sensor Systems Inc.
Oost, A.P., A. Forzoni, A. van der Spek, T. Vermaas (2019). Kustgenese-2 'diepe vooroever' – Core analysis Noordwijk, Terschelling, Amelander Inlet. Report 1220339-004-ZKS-0008, Deltares, The Netherlands.
Oost., A., Marges, V., Vermaas, T., Karaoulis, M. (2019). Kustgenese-2 'diepe vooroever', A description of the multibeam surveys 2017 & 2018. Draft report 220339-000-ZKS-0062, Deltares, The Netherlands
Pearson, S.G., Van Prooijen, B.C., De Wit, F.P. Holzhauer-Meijer, H., De Looff, A.P., Wang Z.B. (2019). Observations of suspended particle size distribution on an energetic ebb-tidal delta. Coastal Sediments '19, May 27-31, 2019, St. Petersburg, Florida.
Provoost, P. et al., 2010. Seasonal and long-term changes in pH in the Dutch coastal zone. Biogeosciences, 7(11), pp.3869–3878.
Ruessink, B.G., Brinkkemper, J.A., Kleinhans, M.G. (2015). Geometry of Wave-Formed Orbital Ripples in Coarse Sand. J. Mar. Sci. Eng. 3, 1568-1594; doi:10.3390/jmse3041568.
Schrijvershof, R., Brakenhoff, L., Grasmeijer, B. (2019). Hydrodynamics and bedforms on the Dutch lower shoreface Analysis of ADCP, ADV, and SONAR observations. Draft report 1220339-007-ZKS-0008, Deltares, The Netherlands.
Seapoint Sensors (2013). Seapoint Turbidity Meter: User Manual. Exeter, NH: Seapoint Sensors, Inc.
Sequoia Scientific, 2015. LISST-100X Particle Size Analyzer User's Manual Version 5.1, Bellevue, WA: Sequoia Scientific, Inc.
Sontek (2008). ADVOcean/Hydra: Expanded Description. San Diego, CA: Sontek /YSI
Teledyne RD Instruments (2018a). WorkHorse Sentinel, Monitor, & Mariner, LongRanger, and QuarterMaster: Commands and Output Data Format. Poway, CA: RD Instruments.

Teledyne RD Instruments (2018b). WorkHorse Sentinel, Monitor, & Mariner: Operation Manual. Poway, CA: RD Instruments.

TRDI (2010), ADCP coordinate transformation. Formulas and calculations. P/N 951-6079-00 (January 2010) © 2010 Teledyne RD Instruments, Inc.

Van Aken, H.M., 2008a. Variability of the salinity in the western Wadden Sea on tidal to centennial time scales. Journal of Sea Research, 59(3), pp.121–132. Available at: http://linkinghub.elsevier.com/retrieve/pii/S1385110107001116.

Van Aken, H.M., 2008b. Variability of the water temperature in the western Wadden Sea on tidal to centennial time scales. Journal of Sea Research, 60(4), pp.227–234. Available at: http://dx.doi.org/10.1016/j.seares.2008.09.001.

Van Prooijen, B.C., Tissier, M.F.S., De Wit., F.P., Pearson, S.G. Brakenhoff, L.B., Van Maarseveen, M.C.G., Mol, J.W., Holzhauer, H., Van der Werf, J.J., Vermaas, T., Gawehn, M., Grasmeijer, B., Elias, E.P.L., Tonnon, P.K., Reniers, A.J.H.M., Wang, Z.B., Den Heijer, K., Van Gelder-Maas, C., Wilmink, R.J.A., Schipper, C.A., De Looff, H. (submitted). Measurements of Hydrodynamics, Sediment, Morphology and Benthos on Ameland Ebb-Tidal Delta and Lower Shoreface. Submitted for publication in Earth System Science Data.

Van der Werf, J., Grasmeijer, B., Hendrik, E., Van der Spek, A. Vermaas, T. (2017). Literature study Dutch lower shoreface. Report 1220339-004-ZKS-0001, Deltares, The Netherlands.

Van Rhijn, T. (2019). Sediment transport during the execution of the pilot nourishment Ameland Inlet. MSc thesis, Technical University of Delft, The Netherlands.

Verduin, E.C., Engelberts, A. (2017). T-nulmeting Benthos Buitendelta Amelander Zeegat 2017 Veldrapportage Benthos boxcorer. Eurofins, Amsterdam, The Netherlands. (in Dutch)

Verduin, E.C., Leewis, L. (2018), T-nulmeting Benthos Buitendelta Amelander Zeegat 2017. Rapportage Benthos boxcorer. Eurofins, Amesterdam, The Netherlands. (in Dutch)

Vermeulen, B. (2015). ADCPtools. Retrieved December 7, 2018, from https://sourceforge.net/projects/adcptools/

Wit, F. de (in prep).

YSI Incorporated, 2012. 6-Series Multiparameter Water Quality Sondes User Manual Revision J., Yellow Springs, Ohio: YSI Incorporated.

Zijderveld, A., Peters, H. (2008). Measurement programme Dutch Wadden Sea. Proceedings International Conference on Coastal Engineering, San Diego, USA, 404-410.

A Overview of instruments on frames

The tables below give per campaign an overview of the instruments on the frames. It includes the instrument height above the bottom of the frame (*z*), which is not necessary the same as the location of measurement volume, as well as the sensor orientation (angle). The angle offset is positive in clockwise direction and relative to a “reference” instrument, which has therefore an angle of 0º. (U) indicates and upward-looking ADCP, and (D) indicates a downward-looking ADCP.

A.1 Amelander Zeegat (AZG)

Frame	Instrument	Code	z (m)	angle offset (º)
1	ADCP (U)	ADC01/ADC06	2.297	0.0
	ADCP-HR (D)	AQD01	0.480	115.6
	ADV	ADV01	0.645	270.3
	ADV	ADV02	0.346	267.8
	SONAR	PFS01	0.971	58.9
	OBS	OBS01	0.798	-
	OBS	OBS02	0.500	-
	OBS	OBS03	0.300	-
	OBS	OBS04	0.193	-
	MPP	MPP01	1.280	-

The instrument orientations were measured on 24 August 2017 (pre-deployment).

Frame	Instrument	Code	z (m)	angle offset (º)
3	ADCP (U)	ADC03/ADC08	2.297	0.0
	ADCP-HR (D)	AQD03	0.471	121.6
	ADV	ADV05	0.651	272.9
	ADV	ADV06	0.350	273.4
	SONAR	PFS03	0.975	57.9
	OBS	OBS09	0.792	-
	OBS	OBS10	0.488	-
	OBS	OBS11	0.301	-
	OBS	OBS12	0.202	-
	MPP	MPP03	1.263	-
	LISST	LIS01	0.605	-

The instrument orientations were measured on 24 August 2017 (pre-deployment).

Frame	Instrument	Code	z (m)	angle offset (º)
4	ADCP (U)	ADC04	2.298	0.0
	ADCP-HR (D)	AQD04	0.522	n/a[1]
	ADV	ADV12	0.926	270.2
	ADV	ADV07	0.651	267.0
	ADV	ADV08	0.358	268.2
	SONAR	PFS04	0.977	59.3
	OBS	OBS13	0.792	-
	OBS	OBS14	0.504	-
	OBS	OBS15	0.302	-
	OBS	OBS16	0.193	-
	MPP	MPP04	1.265	-
	LISST	LIS02	0.597	-

The instrument orientations were measured on 25 August 2017 (pre-deployment).
[1] AQD04 not surveyed because alignment tool does not fit the 90 degrees angle head

Frame	Instrument	Code	z (m)	angle offset (º)
5	ADCP (U)	ADC05/ADC09	2.272	0.0
	ADCP-HR (D)	AQD05	0.481	126.0
	ADV	ADV09	0.981	270.9
	ADV	ADV10	0.681	269.8
	ADV	ADV11	0.382	270.8
	SONAR	PFS05	0.947	80.2
	OBS	OBS17	0.805	-
	OBS	OBS18	0.508	-
	OBS	OBS19	0.203	-
	OBS array	OBS20	0.231	-
	OBS array	OBS21	0.200	-
	OBS array	OBS22	0.169	-
	OBS array	OBS23	0.137	-
	OBS array	OBS24	0.105	-
	Pressure	PRE1	1.910	-
	MPP	MPP05	1.211	-
	LISST	LIS03	0.593	-

The instrument orientations were measured on 23 August 2017 (pre-deployment).

A.2 Diepe Vooroever Ameland (DVA)

Frame	Instrument	Code	z (m)	angle offset (º)
1	ADCP (U)	ADC08	2.297	0.0
	ADCP-HR (D)	AQD01	0.480	115.5
	ADV	ADV01	0.645	269.5
	ADV	ADV02	0.346	267.9
	SONAR	PFS01	0.971	56.8
	OBS	OBS01	0.798	-
	OBS	OBS02	0.500	-
	OBS	OBS03	0.300	-
	OBS	OBS04	0.193	-
	MPP	MPP01	1.280	-
	LISST	LIS03	0.597	

The instrument orientations were measured on 2 November 2017 (pre-deployment).

Frame	Instrument	Code	z (m)	angle offset (º)
3	ADCP (U)	ADC10	2.297	0.0
	ADCP-HR (D)	AQD03	0.471	120.1
	ADV	ADV05	0.651	272.2
	ADV	ADV06	0.350	272.1
	SONAR	PFS03	0.975	57.6
	OBS	OBS09	0.792	-
	OBS	OBS10	0.488	-
	OBS	OBS11	0.301	-
	OBS	OBS12	0.202	-
	MPP	MPP03	1.263	-
	LISST	LIS01	0.605	-

The instrument orientations were measured on 2 November 2017 (pre-deployment).

Frame	Instrument	Code	z (m)	angle offset (º)
4	ADCP (U)	ADC06	2.298	0.0
	ADCP (D)	ADC04	1.151	357.6
	ADCP-HR (D)	AQD05	0.480	359.6
	SONAR	PFS04	0.977	57.5
	MPP	MPP04	1.265	-

The instrument orientations were measured on 2 November 2017 (pre-deployment).

A.3 Diepe Vooroever Terschelling (DVT1, DVT2)

The same frames and instruments were used as during the DVA campaign. Only ADV06 on Frame 3 was replaced by ADV13 and the SONAR was not present on Frame 3 during the DVT2 campaign. The angle offsets were not measured again.

A.4 Diepe Vooroever Noordwijk (DVN)

The same frames and instruments were used as during the DVA campaign. Only ADC10 on Frame 3 was replaced by ADC06, ADC06 on Frame 4 was replaced by ADC10 and the SONAR was not present on Frame 3 during the DVT2 campaign. The angle offsets were not measured again.

B Instrument specifications

B.1 ADCP – Frames

Sampling frequency [Hz]	1.25
Burst length [min:sec]	30:00
Burst interval [min:sec]	30:00 or 60:00
Samples per burst [-]	2250
Internal pressure sensor	Yes*
Acoustic frequency [kHz]	600 (ADC01, ADC03, ADC08, ADC10) 1200 (ADC04, ADC05, ADC06, ADC09)
Blanking distance [m]	0.5, 0.8, or 1
Cell size [m]	0.25, 0.50, 0.80, or 1
Number of cells [-]	18-42

*Internal pressure sensor was not working for certain ADCPs during AZG campaign (**Error! R eference source not found.**).

B.2 ADCP HR – Frames

Sampling frequency [Hz]	4
Burst length [min:sec]	29:00
Burst interval [min:sec]	30:00
Samples per burst [-]	6960
Internal pressure sensor	Yes
Acoustic frequency [kHz]	2000
Blanking distance [m]	0.05
Cell size [m]	0.03
Number of cells [-]	13

B.3 ADCP - Watersheds

Averaging interval [min:sec]	1:00
Internal pressure sensor	Yes
Acoustic frequency [kHz]	2000
Blanking distance [m]	0.10
Cell size [m]	0.10
Number of cells [-]	45

B.4 ADV

	Sontek Hydra	Nortek Vector
Sampling frequency [Hz]	10	16
Burst length [min:sec]	29:00	29:50
Burst interval [min:sec]	30:00	30:00
Blanking distance [m]	0.18	0.15
Samples per burst [-]	17400	28640
Internal pressure sensor	No*	Yes
Acoustic frequency [kHz]	5000	6000

*pressure signals are measured at 4Hz at another location on the frame, and are synchronized in time.

B.5 Pressure sensors

Specifications for OSSI Pressure Sensors.

Sampling frequency [Hz]	10
Burst length [hr:min:sec]	23:59:50
Burst interval [hr:min:sec]	24:00:00
Samples per burst [-]	864000 (including some NaNs in the end)

B.6 LISST

Specifications for LISST-100X Particle Size Analyzer.

Variable	LISST
Measurements per sample	5
Sample interval	1 s
Samples per burst	15
Burst Interval	60 s
Sampling Frequency	1 Hz
Instrument Height	0.60 m
Sensor Height	0.60 m
Optical Path Length	0.05 m
Particle Size Range	Type C (2.5-500 µm)

B.7 Multi-parameter Probe (MPP)

Specifications for YSI 6600v2-4 Multi-parameter Probe.

Variable	Value
Sampling Interval [s]	300
Instrument Height [m]	1.265
Sensor Height [m]	1.265

B.8 OBS

	Campbell	Seapoint	Seapoint Array
Sampling frequency [Hz]	16	10	4
Burst length [min:sec]	29:50	29:00	29:00
Burst interval [min:sec]	30:00	30:00	30:00
Samples per burst [-]	28640	17400	7200
ADVs and OBSs exactly synchronised in time?	No	Yes	Yes

C Data processing techniques

C.1 Coordinate system transform from beam to XYZ to ENU velocities

Three coordinate systems can be distinguished, BEAM, XYZ, and ENU. BEAM coordinates measure velocities along the beam. XYZ coordinates are defined with respect to the instrument, which differs per instrument and can be found in the instrument's manual. ENU coordinates are Earth coordinates, positive in East, North, and Up direction.

The procedure followed to convert from the ADCP beam velocities to ENU velocities is explained in more detail in TRDI (2010); here we summarized the followed methodology. The local ADCP coordinate system is shown in Figure C.1.

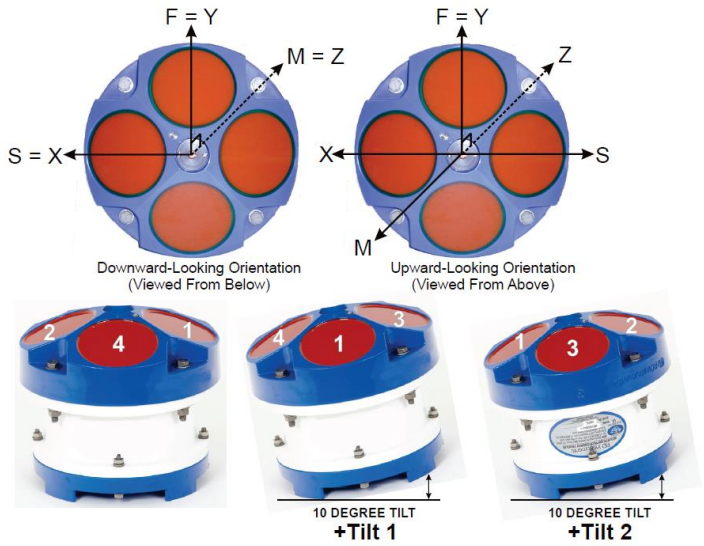

Figure C.1 ADCP Local reference system. Ship coordinates referred as starboard or pitch, forward or roll, and mast or yaw (S,F,M); and instrument axis (X,Y,Z). Figure taken from TRDI (2010)

Firstly, BEAM velocities are transformed in to XYZ velocities using the instruments transformation matrix. For the ADCP this transformation matrix reads:

$$\begin{pmatrix} X \\ Y \\ Z \\ E \end{pmatrix} = \begin{pmatrix} ca(b_1 - b_2) \\ ca(b_4 - b_3) \\ b(b_1 + b_2 + b_4 + b_3) \\ d(b_1 + b_2 - b_4 - b_3) \end{pmatrix} \tag{8.1}$$

in which E is the velocity error, c = +1 or -1 for a convex/concave transducer head, a = 1/[2 sin(θ)], b = 1/[4 cos(θ)], d = a/2, b_n is the beam velocity and θ is the beam angle to the vertical (ADCP head was convex with a 20º beam angle).

Secondly, velocities are transformed from XYZ to ENU. For this second step, the heading, pitch and roll (HPR) of the instrument are needed. Three successive rotations, R about the F axis, P about the levelled S axis and H about the U axis were applied. The instrument frames were

placed almost horizontally (Z- and U-axis are aligned), and so pitch P and roll R only play a marginal role, and the transformation is dominated by the heading H. The rotation matrix (RM) to apply is:

$$T = \begin{pmatrix} \cos H & \sin H & 0 \\ -\sin H & \cos H & 0 \\ 0 & 0 & 1 \end{pmatrix} \begin{pmatrix} 1 & 0 & 0 \\ 0 & \cos P & -\sin P \\ 0 & \sin P & \cos P \end{pmatrix} \begin{pmatrix} \cos R & 0 & \sin R \\ 0 & 1 & 0 \\ -\sin R & 0 & \cos R \end{pmatrix} \quad (8.2)$$

If the orientation of the ADCP device in the frame is upward, in comparison with the standard downward orientation, the axes are rotated 180° about the Y-axis. Thus, S = -X, F = Y, M = -Z (Figure C.1). Since the roll describes the ship axes rather than the instrument axes, in the case of upward-looking orientation, 180 degrees must be added to the measured roll before it is used to calculate RM.

The true heading of an instrument consists of three parts: the compass heading, the local compass deviation and the Earth deviation. The compass heading is measured by the actual instrument. Compass deviation is caused by nearby metal or batteries influencing the compass and can be obtained from the deviation table. The Earth deviation is caused by the fact that there is a deviation between the magnetic north and the true north, which was approximately +1.3 degrees for the time and latitude of this field campaign.

The procedure for determining the deviation table was to rotate the mounting frame annotating every ten degrees the device heading angle (compass heading) and the true angle measured with high accuracy GPS (magnetic heading) not affected by the frame (Figure C.2, Figure C.2). This was repeated in reverse direction. An averaged compass deviation (from the two cycles) at a 10-degree interval was taken for the compass calibration. Not accounting for deviations can lead to directional errors of up to 20 degrees. As an example, Figure C.4 shows the heading (measured and corrected), pitch and roll obtained from ADC08 mounted on Frame 1 during the DVT2 campaign. A 30min running mean was applied to the measured and corrected H, P and R in order to reduce the noise in the signal.

Figure C.2 Compass calibration procedure. The frame was rotated around the centre pole.

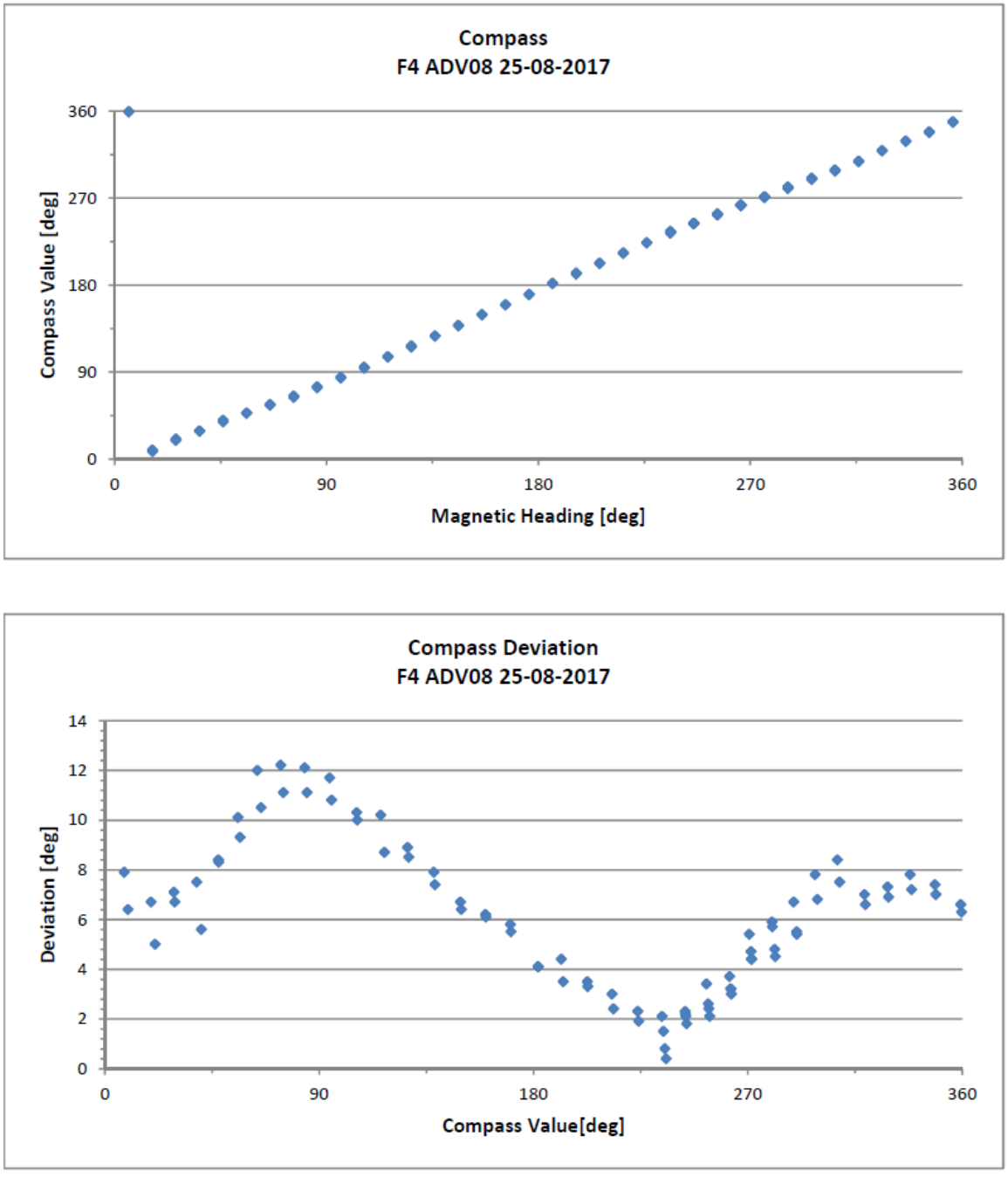

Figure C.3 Example of compass variation curves for ADV08 during the AZG campaign. Top panel shows the exact heading as a function of the compass heading, the bottom panel shows the difference as a function of the compass value.

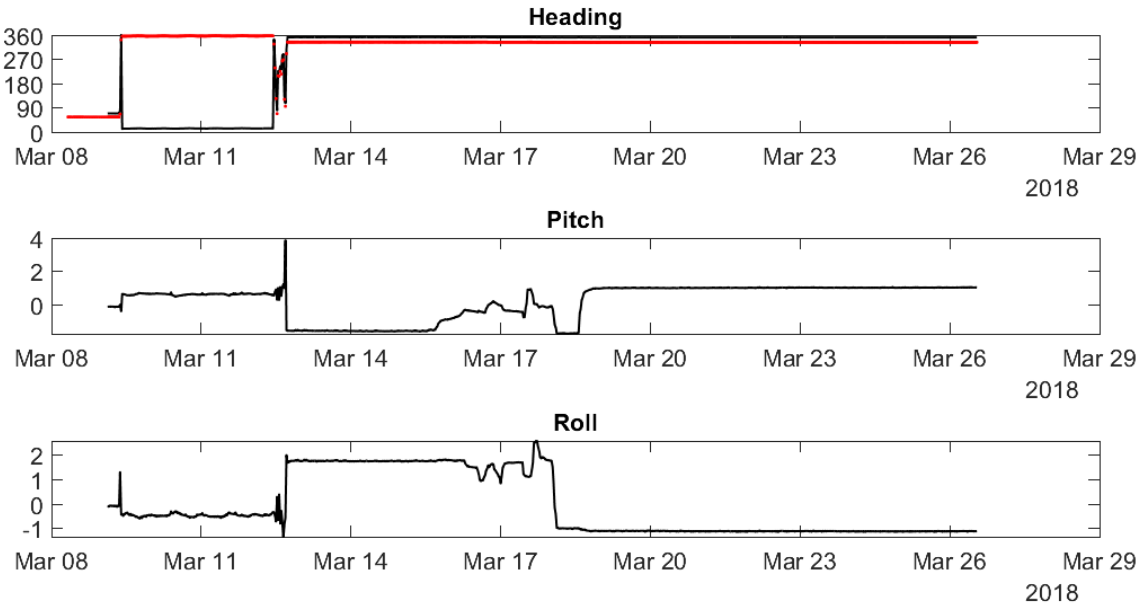

Figure C.4 Heading, pitch and roll 30-minute averaged values [degrees] measured in the ADCP mounted in frame 1 during 2018/03 campaign at Terschelling. This frame was deployed 12-03-2018 17:00 CET. Red dots in heading panel represents the values without correction and the black line the actual values. This frame mounted the ADCP looking upward, thus, the roll shown here has been translated 180 degrees to compute ENU velocities.

Unfortunately, not every instrument was calibrated (e.g. in case of replacement after servicing) and sometimes the calibration was unsuccessful due to a too high magnetic interference, see Table C.1. For those, the true heading will be derived from the heading of a nearby instrument and the angle between the two instruments within the frame for the same timestamps.

This transformation from XYZ to ENU is the net result of three successive rotations in this order: i) R about the F axis, ii) P about the S axis, iii) H about the M axis (Figure C.1). The transformation matrix is:

$$T = \begin{pmatrix} \cos H & \sin H & 0 \\ -\sin H & \cos H & 0 \\ 0 & 0 & 1 \end{pmatrix} \begin{pmatrix} 1 & 0 & 0 \\ 0 & \cos P & -\sin P \\ 0 & \sin P & \cos P \end{pmatrix} \begin{pmatrix} \cos R & 0 & \sin R \\ 0 & 1 & 0 \\ -\sin R & 0 & \cos R \end{pmatrix} \quad (8.3)$$

The roll describes the frame axes rather than the instrument axes, in the case of upward-looking orientation, 180 degrees must be added to the measured roll before it is used to calculate *T*. This is equivalent to negating the first and third columns of *T*.

Table C.1 Overview of instruments for which no (successful) compass calibration was available and the solution to this.

Location	Instrument	Issue	Solution
Frame 1 AZG	ADC06	Replacement ADC01 after 19-09-2017 servicing; no compass calibration available	Use AQD1 compass calibration and difference angle with ADC06 orientation
Frame 1 DVA Frame 1 DVT1 Frame 1 DVT2 Frame 1 DVN	ADC08	Replacement ADC06; no compass calibration available	Use AQD3 compass calibration and difference angle with ADC08 orientation
Frame 1 DVA Frame 1 DVT1 Frame 1 DVT2 Frame 1 DVN	AQD01 ADV01 ADV02	No new compass calibration available	Use compass calibration Frame 1 AZG
Frame 3 AZG	ADC08	Replacement ADC03 after 18-09-2017 servicing; no compass calibration available	Use AQD3 compass calibration and difference angle with ADC08 orientation
Frame 3 DVA Frame 3 DVT1 Frame 3 DVT2 Frame 3 DVN	AQD03 ADV06	No new compass calibration available	Use compass calibration Frame 3 AZG
Frame 3 DVA Frame 3 DVT1 Frame 3 DVT2	ADC10	Replacement ADC08; no compass calibration available	Use AQD3 compass calibration and difference angle with ADC10 orientation
Frame 3 DVT1 Frame 3 DVT2 Frame 3 DVN	ADV13	Replacement for ADV06; no compass calibration available; no sensor orientation available	Assume same orientation as ADV06, and use the same way to compute direction.
Frame 3 DVN	ADC06	Replacement ADC10; no compass calibration available	Use AQD3 compass calibration and difference angle with ADC06 orientation
Frame 4 DVT1 Frame 4 DVT2 Frame 4 DVN	ADC04 ADC06 AQD05	No new compass calibration available	Use compass calibration Frame 4 DVA
Frame 5 AZG	ADC05 ADV09 ADV10 ADV11	Unusable compass calibration due to too much iron	Use AQD5 compass calibration and difference angle with instruments

C.2 Velocity filtering and de-spiking

A first quality check is done by filtering based on correlation and Signal-to-Noise-Ration (SNR). Low correlation indicates that the three or four beams give very different velocities, therefore the average will be unreliable. Low SNR means that the measured signal is the same order of magnitude as the instrument's noise, so the signal is not actually the velocity but instrument noise. Threshold values for correlation and SNR are based on Elgar et al (2005).

Secondly, velocities are de-spiked using the 3D phase space method (Goring and Nikora 2002; Mori et al., 2007), in which velocities and their first and second order derivatives are plotted in a 3D space. Subsequently points outside a given ellipsoid are excluded. An example of measured data before and after de-spiking is given in Figure C.5.

Both methods above remove data from the velocity time-series. These removed data points are then logged as NaNs (Not a Number). Further treatment of these points is based on the number of NaNs and the number of subsequent NaNs:

- If a gap between correct data points is smaller than 1 second, velocities are linearly interpolated between these points.
- If the gap between correct data points is larger than 1 second, (parts of) waves are removed if linearly interpolation would be applied. Therefore, velocity points are then estimated based on a moving average through all bad data points.
- If more than 5% of data is NaN, the full half-hourly burst is disregarded.

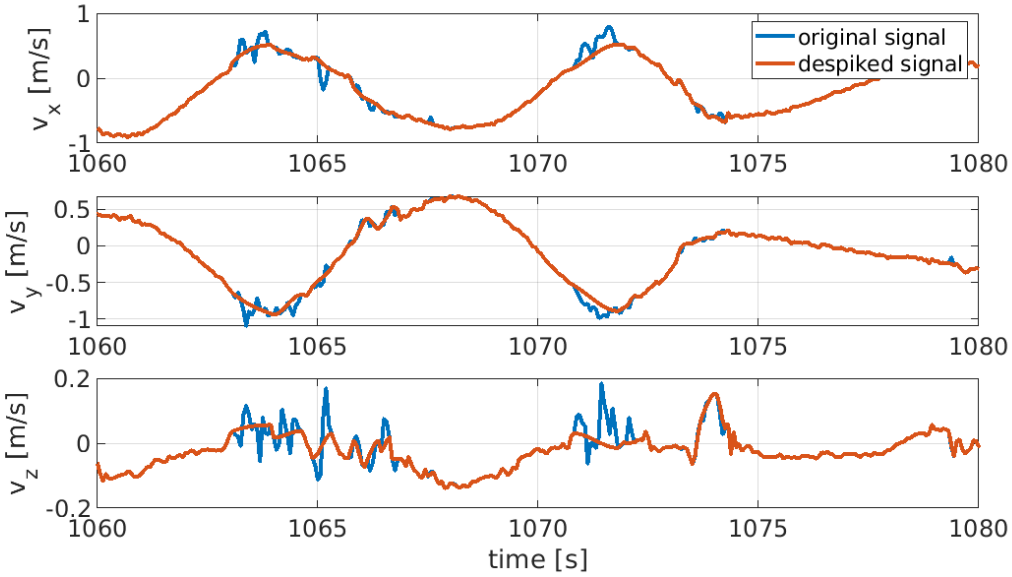

Figure C.5 Effect of the de-spiking toolbox. x-velocities (top panel), y-velocities (middle panel) and z-velocities (bottom panel) are shown with (red) and without (blue) de-spiking for a period of 20 seconds.

C.3 Depth-averaging ADCP velocities

Depth-averaged velocities can be derived from the ADCP instruments through various approaches. The main challenge consists of dealing with absent data between the bed and the first measurement cell above the bd. For the frames, roughly the first three meters from the bed were not measured (sensor elevation + blanking distance). This is a significant fraction of the water depth, especially for the shallow frames.

Three approximations for the depth averaged velocity were considered (name of the NetCDF variable is mentioned in italics):

1 The first approximation (*velocity_da037d*) simply equals the depth-averaged velocity to the velocity at 37% of the water depth. This is based on the fact that for an exact logarithmic velocity profile, the velocity at this depth equals the mean velocity over the water column. Note that for some of the shallow frames, this 37% of the water depth is below the lowest measurement cell at low water levels.

2 The second approximation (*velocity_dabmean*) simply averages the equidistant bins below the water level, ignoring the fact that the bins do not cover the full water depth.

3 The most advanced approximation (*velocity_dalogf*) fits a logarithmic fit to the measured data, to fill in the missing data near the bed, before averaging over depth. The fit is based on the following equation:

$$u(z) = \frac{u_*}{\kappa} \ln\left(\frac{z}{z_0}\right) \tag{8.4}$$

with u_* the shear velocity, κ the Von Karmann constant (= 0.4), z the height above the bed, and z_0 the near-bed vertical level where the velocity is zero. Both the shear velocity as z_0 follows from a fit to the data, while z_0 was limited to 0.001 m to prevent unrealistic fits. Finally, the depth-averaged velocity estimate follows by averaging the velocity measurements of the ADCP combined with the fitted velocity profile outside the range of the ADCP instruments (below the sensor height + the blanking distance).

For all methods, the data of each bin is averaged on 10-minute intervals (profiles were recorded every second) by averaging over all the data available in the 5 minutes before and after the target time moment (600 samples). Measurements (bins) that are located above the water surface were ignored. For this step, the local water depth was determined using pressure measurements (after correction for atmospheric pressure fluctuations, see Section C.4) from the ADCP instruments or from the pressure measurements of the ADCP-HR instrument on the same frame in case an ADCP pressure was not available.

Note that none of the estimates is perfect, simply as the vertical profile of the measurements is seldom perfectly logarithmic (assumption for approximations 1 and 3) and that the measured bins over part of the water column are not completely representative for the full water column (assumption for approximation 2). However, as a relatively large part of the water column is measured by the ADCP, the different considered methods provide robust estimates (Figure C.6). Therefore, there is confidence in the accuracy of the approaches. The logarithmic fit method is considered most appropriate, as it fills in the near-bed missing data.

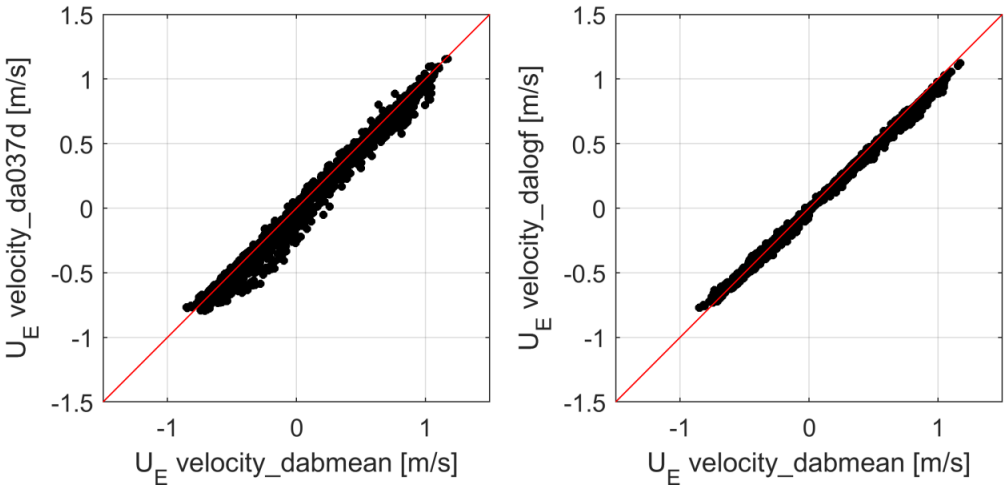

Figure C.6 Comparison of estimates of the depth-averaged eastern velocity component by the different methods for DVA campaign Frame 3.

C.4 Air pressure corrections

Pressure signals are measured by the ADVs, ADCPs, LISST, MPP and standalone pressure sensors. The pressure sensors measure the total pressure, which is the combination of atmospheric pressure and water pressure. Some instruments measure pressure with respect to a certain number (for instance 1 bar). If this is the case, this number is added to obtain the total pressure. To obtain the water pressure, the total pressure is reduced by the air pressure.

The air pressure is obtained from the nearest KNMI meteo station, which varies depending on the campaign (Figure C.7). Finally, the pressure is expressed in SI units [Pascal] in order to be consistent between all instruments (1 bar = 100.000 Pa).

Figure C.7 Location of KNMI meteorological stations in the Netherlands.

D Directional comparison frame-mounted velocity measurements

To verify that the compass orientations of the hydrodynamic measurements from each campaign are correct, we performed a consistency check between the instruments of each frame. The magnetism of the frame, different orientations of the instruments on each frame, and natural variations in the Earth's magnetic field all contribute to variations in the compass readings, which were corrected in Appendix C.1. In principle, aside from minor variations due to different elevations above the bed and possible disturbances in the flow field by the frame, the flow direction measured by each instrument should be similar at each point in time.

To provide a consistent basis for comparison, velocity measurements from the ADCP, ADVs, ADCP-HR, and downward-looking ADCP were averaged over the same 30 min periods. Velocity profiles obtained from ADCP-type measurements were vertically averaged to simplify the comparison with ADV point measurements. Errors in reading the data were logged and classified according to their cause (Table D.1):

- *file does not exist*. The ADVs on AZG Frame 5 have not been processed yet, because the file structure is different from the ADVs on the other frames. Also the data from the highest ADV on AZG Frame 4 has not yet been processed with the latest script. Both will be done at a later stage.
- *all_fillValues*. The data-files contain non-physical fill (dummy) values. The information of the heading, pitch and roll were missing for the ADV low on DVT1 Frame 3, DVT2 Frame 3 and DVN Frame 3 such that the ENU-velocities could not be computed. The same applies for the ADCP-HR on DVA Frame 4, DVT1 Frames 1 and 4, DVT2 Frame 4 and DVN Frame 4.
- *2nd ADV missing*. There is no data of the ADV low on DVT2 Frame 1 in the processed NetCDF file, because there was no raw data file.
- *% Blank*. The percentage of the time where no velocity values are available.

The mean flow direction during each burst was calculated clockwise from North. To identify inconsistencies in direction between instruments, the directional time series were plotted and summarized in histograms (e.g. Figure D.1).

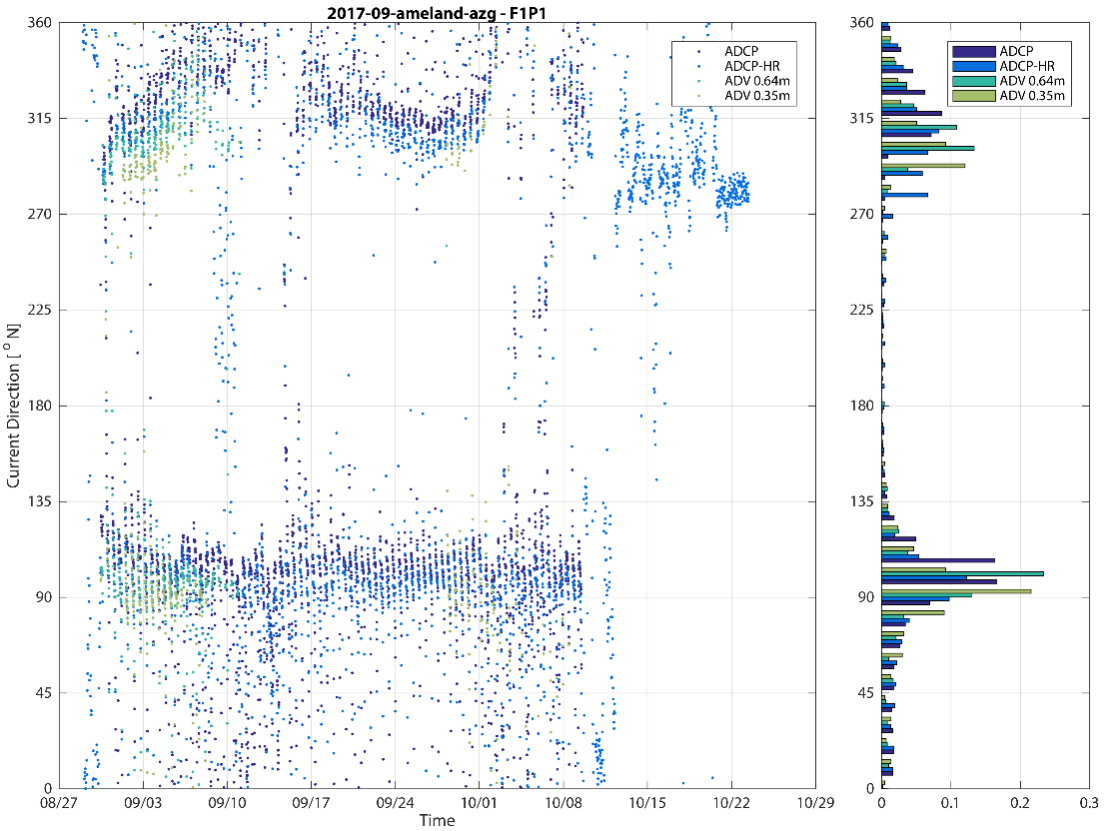

Figure D.1 Example of directional consistency QC plot for DVA F1. On the left is a time series of the 30-min burst-averaged flow direction. The right panel summarizes this information over the entire measurement period, indicating prominent peaks associated with the main ebb and flood directions. Misalignment of these peaks between instruments attached to the same frame may indicate an error in processing. Note that this frame was retrieved on 9 October 2017 (see Table 2.2), so the ADCP values thereafter have no physical meaning.

As a first-order check on the quality of the data, the likely major axis of tidal flow was estimated based on shoreline orientation and the assumption that the dominant flow direction is shore-parallel or along-channel. The first mode (largest peak) of the histograms computed based on the directional time series for each instrument (e.g. Figure D.1) was compared with the estimated tidal axis direction (Table D.1). Results within 15 degrees of the estimated direction were considered reasonable (highlighted in green). Based on this criterion, most instruments show directional consistency with the other instruments on their particular frame.

The ADVs on AZG Frame 4 have not been processed yet with the latest scripts due to memory problems, as a result of which the velocity angles are 90 degrees off. This will be solved at a later stage. For more discussion on the data-quality see Section 2.2.

Table D.1 Quality control checks for the mean directional consistency of flow velocity measuring instruments on each frame of each campaign. The status indicates whether the instrument was functional, missing, or if data files were blank/filled with non-numeric values. The estimated main axis of tidal flow based on local coastline orientation is indicated, along with the dominant flow direction calculated from the first mode of the velocity histogram as a function of direction. Instruments where the measured flow direction matched the estimated tidal axis (+/- 15) are highlighted in green, while discrepancies are highlighted in red.

Frame	Instrument	Status	% Blank	Estimated Tidal Dir		Dominant Flow Dir
AZG F1P1	ADCP	functional	53%	90	270	100
	ADCP-HR	functional	0%	90	270	100
	ADV middle	functional	58%	90	270	100
	ADV low	functional	61%	90	270	90
AZG F3P3	ADCP	functional	55%	0	180	180
	ADCP-HR	functional	0%	0	180	350
	ADV middle	functional	82%	0	180	170
	ADV low	functional	81%	0	180	170
AZG F4P5	ADCP	functional	37%	90	270	90
	ADCP-HR	functional	0%	90	270	100
	ADV high	file does not exist	100%	90	270	NaN
	ADV middle	functional	16%	90	270	180
	ADV low	functional	39%	90	270	180
AZG F5P4	ADCP	functional	52%	90	270	80
	ADCP-HR	functional	0%	90	270	120
	ADV high	file does not exist	100%	90	270	NaN
	ADV middle	file does not exist	100%	90	270	NaN
	ADV low	file does not exist	100%	90	270	NaN
DVA F1P1	ADCP	functional	49%	90	270	100
	ADCP-HR	functional	0%	90	270	80
	ADV middle	functional	46%	90	270	90
	ADV low	functional	59%	90	270	80
DVA F3P2	ADCP	functional	46%	90	270	100
	ADCP-HR	functional	0%	90	270	90
	ADV middle	functional	67%	90	270	90
	ADV low	functional	86%	90	270	90
DVA F4P3	ADCP	functional	44%	90	270	100
	ADCP-HR	all_fillValues	100%	90	270	NaN
	ADCP-DOWN	functional	54%	90	270	100
DVT1 F1P1	ADCP	functional	1%	75	255	90
	ADCP-HR	all_fillValues	100%	75	255	NaN
	ADV middle	functional	1%	75	255	80
	ADV low	functional	42%	75	255	70
DVT1 F3P2	ADCP	functional	44%	75	255	100

	ADCP-HR	functional	0%	75	255	260
	ADV middle	functional	1%	75	255	80
	ADV low	all_fillValues	100%	75	255	NaN
DVT1 F4P3	ADCP	functional	50%	75	255	90
	ADCP-HR	all_fillValues	100%	75	255	NaN
	ADCP-DOWN	functional	56%	75	255	80
DVT2 F1P1	ADCP	functional	60%	75	255	270
	ADCP-HR	functional	0%	75	255	260
	ADV middle	functional	24%	75	255	260
	ADV low	2nd ADV missing	100%	75	255	NaN
DVT2 F3P2	ADCP	functional	60%	75	255	260
	ADCP-HR	functional	0%	75	255	260
	ADV middle	functional	25%	75	255	260
	ADV low	all_fillValues	100%	75	255	NaN
DVT2 F4P3	ADCP	functional	51%	75	255	270
	ADCP-HR	all_fillValues	100%	75	255	NaN
	ADCP-DOWN	functional	65%	75	255	270
DVN F1P1	ADCP	functional	44%	30	210	50
	ADCP-HR	functional	0%	30	210	220
	ADV middle	functional	12%	30	210	220
	ADV low	functional	35%	30	210	210
DVN F3P2	ADCP	functional	43%	30	210	210
	ADCP-HR	functional	0%	30	210	30
	ADV middle	functional	2%	30	210	30
	ADV low	all_fillValues	100%	30	210	NaN
DVN F4P3	ADCP	functional	44%	30	210	40
	ADCP-HR	all_fillValues	100%	30	210	NaN
	ADCP-DOWN	functional	51%	30	210	220

E Contents data files

E.1 ADCP – Frames

The non-depth-averaged ADCP NetCDF files:

Variable	Size	Full Name
time	time x 1	time [seconds since 01-01-1970 00:00:00 0:00]
lon	1 x 1	longitude [degree]
lat	1 x 1	latitude [degree]
x	1 x 1	x_local [m]
y	1 x 1	y_local [m]
z	1 x 1	z_local [m]
z_measures	z_measures x 1	depth at bin center [m]
pressure	time x 1	pressure [Pa]
velocity_beam	z_measures x 1	beam velocity components [m/s]
heading_corrected	time x 1	corrected heading [°]
pitch	time x 1	pitch [°]
roll	time x 1	roll [°]
heading_correction	time x 1	heading deviation [°]
pressure_corrected	time x 1	pressure with atmospheric pressure removed [Pa]
velocity_east	z_measures x time	velocity east component [m/s]
velocity_north	z_measures x time	velocity north component [m/s]
velocity_up	z_measures x time	velocity up component [m/s]
heading_30	time x 1	heading 30 min averaged [°]
pitch_30	time x 1	pitch 30min averaged [°]
roll_30	time x 1	roll 30 min averaged [°]

The depth-averaged NetCDF files:

Variable	Size	Full Name
time	time x 1	time [seconds since 01-01-1970 00:00:00 0:00]
x	1 x 1	x_local [m]
y	1 x 1	y_local [m]
z	1 x 1	z_local [m]
lon	1 x 1	longitude [degree]
lat	1 x 1	latitude [degree]
z_measures	z_measures x 1	depth at bin center [m]
velocity_dabmean	time x xyz	depth averaged velocity beam mean [m/s]
velocity_da037d	time x xyz	depth averaged velocity, velocity at 37% of water depth [m/s]
velocity_dalogf	time x xyz	depth averaged velocity logarithmic fit [m/s]
pressure_corrected	time x 1	pressure with atmospheric pressure removed [Pa]
velocity_east	time x z_measures	velocity east component [m/s]
velocity_north	time x z_measures	velocity north component [m/s]
velocity_up	time x z_measures	velocity up component [m/s]
water_depth	time x 1	water depth [m]

E.2 ADCP HR – Frames

The velocity data:

Variable	Size	Full Name
instrument	1 x 1	ADV instrument name [-]
cell	cell x 1	Cell number, indicating depth of measurement [-]
time	time x 1	time of measurement [seconds since 1970-01-01 00:00:00]
lat	1 x 1	instrument latitude [degrees_north]
lon	1 x 1	instrument longitude [degrees_east]
Z	1 x 1	instrument height in frame [m]
Heading	1 x time	Heading [degree]
Pitch	1 x time	Pitch [degree]
Roll	1 x time	Roll [degree]
x_raw	cell x 1	flow velocity of water in one direction [m/s]
y_raw	cell x 1	flow velocity of water in one direction [m/s]
z_raw	cell x 1	flow velocity of water in one direction [m/s]
East	cell x 1	flow velocity of water in one direction [m/s]
North	cell x 1	flow velocity of water in one direction [m/s]
Up	cell x 1	flow velocity of water in one direction [m/s]

The pressure data:

Variable	Size	Full Name
instrument	1 x 1	ADV instrument name [-]
lat	1 x 1	instrument latitude [degrees_north]
lon	1 x 1	instrument longitude [degrees_east]
Z	1 x 1	instrument height in frame [m]
time	time x 1	time of measurement [seconds since 1970-01-01 00:00:00]
P	1 x time	raw pressure of sea water (at frame) [Pa]
P_APC	1 x time	pressure of sea water (at frame), corrected for air pressure [Pa]

The temperature data:

Variable	Size	Full Name
instrument	1 x 1	ADV instrument name [-]
lat	1 x 1	instrument latitude [degrees_north]
lon	1 x 1	instrument longitude [degrees_east]
Z	1 x 1	instrument height in frame [m]
time	time x 1	time of measurement [seconds since 1970-01-01 00:00:00]
T	1 x time	temperature of sea water (at frame) [degrees_C]

E.3 ADCP – Watersheds

Variable	Size	Full Name
velocityEastDS	time x 1	despiked flow velocity of water in east direction [m/s]
velocityNorthDS	time x 1	despiked flow velocity of water in north direction [m/s]
velocityUpDS	time x 1	despiked flow velocity of water in up direction [m/s]
velocityEast	time x 1	raw flow velocity of water in east direction [m/s]
velocityNorth	time x 1	raw flow velocity of water in north direction [m/s]
velocityUp	time x 1	raw flow velocity of water in up direction [m/s]
p	time x 1	pressure [-]
time	time x 1	time [seconds since 1970-01-01 00:00:00 (unix)]
bins	bin x 1	distance from sensor to measurement cell/bin centre [-]
lat	1 x 1	instrument latitude [degrees_north]
lon	1 x 1	instrument longitude [degrees_east]
Z	1 x 1	sensor elevation [m NAP]

E.4 ADV

Velocity data:

Variable	Size	Full Name
instrument	instrument x 1	ADV instrument name [-]
lat	instrument x 1	instrument latitude [degrees_north]
lon	instrument x 1	instrument longitude [degrees_east]
Z	instrument x 1	instrument height in frame [m]
Z_pres	instrument x 1	height of pressure sensor [m]
Z_vel	instrument x 1	height of velocity sensor [m]
time	time x 1	time of measurement [seconds since 1970-01-01 00:00:00]
x_raw	instrument x time	Flow velocity of water in one direction [m/s]
y_raw	instrument x time	Flow velocity of water in one direction [m/s]
z_raw	instrument x time	Flow velocity of water in one direction [m/s]
Heading	instrument x time	Heading [degree]
Pitch	instrument x time	Pitch [degree]
Roll	instrument x time	Roll [degree]
East	instrument x time	Flow velocity of water in one direction [m/s]
North	instrument x time	Flow velocity of water in one direction [m/s]
Up	instrument x time	Flow velocity of water in one direction [m/s]

Pressure data:

Variable	Size	Full Name
instrument	instrument x 1	ADV instrument name [-]
lat	instrument x 1	instrument latitude [degrees_north]
lon	instrument x 1	instrument longitude [degrees_east]
Z	instrument x 1	instrument height in frame [m]
Z_pres	instrument x 1	height of pressure sensor [m]
Z_vel	instrument x 1	height of velocity sensor [m]
time	time x 1	time of measurement [seconds since 1970-01-01 00:00:00]
P	instrument x time	raw pressure of sea water (at frame) [Pa]
P_APC	instrument x time	pressure of sea water (at frame), corrected for air pressure [Pa]

Temperature data:

Variable	Size	Full Name
instrument	instrument x 1	ADV instrument name [-]
lat	instrument x 1	instrument latitude [degrees_north]
lon	instrument x 1	instrument longitude [degrees_east]
Z	instrument x 1	instrument height in frame [m]
Z_pres	instrument x 1	height of pressure sensor [m]
Z_vel	instrument x 1	height of velocity sensor [m]
time	time x 1	time of measurement [seconds since 1970-01-01 00:00:00]
T	instrument x time	temperature of sea water (at frame) [degree_C]

E.5 Moving boat ADCP

The ADCP measurements:

Variable	Size	Full Name
time	time x 1	time [seconds since 1970-01-01 00:00:00]
lat	time x 1	latitude [degrees_north]
lon	time x 1	longitude [degrees_east]
crs	1 x 1	[-]
depth	depth x 1	depth_below_sea_surface [Z]
bottom	time x 1	sea_floor_depth_below_sea_surface [m]
eastvel	depth x time	eastward_sea_water_velocity [m/s]
northvel	depth x time	northward_sea_water_velocity [m/s]
velmagn	depth x time	sea_water_speed [m/s]
veldir	depth x time	sea_water_to_direction [degrees]
errvel	depth x time	error_of_velocity [m/s]

The derived flux discharges:

Variable	Size	Full Name
time	time x 1	average time between bounds [seconds since 1970-01-01 00:00:00]
time_bnds	2 x time	[-]
lat	time x 1	average latitude between bounds [degrees_north]
lon	time x 1	average longitude between bounds [degrees_east]
lat_bnds	2 x time	average latitude between bounds [degrees_north]
lon_bnds	2 x time	average longitude between bounds [degrees_east]
course	time x 1	direction [degrees]
boat_errors	time x 1	boat_errors []
boat_distance	time x 1	boat_distance [m]
made_good_boat_distance	time x 1	corrected_boat_distance [m]
navigation_distance	time x 1	boat_navigation [m]
made_good_navigation_distance	time x 1	corrected_boat_navigation [m]
discharge	time x 1	total_discharge [m3/s]
Flux	time x 1	total_sediment_flux [g/s]

E.6 Pressure sensors

Variable	Size	Full Name
pressure	time x 1	pressure measured at sensor [Pa]
sensor_height	1 x 1	sensor height above the undisturbed bed [m]
latitude	1 x 1	latitude [degrees north]
longitude	1 x 1	longitude [degrees east]
mean_depth	1 x 1	mean water depth [m]
pressure_apc	time x 1	pressure measured at sensor, corrected for air pressure [Pa]
time	time x 1	time [seconds since 1970-01-01 00:00:00 0:00]

E.7 Meteo

Variable	Size	Full Name
station	station x 1	station name [-]
time	time x 1	time of measurement [seconds since 1970-01-01 00:00:00]
lat	station x 1	station latitude [degrees_north]
lon	station x 1	station longitude [degrees_east]
projection	1 x 1	[-]
DD	station x time	Vector average wind direction [degree]
FH	station x time	Vector average wind speed [m/s]
P	station x time	Air pressure at sea level [hPa]

E.8 Wave Buoy

Basic data:

Variable	Size	Full Name
buoy	buoy x 3	[-]
time	time x buoy	time [seconds since 01-01-1970 00:00:00 0:00]
x	buoy x 1	x_rks [m]
y	buoy x 1	y_rks [m]
depth	buoy x 1	depth [m]
hm0	time x buoy	zero moment wave height [m]
tm02	time x buoy	second order moment wave period [s]
th0	time x buoy	mean wave direction [degrees]

Spectrum data:

Variable	Size	Full Name
buoy	buoy x 3	[-]
time	time x buoy	time [seconds since 01-01-1970 00:00:00 0:00]
x	buoy x 1	x_rks [m]
y	buoy x 1	y_rks [m]
depth	buoy x 1	depth [m]
Czz10	time x 1	wave energy density [cm2/Hz]
degfree	time x buoy	degrees of freedom of the wave spectrum [degrees of freedom]
Th010	time x 1	wave direction [°]
SObh10	time x 1	wave spreading [°]
Czzfreq	Czzfreq x 1	range of frequencies for energy density [mHz]
ThSpfreq	ThSpfreq x 1	range of frequencies for directions and spreading [mHz]

E.9 LISST

Variable	Size	Full Name
dBinLower	grainsizebins x 1	grain size (bin lower bound) [um]
dBinUpper	grainsizebins x 1	grain size (bin upper bound) [um]
dBinMedian	grainsizebins x 1	grain size (bin median) [um]
ringnum	grainsizebins x 1	ring number []
Conc	time x grainsizebins	volume concentration per size class [uL/L]
lasertrans	time x 1	laser transmission sensor [mW]
Voltage	time x 1	battery voltage [V]
Aux	time x 1	external auxiliary input [mW]
laserref	time x 1	laser reference sensor [mW]
pressure	time x 1	pressure [m]
temperature	time x 1	temperature [C]
opticaltrans	time x 1	computed optical transmission over path [-]
attenuation	time x 1	beam attenuation (c) [1/m]
time	time x 1	time [seconds since 1970-01-01 00:00:00 0:00]

E.10 Multi-parameter Probe (MPP)

Variable	Size	Full Name
temperature	time x 1	temperature [C]
conductivity	time x 1	conductivity [mS/cm]
depth	time x 1	depth [m]
salinity	time x 1	salinity [PSU]
pH	time x 1	pH [pH]
turbidity	time x 1	turbidity [NTU]
Chl	time x 1	chlorophyll [ug/L]
bga_pc	time x 1	blue green algae (phycocyanin pigment) [RFU]
odo	time x 1	dissolved oxygen [mg/L]
time	time x 1	time [seconds since 1970-01-01 00:00:00 0:00]

E.11 OBS

Variable	Size	Full Name
instrument	instrument x 1	OBS instrument name [-]
lat	instrument x 1	instrument latitude [degrees_north]
lon	instrument x 1	instrument longitude [degrees_east]
Z	instrument x 1	instrument height in frame [m]
Z_pres	instrument x 1	height of pressure sensor [m]
Z_vel	instrument x 1	height of velocity sensor [m]
time	time x 1	time of measurement [seconds since 1970-01-01 00:00:00]
OBS	instrument x time	voltage of analog input of obs [V]

E.12 Water samples

Variable	Size	Full Name
observation	sample x 1	identifier, sample number [-]
time	sample x 1	[seconds since 1970-01-01 00:00:00]
lat	sample x 1	latitude [degrees_north]
lon	sample x 1	longitude [degrees_east]
crs	1 x 1	[-]
Cond	sample x 1	[mS/cm]
D	sample x 1	[m]
T	sample x 1	[c]
Turb	sample x 1	[ntu]
SSC	sample x 1	[mg/l]

E.13 SONAR

Two series of files with results from the 0.05 m and 0.1 m LOESS filter. Each file contains the following variables:

Variable	Size	Full Name
x	nx x ny	x-coordinate [m]
y	nx x ny	y-coordinate [m]
time	time x 1	time [seconds since 1970-01-01 00:00:00 0:00]
z	time x 1	depth [m]
error	time x 1	error [m]
flag	time x 1	flag [-]
z_mean	time x 1	z_mean [-]

E.14 XBand radar

Variable	Size	Full Name
time	1 x 1	posixtime [seconds since 1970-01-01 00:00:00 0:00]
RDy	cell x 1	rijksdriehoekscoordinate Y [m]
RDx	cell x 1	rijksdriehoekscoordinate X [m]
px_x	cell x 1	image pixel coordinate X [m]
px_y	cell x 1	image pixel coordinate Y [px]
d	cell x 1	inverted depth [m]
d pred	cell x 1	predicted depth [m]
U	cell x 1	surface current velocity magnitude [m s-1]
Udir	cell x 1	surface current direction [degree]
Tm	cell x 1	mean wave period from radar [s]
Tp	cell x 1	peak wave period from radar [s]
MWD	cell x 1	mean wave direction from radar [degree]
PkWD	cell x 1	peak wave direction from radar [degree]
R2	cell x 1	r2 of conefit [-]
RMSE	cell x 1	rmse of conefit [degree]
Lim	cell x 1	chosen spectral threshold [-]
d_Ci	cell x 2	95% confidence bounds of conefit [m]
CPU time	1 x 1	CPU time [s]
WL (external)	1 x 1	water level used in depth prediction (buoy info from Terschelling) [m NAP]
SETTINGS cb_size	3 x 1	cube size in space x,y and time [px]
SETTINGS NwAvg	1 x 1	spectral bin size for averaging [frames]
SETTINGS NwOverlap	1 x 1	spectral overlap of bins [frames]
SETTINGS T_lims	2 x 1	spectral wave period limits [s]
SETTINGS d_lims	2 x 1	depth limits of wide dispersion filter [m]
SETTINGS U_lims	2 x 1	surface current magnitude limits [m s-1]
SETTINGS UpperConeFac	1 x 1	upper wide dispersion cone scaling factor [-]
SETTINGS DepMargin	1 x 1	allowed deviation from running bathymetry average [m]
SETTINGS BathyAvgNr	1 x 1	number of valid estimates used for running bathymetry average [-]
RADAR location	2 x 1	rijksdriekhoekcoordinates x,y of radar [m]
RADAR range	1 x 1	radar range [m]
RADAR range cutoff	1 x 1	radar range cutoff [m]
RADAR pixres	1 x 1	radar pixel resolution [m]
RADAR rottime	1 x 1	radar rotation time [s]
RADAR ImgSize	1 x 1	radar image size [px]

E.15 Singlebeam (Vaklodingen)

Variable	Size	Full Name
oblique_stereographic	1 x 1	CRS definition [-]
x	nx x 1	x coordinate of projection [m]
y	ny x 1	y coordinate of projection [m]
Altitude	nx x ny	altitude [m]

E.16 Multibeam

Variable	Size	Full Name
oblique_stereographic	1 x 1	CRS definition [-]
x	nx x 1	x coordinate of projection [m]
y	ny x 1	y coordinate of projection [m]
altitude	nx x ny	altitude [m]
time	1 x 1	[days since 1970-01-01]

E.17 Boxcores Ameland Inlet

Variable	Size	Full Name
Time	time x 1	time [seconds since 1970-01-01 00:00:00]
Lat	time x 1	latitude [degrees_north]
Lon	time x 1	longitude [degrees_east]
Crs	1 x 1	[-]
Id	id x time	identifier []
Depth	time x 1	depth_below_sea_surface [m]
D10	time x 1	particle_size_d10 []
D50	time x 1	particle_size_d50 []
D90	time x 1	particle_size_d90 []
Comments	id x time	comments []
Diameters	id x 11	diameters []
particle_size_density_function	11 x time	particle size density function []

E.18 Boxcores Ameland Inlet Borndiep

Variable	Size	Full Name
time	time x 1	time [seconds since 1970-01-01 00:00:00]
lat	time x 1	latitude [degrees_north]
lon	time x 1	longitude [degrees_east]
crs	1 x 1	[-]
id	id x time	identifier []
depth	23 x 1	depth_below_sea_surface [m]
url_photo	id x time	url of sediment photo []
sea_water_speed	time x 1	sea_water_speed [m/s]
direction_of_sea_water_velocity	time x 1	direction_of_sea_water_velocity [degrees]
D10	time x 1	particle_size_d10 []
D50	time x 1	particle_size_d50 []
D90	time x 1	particle_size_d90 []
comments	id x time	comments []
diameters	id x 33	diameters []
particle_size_density_function	33 x time	particle size density function []

E.19 Boxcores lower shoreface

Variable	Size	Full Name
time	time x 1	time [seconds since 1970-01-01 00:00:00]
lat	time x 1	latitude [degrees_north]
lon	time x 1	longitude [degrees_east]
crs	1 x 1	[-]
id	id x time	identifier []
depth	time x 1	depth_below_sea_surface [m]
url_photo	id x time	url of sediment photo []
core_length	time x 1	core_length [m]
sea_water_speed	time x 1	sea_water_speed [m/s]
direction_of_sea_water_velocity	time x 1	direction_of_sea_water_velocity [degrees]
wind_speed	time x 1	wind_speed [m/s]
wind_direction	time x 1	wind_direction [degrees]
number_of_core_parts	id x time	number of core parts []
D10	90 x 1	particle_size_d10 []
D50	90 x 1	particle_size_d50 []
D90	90 x 1	particle_size_d90 []
comments	id x time	comments []
diameters	id x 33	diameters []
particle_size_density_function	33 x time	particle size density function []

E.20 Vibrocores lower shoreface

Variable	Size	Full Name
time	time x 1	time [seconds since 1970-01-01 00:00:00]
lat	time x 1	latitude [degrees_north]
lon	time x 1	longitude [degrees_east]
crs	1 x 1	[-]
id	id x time	identifier []
depth	time x 1	depth_below_sea_surface [m]
url_photo	id x time	url of sediment photo []
core_length	time x 1	core_length [m]
penetration_depth	time x 1	penetration_depth [m]
number_of_core_parts	time x 1	number_of_core_parts []
sea_water_speed	time x 1	sea_water_speed [m/s]
direction_of_sea_water_velocity	time x 1	direction_of_sea_water_velocity [degrees]
wind_speed	time x 1	wind_speed [m/s]
wind_direction	time x 1	wind_direction [degrees]

Rijkswaterstaat
Ministry of Infrastructure and Water Management